

Host influenced geochemical signature in the parasitic foraminifer *Hydrokin sarcophaga*

Nicolai Schleinkofer^{1,2}, David Evans^{1,2}, Max Wisshak³, Janina Vanessa Büscher^{4,5}, Jens Fiebig^{1,2}, André Freiwald³, Sven Härter¹, Horst R. Marschall^{1,2}, Silke Voigt^{1,2}, Jacek Raddatz^{1,2}

¹Goethe Universität Frankfurt, Institut für Geowissenschaften, Frankfurt am Main, Germany

²Goethe Universität Frankfurt, Frankfurt Isotope and Element Research Center (FIERCE), Frankfurt am Main, Germany

³Senckenberg am Meer, Marine Research Department, Wilhelmshaven, Germany

⁴National University of Ireland Galway, Department of Earth and Ocean Sciences, Galway, Ireland

⁵GEOMAR Helmholtz Centre for Ocean Research Kiel, Department of Biological Oceanography, Kiel, Germany

Corresponding Author: Nicolai Schleinkofer (schleinkofer@em.uni-frankfurt.de)

Abstract

Hydrokin sarcophaga is a parasitic ~~foraminifer~~foraminifera that is commonly found in cold-water coral reefs where it infests the file clam *Acesta excavata* and the scleractinian coral *Desmophyllum pertusum* (formerly known as *Lophelia pertusa*). Here, we present measurements of the ~~elemental trace~~element and isotopic composition of ~~this~~these parasitic ~~foraminifer for the first time~~foraminifera, analyzed by inductively coupled optical emission spectrometry (ICP-OES), electron probe micro analysis (EPMA) and mass spectrometry (~~Gas-source-MS and Inductively-coupled-plasma~~-MS).

Our results reveal that the geochemical signature of *H. sarcophaga* depends on the host organism it infests. Sr/Ca ratios are 1.1 mmol mol⁻¹ higher in *H. sarcophaga* that infest ~~L. pertusa~~D. pertusum, which could be an indication that dissolved host carbonate material is utilised in shell calcification, given that the aragonite of ~~L. pertusa~~D. pertusum has a naturally higher Sr concentration compared to the calcite of *A. excavata*. Similarly, we measure 3.1 ‰ lower δ¹³C and 0.25 ‰ lower δ¹⁸O values in *H. sarcophaga* that lived on ~~L. pertusa~~D. pertusum, which might be caused by the direct uptake of the host's carbonate material with a more negative isotopic composition or different pH regimes in these foraminifera (pH can exert a control on the extent of CO₂ hydration/hydroxylation) due to the uptake of body fluids of the host. We also observe higher Mn/Ca ratios in ~~foraminifers~~foraminifera that lived on *A. excavata* but did not penetrate the host shell compared to specimen that penetrated the shell, which could be interpreted as a change in food source, changes in the calcification rate, Rayleigh fractionation or changing oxygen conditions.

While our measurements provide an interesting insight into the calcification process of this unusual ~~foraminifer~~foraminifera, these data also indicate that the geochemistry of this parasitic ~~foraminifer~~foraminifera is unlikely to be a reliable indicator of paleoenvironmental conditions using

Formatvorlagendefinition: Beschriftung: Schriftfarbe: Text 1

Sr/Ca, Mn/Ca, $\delta^{18}\text{O}$ or $\delta^{13}\text{C}$ unless the host organism is known and its geochemical composition can be accounted for.

1. Introduction

~~Foraminifera are a very diverse group of marine shelly organisms that are commonly used for paleoenvironmental reconstructions using the isotopic or elemental composition that is recorded in their carbonate shell (Costa et al., 2016; Gray and Evans, 2019; Sen Gupta, 2003; Hönisch et al., 2011; Lear and Rosenthal, 2006; Petersen et al., 2018; Raddatz et al., 2017). They first appeared in the Cambrian and, over the course of the Phanerozoic, occupied oceanic settings from coastal waters to the open ocean, as well as the benthic habitats of the deep sea (Goldstein, 1999). Multiple feeding methods are known from foraminifera, including suspension feeding, grazing, predation and parasitism (Hancock et al., 2015). The latter is probably the least common feeding mechanism among the foraminifera with only nine species that are known to be parasitic and a further 13 that are suspected to be (Walker et al., 2017). One of the known parasitic species is *Hyrrokin sarcophaga* (Cedhagen, 1994), a common foraminifera in cold water coral reefs in the NE Atlantic (Beuck et al., 2008). *H. sarcophaga* preferentially colonises the file clam *Acesta excavata*, but also other organisms such as the bivalve *Delectopecten vitreus*, sponges of the family Geodiidae and Ancorinidae, cold water corals such as *Lophelia pertusa*, *Madrepora oculata* and *Flabellum japonicum*, as well as other foraminifera (Beuck et al., 2008; Cheng and Dai, 2016). Besides biogenic hardgrounds, *H. sarcophaga* can also be found settling on rocks which shows that it can at least survive short periods without a host (Cedhagen, 1994). *H. sarcophaga* forms an attachment etching, i.e. mirroring its outline on the host. From this depression the foraminifer bores a canal into the shell of the host (Cedhagen, 1994)(Fig. 1). This allows the foraminifera to feed on the host tissue (Cedhagen, 1994) and possibly assimilate amino acids from the calcifying fluid (Alexander and Delaca, 1987; Schweizer et al., 2012).~~

The foraminifera are a very diverse group of marine shelly organisms that are commonly used for paleoenvironmental reconstructions using the isotopic or elemental composition of their carbonate shell (Petersen et al., 2018; Hönisch et al., 2011; Gray and Evans, 2019; Lear and Rosenthal, 2006; Raddatz et al., 2017). They first appeared in the Cambrian and, over the course of the Phanerozoic, occupied oceanic settings from coastal waters to the open ocean, as well as deep sea benthic habitats (Goldstein, 1999). Multiple feeding methods are known from foraminifera, including suspension feeding, grazing, predation and parasitic feeding (Hancock et al., 2015). The latter is probably the least common feeding mechanism among the foraminifera with only nine species that are known to be parasitic and a further 13 that are suspected to be (Walker et al., 2017). One of the known parasitic

65 species is *Hyrrokin sarcophaga* (Cedhagen, 1994), a common foraminifera in cold-water coral reefs in
66 the NE-Atlantic (Beuck et al., 2008). *H. sarcophaga* preferentially colonises the file clam *Acesta*
67 *excavata*, but also other organisms such as the bivalve *Delectopecten vitreus*, sponges of the family
68 Geodiidae and Ancorinidae, cold-water corals such as *Desmophyllum pertusum* (formerly known as
69 *Lophelia pertusa* (Addamo et al., 2016)), *Madrepora oculata* and *Flabellum japonicum*, as well as other
70 foraminifera (Beuck et al., 2008; Cheng and Dai, 2016; Cedhagen, 1994). Besides biogenic hard
71 substrates, *H. sarcophaga* can also be found settling on rocks which shows that it can at least survive
72 short periods without a host (Cedhagen, 1994). *H. sarcophaga* forms an attachment etching, i.e.
73 mirroring its spiral outline on the host. From this depression the foraminifera etch a canal into the shell
74 of the host (Cedhagen, 1994) (Fig. 1). This allows the foraminifera to feed on the bivalve host's tissue
75 (Cedhagen, 1994) and possibly assimilate amino acids from its extrapallial calcifying fluid (Schweizer et
76 al., 2012; Alexander and Delaca, 1987).

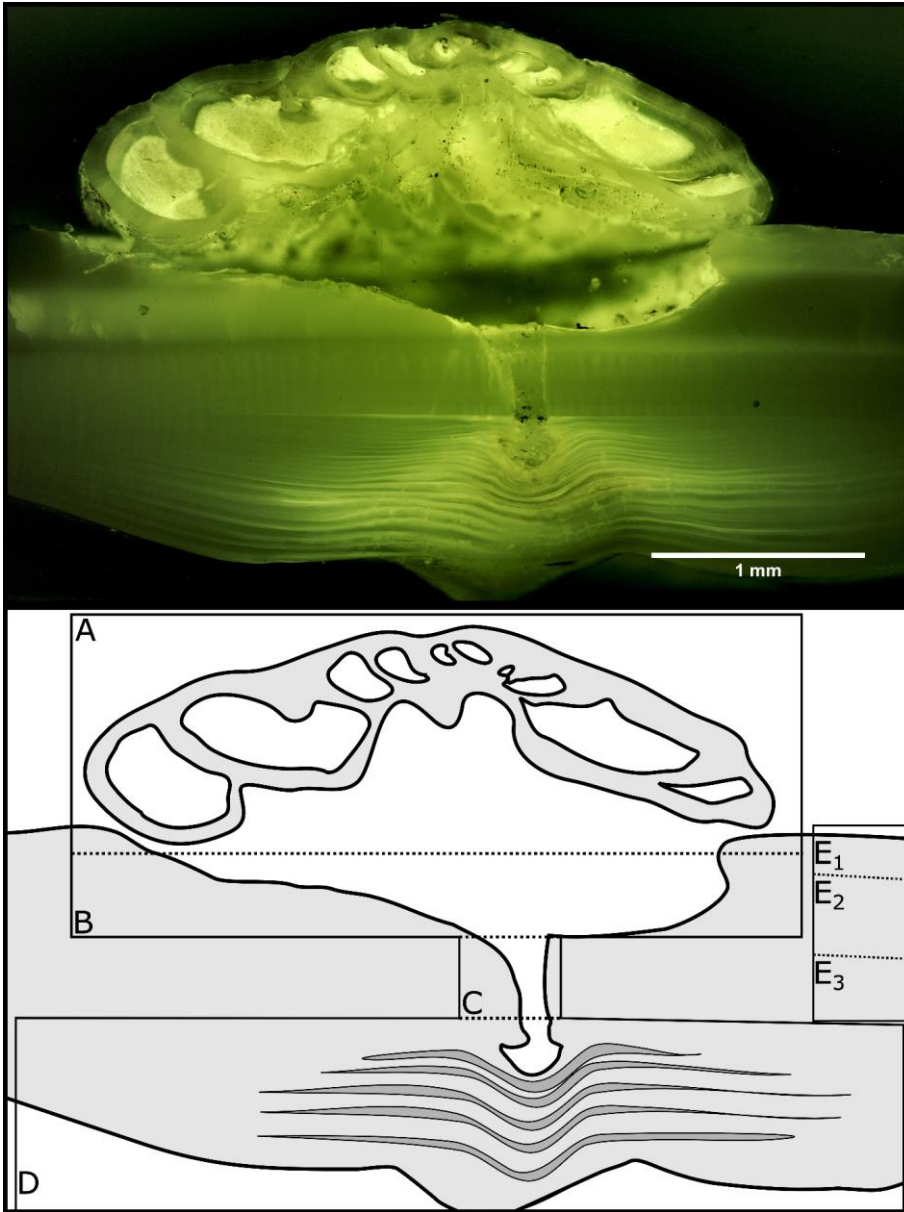


Figure 1 Fluorescence microscopic image (excitation 420 – 490 nm) and schematic figure of *H. sarcophaga* on *A. excavata*. A: *H. sarcophaga*, B: Attachment depression corroded by *H. sarcophaga*, C: Bored canal, D: Callus built by *A. excavata* (SRZ = shell repair zone), E: Undisturbed shell, E₁: Calcitic shell layer (fibrous), E₂: Calcitic shell layer (microgranular), E₃: Aragonitic shell layer

~~A. excavata reacts by building a callus to seal this boring (Fig 1D). This callus is a layered formation of aragonite rich in organic material that seals the boring of H. sarcophaga to defend the organism from the parasite's attack (Beuck et al., 2008). In L. pertusa, borings into the inner calyx area were not observed (Beuck et al., 2008). Instead multiple "whip"-shaped filaments protrude into the corals skeleton, which probably serve an anchoring function (Beuck et al., 2008). The pit is possibly formed either as a way to protect itself from cleaning attempts of the host and increase attachment strength or to satisfy calcium requirements in order to calcify (Beuck et al., 2008; Cedhagen, 1994).~~

~~As the parasitic foraminifera ingests material from its host, the question arises whether this process exerts an influence on the shell geochemistry of the parasite. Should this be the case, this factor may need to be accounted for, especially as some parasitic foraminifera, such as Cibicides refulgens, are also used in geochemical studies for paleoenvironmental reconstructions (Alexander and Delaca, 1987; García-Gallardo et al., 2017; Mackensen and Nam, 2014; Raddatz et al., 2011; Rathburn and De Deckker, 1997). If the geochemistry of the foraminifera shell depends systematically on the type of host that is infected, and these effects remain unknown, this could lead to erroneous palaeoenvironmental reconstructions. As far as we are aware, no previous studies have been conducted to test for this effect of different hosts on the geochemical composition of parasitic foraminifera.~~

~~HereThe bivalve reacts by building a callus (layered aragonite rich in organics) to seal this boring (Fig 1D) and defend the organism from the parasite's attack (Beuck et al., 2008). In D. pertusum, borings into the inner calyx area were not observed (Beuck et al., 2008). Instead, multiple "whip"-shaped tunnels protrude into the coral's skeleton, which possibly serve an anchoring function (Beuck et al., 2008). The pit is possibly formed either as a way to protect itself from cleaning attempts of the host and increase attachment strength or to serve the foraminifera's need for calcium and/or DIC (Beuck et al., 2008; Cedhagen, 1994).~~

~~As the parasitic foraminifera ingests material from its host, the question arises whether this process exerts an influence on the shell geochemistry of the parasite. Should this be the case, this factor may need to be accounted for, especially as some parasitic foraminifera, such as Cibicides refulgens, are also used in geochemical studies for paleoenvironmental reconstructions (García-Gallardo et al., 2017; Mackensen and Nam, 2014; Rathburn and de Deckker, 1997; Raddatz et al., 2011; Alexander and Delaca, 1987).~~

~~Here, we present element to Ca ratios (Mg/Ca, Sr/Ca, Na/Ca and Mn/Ca) and stable isotope data (oxygen and carbon) measuredanalyzed in H. sarcophaga collected from different host organisms (A. excavata and L. pertusaD. pertusum) from the Trondheimsfjord (Norway) to explore if and how the~~

different hosts influence the geochemical composition of the ~~test of~~ foraminifera ~~shell~~. In addition, we present element maps ~~measured~~ analyzed by electron microprobe analysis (EPMA) of the callus region of *A. excavata* in order to explore geochemical differences between the callus region and undisturbed shell areas.

2. Material and Methods

2.1. Sampling

~~All investigated samples were collected in the Leksa Reef, located at the entrance to the Trondheimsfjord in Norway (N 63.613056/E 9.384167, depth ~ 200 m) by means of the manned submersible JAGO (Hissmann and Schauer, 2017) during the scientific cruises POS473 and POS525 with R/V POSEIDON (Büscher, 2018; Form et al., 2015; Lackschewitz and Heinitz, 2015). In total we measured 28 specimen of *H. sarcophaga*, which were divided into three groups: 1. *H. sarcophaga* that infested *A. excavata* with callus formation (henceforth called HAW), 2. *H. sarcophaga* that infested *A. excavata* without callus formation (henceforth called HAO, HAW + HAO = HA), 3. *H. sarcophaga* that infested *L. pertusa* (henceforth called HL). Samples of *A. excavata* and *L. pertusa* were picked alive. For *H. sarcophaga* we cannot be entirely certain that they were still alive when sampled, however, when dead they are easily removed from the shell. Therefore, in case the foraminifera were dead when sampled, they died close to the time of sampling.~~

~~For electron probe micro analysis (EPMA) we used two samples of *A.*~~ All investigated samples were collected in the Leksa Reef, located at the entrance to the Trondheimsfjord in Norway (N 63.613056/E 9.384167, depth ~ 200 m) by means of the manned submersible JAGO (GEOMAR Helmholtz-Zentrum für Ozeanforschung, 2017) during the scientific cruises POS473 and POS525 with RV Poseidon (Form et al., 2015; Büscher, 2018; GEOMAR Helmholtz-Zentrum für Ozeanforschung, 2015). In total we analyzed 30 specimens of *H. sarcophaga*, which were divided into three groups: 1. *H. sarcophaga* that infested *A. excavata* with callus formation (henceforth called HAW), 2. *H. sarcophaga* that infested *A. excavata* without callus formation (henceforth called HAO; HAW + HAO = HA), 3. *H. sarcophaga* that infested *D. pertusum* (henceforth called HL). Samples of *A. excavata* and *D. pertusum* were alive when sampled. We cannot be entirely certain that *H. sarcophaga* were still alive when sampled, but upon death they easily become detached from the shell whereas in our samples the foraminifera were still firmly attached. For ICP-OES, ICP-MS and GS-MS, the samples were ultrasonically rinsed in deionized water for five minutes and allowed to dry before crushing in an agate mortar

~~*excavata* with attached *H. sarcophaga*. The area of interest was cut from the shell with a handheld drilling tool, mounted vertically into circular mounts and embedded in epoxy resin. The sample surface~~

Formatiert: Schriftart: Kursiv

Formatiert: Englisch (Vereinigte Staaten), Muster: Transparent (Weiß)

was ground with 9 µm grid with silicon carbide sanding paper and then polished using 3 µm diamond water based lapping paste.

~~For stable isotope measurements we used nine HAW, nine HAO and ten HL. The samples were ultrasonically rinsed in deionised water for five minutes and allowed to dry. Afterwards the samples were crushed in an agate mortar. About 100 µg of sample powder was transferred to borosilicate glass tubes and sealed with plastic caps.~~

~~For ICP-OES measurements we used ten HAW, ten HAO and ten HL samples. The samples were ultrasonically rinsed in deionised water for five minutes and allowed to dry. Afterwards the samples were crushed in an agate mortar. About 120 µg of sample powder was transferred to Eppendorf tubes and sealed.~~

Bivalve and coral samples were treated similarly to foraminifera samples. For stable isotopes and E/Ca analysis we used three shells. We took 15–20 samples per shell from the outermost shell section along the main growth axis, starting at the ventral margin. The corals were sampled randomly over the whole calyx area.

~~The manganese concentration of *L. pertusa* had to be determined by ICP-MS because it was below the limit of detection by ICP-OES. We used three specimens (two from the Leksa Reef, one from the Sula Reef) of which we sampled 150 µg from the fibrous shell section.~~

~~Samples of the ambient water were collected during scientific cruise POS525 with R/V POSEIDON in July 2018 (Büscher, 2018; Lackschewitz and Heinitz, 2015). A Rosette Sampler equipped with conductivity, temperature and depth sensors (CTD) was used to sample water from the investigated reefs. The water samples were transferred from 12 L Niskin bottles to 250 mL borosilicate bottles and sealed after adding 100 µL HgCl₂ to prevent biological activity of microorganisms that may alter the isotopic composition. The samples were stored in a fridge at 4 °C until measurement.~~

2.2.Shell carbonate polymorph

~~The polymorph of the foraminiferal shell was determined using cobalt nitrate solution (Meigen solution). The foraminifera samples were crushed in an agate mortar and transferred to Eppendorf containers. The samples were mixed with 0.38. Aragonite stains purple/pink in cobalt nitrate solution, whereas calcite is unaffected (Kato et al., 2003)~~

2.2.Shell carbonate polymorph

~~The polymorph of the foraminiferal shell was determined using cobalt nitrate solution (Meigen solution). The foraminifera samples were crushed in an agate mortar and transferred to Eppendorf~~

containers. The samples were mixed with 10 wt% $\text{Co}(\text{NO}_3)_2$ aqueous solution and allowed to react at 95°C for 20 minutes. Afterwards the samples were washed four times with deionized-water and inspected under a KEYENCE VHX-S660E microscope. Aragonite stains purple/pink in cobalt nitrate solution, whereas calcite remains unaffected (Kato et al., 2003)

2.3. Fluorescence microscopy

We used fluorescence microscopy to investigate the distribution of the organic material in the foraminifera and the underlying bivalve shell. The sample was cut, ultrasonically cleaned in deionized-water, embedded in epoxy resin (Araldite 2020) and polished with 3 μm diamond-lapping paste. Fluorescent images were taken using a Leica DMRX-POL microscope with fluorescent front light and a 50 W mercury lamp. The microscope was equipped with an H3 filter cube, which excites in the wavelength range of blue to violet (Bandpass filter: 420 – 490 nm) The pictures were taken with a digital camera connected to the microscope with 0.25 s exposure time.

2.4. EPMA

Two samples of *A. excavata* with attached *H.* Electron-probe micro-analyses were conducted at Goethe Universität Frankfurt on a JEOL JXA-8530F Plus Field Emission Gun Electron Probe Micro Analyzer (FEG-EPMA). Analysis conditions were: 15 kV acceleration voltage, 20 nA current with a beam diameter of 3 μm . We used TAP crystal for Mg, TAPL for Na and Sr and PETH for S. Detection limits are calculated with the equation given in Goldstein et al., 2017 and amount to: Mg = 178 $\mu\text{g g}^{-1}$ (Mg/Ca = 0.7 mmol mol^{-1}), Na = 170 $\mu\text{g g}^{-1}$ (Na/Ca = 0.7 mmol mol^{-1}), Sr = 129 $\mu\text{g g}^{-1}$ (Sr/Ca = 0.1 mmol mol^{-1}), S = 152 $\mu\text{g g}^{-1}$ (S/Ca = 0.4 mmol mol^{-1}) and Ca = 195 $\mu\text{g g}^{-1}$. The chemical maps were recorded with a beam diameter of 2 μm , 15 kV acceleration voltage and 20 nA current.

sarcophaga were analysed by electron probe micro analysis (EPMA). The area of interest was cut from the shell with a handheld drilling tool, ultrasonically cleaned in deionized-water for five minutes, mounted vertically into circular mounts and embedded in epoxy resin (Araldite 2020). The sample surface was ground with 9 μm grid with silicon carbide sanding paper and then polished using 3 μm diamond-water based lapping paste. After polishing the samples were coated with carbon.

The EPMA analyses were conducted at Goethe University Frankfurt on a JEOL JXA-8530F Plus Field Emission Gun Electron Probe Micro Analyzer (FEG-EPMA). Analysis conditions were: 15 kV acceleration voltage, 20 nA current with a beam diameter of 3 μm . We used a TAP crystal for Mg, TAPL for Na and Sr and PETH for S. Detection limits are calculated with the equation given in Goldstein et al., 2017 and amount to: Mg = 178 $\mu\text{g g}^{-1}$ (Mg/Ca = 0.7 mmol mol^{-1}), Na = 170 $\mu\text{g g}^{-1}$ (Na/Ca = 0.7 mmol mol^{-1}), Sr = 129 $\mu\text{g g}^{-1}$ (Sr/Ca = 0.1 mmol mol^{-1}), S = 152 $\mu\text{g g}^{-1}$ (S/Ca = 0.4 mmol mol^{-1}) and Ca = 195 $\mu\text{g g}^{-1}$. Molar ratios were calculated from the weight fractions of the specific oxides (CaO, MgO, Na_2O , SrO, SO_3) by

Formatiert: Schriftart: Kursiv

calculating the concentration of the observed elements (in $\mu\text{g/g}$) and normalization to Ca accounting for their relative atomic mass. The chemical maps were recorded with a beam diameter of 2 μm , 15 kV acceleration voltage and 20 nA current.

2.5. ICP-OES

For ICP-OES measurements we used ten HAW, ten HAO and ten HL samples. About 120 μg of sample powder was transferred to Eppendorf tubes (acid cleaned with 5 % HNO_3) and sealed. Each sample was analyzed three times.

Elemental ratios Mg/Ca, Sr/Ca, Na/Ca and Mn/Ca (only for foraminifera and bivalves) were analyzed by inductively coupled plasma-optical emission spectrometry (ICP-OES). ~~The~~ ICP-OES analysis was carried out ~~with~~ using a ThermoScientific iCap 6300 Duo at the Institute of Geosciences, Goethe ~~Universität~~ University Frankfurt. The sample powder ($\approx 140 \mu\text{g}$) was dissolved in 500 μL HNO_3 (2-%) and ~~300 μL~~ 300 μL aliquots were separated. Subsequently 1500 μL of 1.2 mg L^{-1} yttrium solution was added to each aliquot as an internal standard resulting in a concentration of Y = 1 mg L^{-1} and Ca = 25 mg L^{-1} . The intensity data were background ~~subtracted and corrected~~, standardized internally to Y and normalized to Ca. ~~The reproducibility~~ Accuracy is reported in % deviation from values of standard reference material JCP1 and USGS MACS-3 (n = 5) (Jochum et al., 2005) and is better than 1% for Mg/Ca and Sr/Ca, 5% for Na/Ca and 3% for Mn/Ca. Precision is reported in relative standard deviation; % RSD of the USGS MACS-3 and JCP1 carbonate reference material (n = 5) (Jochum et al., 2005) was (Jochum et al., 2005) and is better than 3% (relative standard deviation; % RSD) for Mg/Ca, Na/Ca, Sr/Ca and Mn/Ca. Accuracy is reported in % deviation from reported values of standard reference material for all analyzed elements.

Bivalve (n = 3) and coral (n = 3) samples were treated similarly to foraminifera samples. We took 15 - 20 samples per shell from the outermost shell section along the main growth axis, starting at the ventral margin resulting in a total of 49 samples. The corals were sampled randomly over the whole calyx area resulting in 44 samples.

2.6. ICP-MS

The manganese concentration of *D. pertusum* had to be determined by ICP-MS because it was below the limit of detection by ICP-OES. We used three specimens (two from the Leksa Reef, one from the Sula Reef) of which we sampled 150 μg from the fibrous shell section. ~~For solution-based ICP-MS measurements we used 150 μg of sample powder and dissolved it in 500 μL 2% HNO_3 . The dissolved sample (300 μL) was mixed with 1500 μL 1.2 mg L^{-1} Yttrium solution which was used as the internal standard. The reference material ECRM 752 (Greaves et al., 2008) was used to monitor measurement~~

Formatiert: Englisch (Vereinigtes Königreich)

precision. The reproducibility of the ECRM 752 carbonate reference material (n = 3) was better than 1% for Mn/Ca

Each sample was measured twice.

For solution based ICP-MS measurements we used 150 µg of sample powder and dissolved it in 500 µL 2% HNO₃. The dissolved sample (300 µL) was mixed with 1500 µL 1.2 mg L⁻¹ yttrium solution which was used as the internal standard. The reference material ECRM 752-1 (Greaves et al., 2008) was used to monitor measurement precision and accuracy, reported in %-deviation from the reported values of the standard reference material ECRM 752-1 (n = 3) (Greaves et al., 2005) and equals 7% for this analytical session. Precision is reported in relative standard deviation; % RSD of the ECRM 752 carbonate reference material (n = 3) is better than 1% for Mn/Ca

2.7. Stable oxygen and carbon isotopes

We used nine HAW, nine HAO and ten HL for stable isotope measurements. About 100 µg of sample powder was transferred to borosilicate glass tubes and sealed with plastic caps. Each sample was measured three times.

Stable isotopes were measured at Goethe ~~Universität~~University Frankfurt on a Thermo MAT 253 Mass Spectrometer interfaced with a Thermo Fisher Scientific GasBench II. The sample material (100 µg) was reacted with 99% H₃PO₄ at 72°C in continuous flow mode. Analytical procedures followed ~~Spötl and Vennemann (2003).~~Spötl and Vennemann (2003). δ¹³C and δ¹⁸O values are reported in δ-notation, i.e. ‰-deviation relative to Vienna Pee Dee Belemnite (VPDB) and Vienna Standard Mean Ocean (VSMOW), respectively. Internal precision is better than 0.06-‰ (δ¹³C) and 0.08-‰ (δ¹⁸O).

Samples of the ambient water were collected during scientific cruise POS525 with R/V Poseidon in July 2018 (Büscher, 2018; GEOMAR Helmholtz-Zentrum für Ozeanforschung, 2015). A Rosette Sampler equipped with conductivity, temperature and depth sensors (CTD, Sea-Bird Scientific. SBE 911 Plus) was used to sample water from the investigated reefs. The water samples were transferred from 12 L Niskin bottles to 250 mL borosilicate bottles and sealed after adding 100 µL HgCl₂ to prevent biological activity of microorganisms that may alter the isotopic composition. The samples were stored in a fridge at 4°C until measurement.

Water samples were analyzed for their isotopic composition at Friedrich-Alexander ~~Universität~~University Erlangen-Nürnberg by an automated equilibration unit (Gasbench II; Thermo Fisher Scientific) coupled in continuous flow mode to a Delta *plus* XP isotope ratio mass spectrometer (Thermo Fisher Scientific, Bremen, Germany).

Water for $\delta^{13}\text{C}$ analyses was extracted from the sample bottles by a 1-mL disposable syringe through the septa without opening the bottle to avoid loss of CO_2 during sample transfer. During water extraction, the removed volume was simultaneously replaced by inert gas through a second needle connected to an argon-filled gas sampling bag (Grace, Deerfield, IL, USA). The samples were injected into 12 mL Labco Exetainers™ (Labco Ltd. Lampeter, U.K) that were prepared with phosphoric acid and pre-flushed with helium (purity 99.999%). For seawater the injection volume was 0.85 mL per vial. Samples were analyzed in duplicates and the reported values are arithmetic means. All values are reported in the standard δ -notation in per mille (‰) vs. VPDB.

Sample bottles for $\delta^{18}\text{O}$ were de-capped and 0.5 mL water were extracted with a pipette for CO_2 equilibration. The samples were transferred into 12 mL Labco Exetainers™ (Labco Ltd. Lampeter, U.K) and subsequently flushed with 0.3% CO_2 in helium. Equilibration time was 24 hours at 25 °C. All samples were measured in duplicates and the reported values are arithmetic means. All values are reported in the standard δ -notation in per mille (‰) vs. VSMOW. External reproducibility based on repeated analysis of control samples was better than 0.1‰ and 0.05-‰ for $\delta^{13}\text{C}$ and $\delta^{18}\text{O}$, respectively.

2.8. Statistical computation

We used one-way ANOVA to test the effect of the host species on the elemental and isotopic composition in *H. sarcophaga*. Shapiro-Wilk test and Levene's test were used to ensure normal distribution and equal variance of the target variables. Most groups and target variables are normally distributed except for Na/Ca in the HAO group and $\delta^{18}\text{O}$ in the HL group. All target variables except for Mn/Ca and Sr/Ca show equal variance based on the Levene's test. Normal distribution and equal variance are considered a prerequisite for ANOVA. ~~As these prerequisites are not met in some groups we additionally tested the data with a Kruskal-Wallis test which can be regarded as a non-parametric alternative to ANOVA (Lantz, 2013). R scripts are available from the corresponding author.~~ As these prerequisites are not met in some sample groups, we additionally tested the data with a Kruskal-Wallis test which is a non-parametric alternative to ANOVA (Lantz, 2013). Pairwise comparison of the different groups was accomplished with Bonferroni adjusted Tukey-HSD test. All reported *p*-values are Bonferroni adjusted.

3. Results

3.1. Carbonate Polymorph

~~The investigated *H. sarcophaga* samples show no staining (Supplement S2) under the influence of cobalt nitrate solution. Consequently the shells are built of calcite like other species of the order Rotaliida (Horton et al., 2021).~~

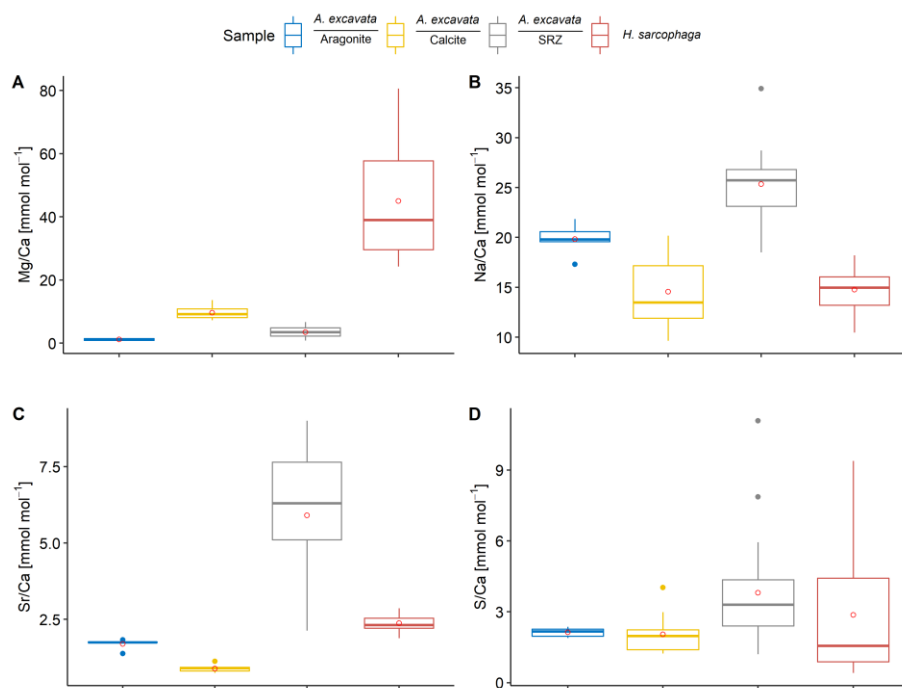
The investigated *H. sarcophaga* samples show no staining (Supplement S1) under the influence of cobalt nitrate solution. Consequently, the shells are calcitic as is the case for other species of the order Rotaliida (Horton et al., 2021).

3.2. Fluorescence microscopy

The fluorescence microscopic image of *H. sarcophaga* attached to *A. excavata* (Fig. 1) shows distinct fluorescent and non-fluorescent layers in the shell repair zone (SRZ) of the bivalve. Highly fluorescent material is also observable on *H. sarcophaga*, especially in the foramen test apertures.

The SRZ has a maximum thickness of 900 µm, decreasing in all directions. The fluorescent layers in the SRZ are 20 – 40 µm thick. These layers taper off distally from the bore canal and disappear. Non-fluorescent layers are generally smaller ranging from 9- 20 µm. The asymmetric pit that is produced by the foraminifera is observable, one side of the pit is rising steeply whereas the other side has a shallower angle. The bore canal, which starts at the bottom of the attachment etching, is 400 µm long in the undisturbed bivalve shell, but continues in the callus by another 240 µm. At the start of the bore the canal is 340 µm in diameter and continuously narrows to 140 µm. The canal ends in the SRZ with a “mushroom-like” shape.

3.3. Element composition of point measurements (EPMA)



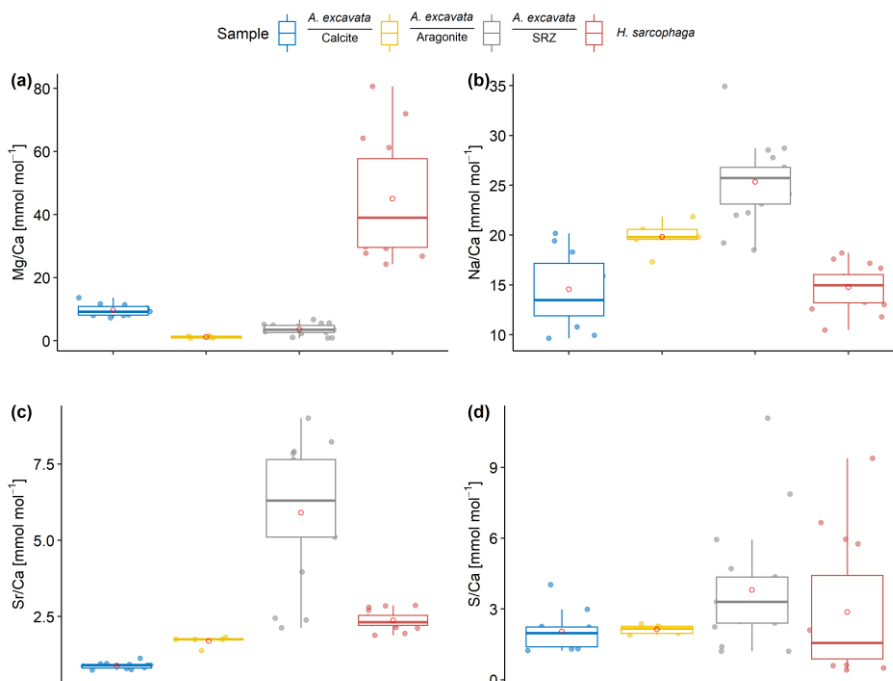


Figure 2 Results of point measurements by EPMA in different sections of *A. excavata* and *H. sarcophaga* (two specimens each). A: Mg/Ca, B: Na/Ca, C: Sr/Ca, D: S/Ca. Boxes display the interquartile range (IQR) and lines the median values. The whiskers show min and max values that are within the range of $Q1 - 1.5 \times IQR - Q3 + 1.5 \times IQR$. Red circles show the mean values. Sample size = 11, 5, 17, 16 (Calcite, Aragonite, SRZ, *H. sarcophaga*). Text below the horizontal lines in the legend is the sampled area.

Table 1 Wilcoxon-Mann-Whitney test results of E/Ca comparison between the observed shell sections. Bold fields show significant differences between the two groups. *p*-values are Bonferroni adjusted.

Wilcoxon-Mann-Whitney Test			
	Group 1	Group 2	<i>p</i>
Mg/Ca	Calcite	Aragonite	0.003
	Calcite	SRZ	<0.001
	Calcite	<i>H. sarcophaga</i>	<0.001
	Aragonite	SRZ	0.051
	Aragonite	<i>H. sarcophaga</i>	<0.001
	SRZ	<i>H. sarcophaga</i>	<0.001
Na/Ca	Calcite	Aragonite	0.052
	Calcite	SRZ	<0.001
	Calcite	<i>H. sarcophaga</i>	1
	Aragonite	SRZ	0.027
	Aragonite	<i>H. sarcophaga</i>	0.002
	SRZ	<i>H. sarcophaga</i>	<0.001
Sr/Ca	Calcite	Aragonite	0.003
	Calcite	SRZ	<0.001

Formatiert: Englisch (Vereinigtes Königreich)

	<u>Calcite</u>	<u>H. sarcophaga</u>	<u><0.001</u>
	<u>Aragonite</u>	<u>SRZ</u>	<u><0.001</u>
	<u>Aragonite</u>	<u>H. sarcophaga</u>	<u><0.001</u>
	<u>SRZ</u>	<u>H. sarcophaga</u>	<u><0.001</u>
<u>S/Ca</u>	<u>Calcite</u>	<u>Aragonite</u>	<u>1</u>
	<u>Calcite</u>	<u>SRZ</u>	<u>0.116</u>
	<u>Calcite</u>	<u>H. sarcophaga</u>	<u>1</u>
	<u>Aragonite</u>	<u>SRZ</u>	<u>0.286</u>
	<u>Aragonite</u>	<u>H. sarcophaga</u>	<u>1</u>
	<u>SRZ</u>	<u>H. sarcophaga</u>	<u>0.66</u>

Within the bivalve shell Mg/Ca varies between 0.762 and 13.67 mmol mol⁻¹ (Fig. 2). Lowest values were found in the aragonitic shell layer (Fig 1/E₃) and highest values are measured in the microgranular calcitic shell layerslayer (Fig 1/E_{1&2}). With a mean ratio of 3.47 mmol mol⁻¹, the SRZ is enriched in Mg/Ca compared to the undisturbed bivalve aragonite.E₂). The highest Mg/Ca ratios are measured in the foraminiferal calcite (mean = 45.030 ± 17.9 mmol mol⁻¹, max = 80.6 mmol mol⁻¹).

Na/Ca ratio showare characterized by similar values in the different sections when considering the carbonate polymorph, that they are built of. The aragonitic sections (Fig 1/E₃), bivalve aragonite and SRZ, have mean Na/Ca ratios of 22.0 and 25 ± 2.3 mmol mol⁻¹ (mean ± sd) and 25.3 ± 3.8 mmol mol⁻¹ respectively. The SRZ displays a higher variability than the undisturbed aragonite. Both calcitic regions areThe microgranular calcite is characterised by a mean Na/Ca of 14.8 ± SD = 3.7 mmol mol⁻¹ (Fig 1/E_{1&2}E₂).

The SRZ is enriched in Sr/Ca compared to the undisturbed shell sections. Mean ratios are with 5.91 mmol mol⁻¹nearlynearly four times higher than in the undisturbed aragonitic shell parts (mean = 1.54 ± 0.2 mmol mol⁻¹ compared to 1.5 ± 0.2 mmol mol⁻¹). Lowest values are measured in the bivalvebivalve's microgranular calcite (mean = 0.899 ± 0.1 mmol mol⁻¹).

S/Ca ratios are comparable in the undisturbed bivalve aragonite and microgranular calcite, with 1.9 ± 0.3 mmol mol⁻¹ and 2.1 mmol mol⁻¹ ± 0.8 mmol mol⁻¹, respectively. Similar to Sr/Ca, the highest mean and maximum S/Ca ratios are measured in the SRZ (mean = 3.8 ± 2.5 mmol mol⁻¹, max = 11.1 mmol mol⁻¹). However, all these differences are insignificant (Table 1).

The Ca concentration in the different samples varies between 36.7 w% and 39.3 w%. Variations in E/Ca ratios are therefore not necessarily controlled by changes of the observed element but can also change according to the Ca concentration. However, changes in the Ca concentration are negligible in the context of this study as the maximum deviation of the calculated E/Ca ratios amounts to 2 mmol mol⁻¹ for Mg/Ca at 80 mmol mol⁻¹.

Formatiert: Englisch (Vereinigte Staaten), Muster: Transparent (Weiß)

Formatiert: Englisch (Vereinigte Staaten), Muster: Transparent (Weiß)

Formatiert: Englisch (Vereinigte Staaten), Muster: Transparent (Weiß)

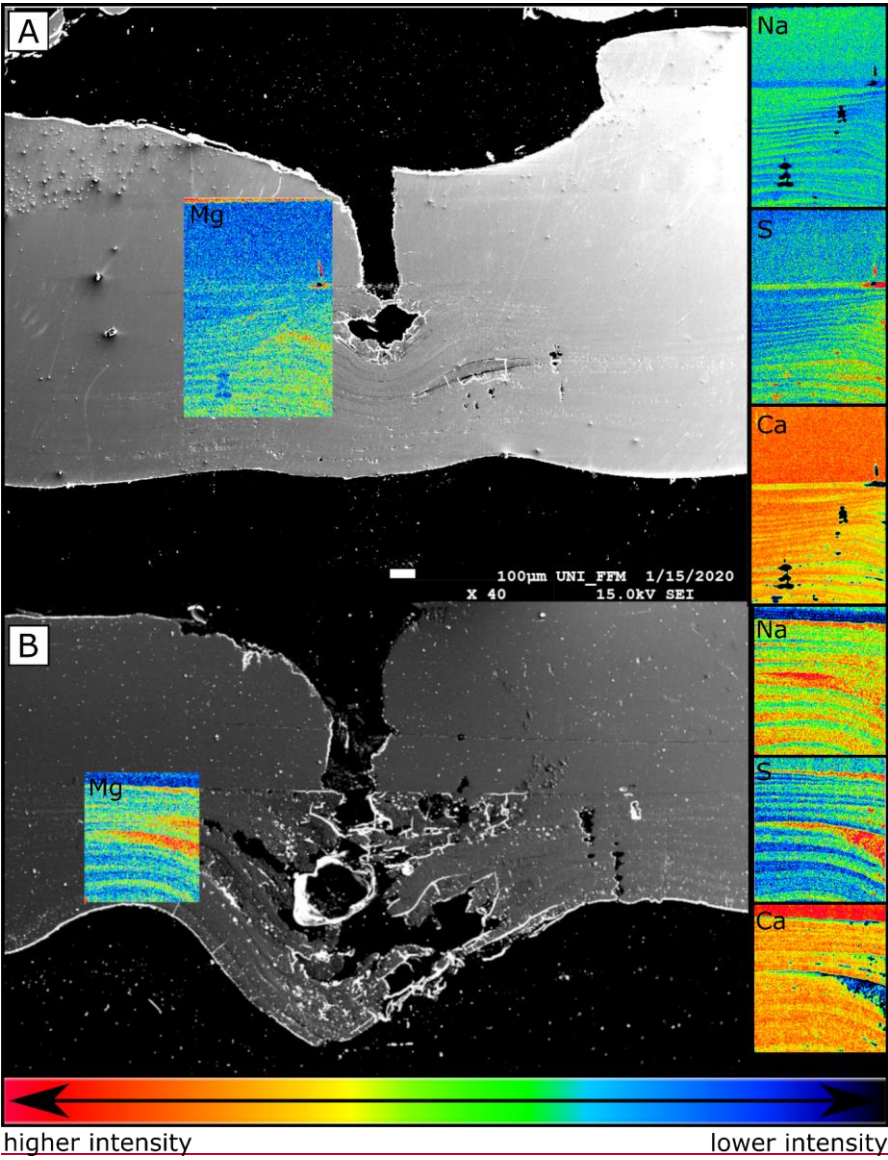
Formatiert: Englisch (Vereinigte Staaten), Muster: Transparent (Weiß)

Formatiert: Englisch (Vereinigte Staaten), Muster: Transparent (Weiß)

Formatiert: Englisch (Vereinigtes Königreich), Nicht Hochgestellt/ Tiefgestellt, Muster: Transparent

364

3.4-EPMA-element maps



365

366

367

368

Elemental composition of the SRZ

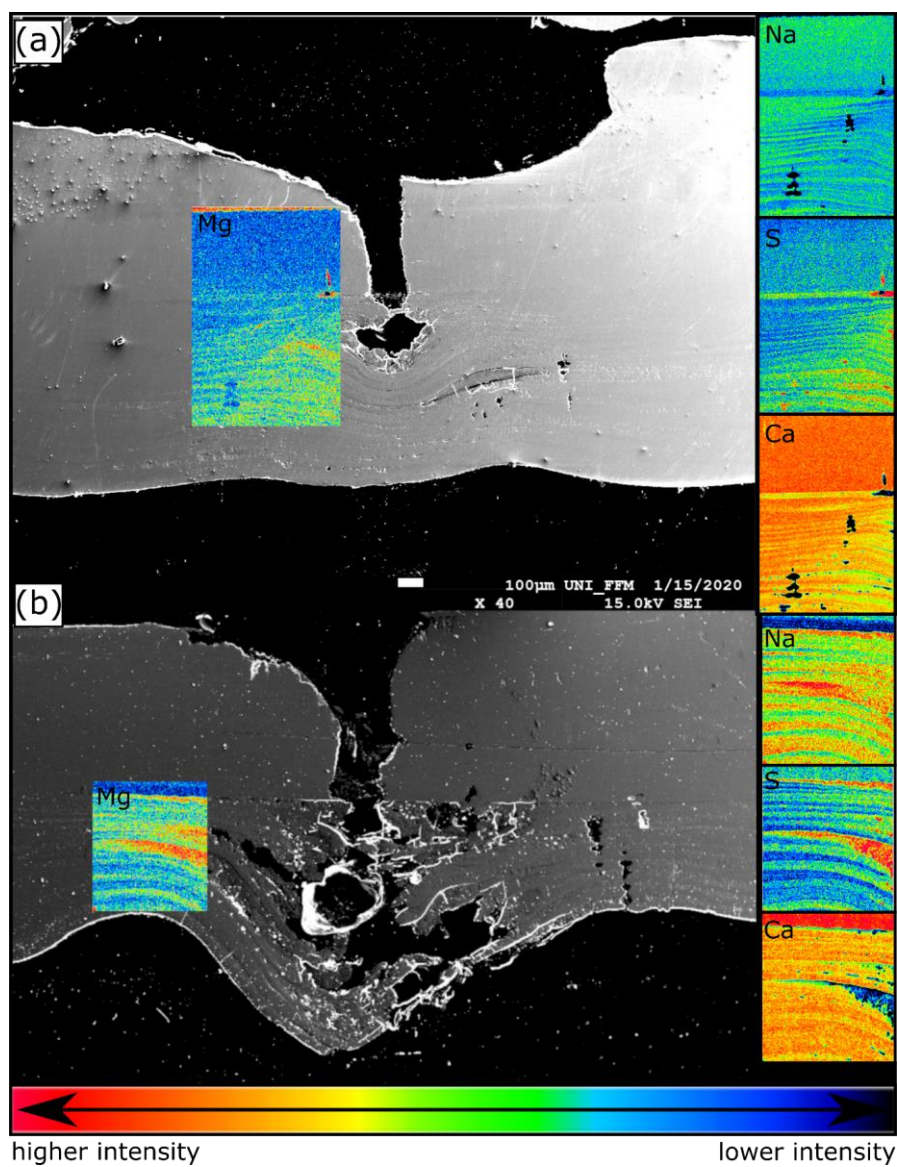


Figure 3 EPMA element maps and secondary-electron image from an SEM of the callus area of *A. excavata*—two specimen (A & B) of *A. excavata*. Intensity scale in counts per second (cps). Min-Max counts amount to: Mg (10-24 cps), Na (76-132 cps) Ca (7600-8650 cps), S (8.5-33)

As was visible in the fluorescence image (Fig. 1), the EPMA chemical maps show a similar layering pattern (Fig. 3). Areas rich in magnesium also show increased sodium and sulfur intensities whereas calcium intensities are lower.

As also visible in the fluorescence image (Fig. 1), the EPMA chemical maps show a layering pattern (Fig. 3). Highly fluorescent layers, that coincide with Mg and S maxima and Ca minima are variable in size ranging from 15 to 80 μm in thickness. Non-fluorescent layers that coincide with Mg and S minima and Ca maxima are more uniform in size, ranging from 12.5 to 30 μm in thickness. Mean composition of the fluorescent (fl) and non-fluorescent (nfl) layers, based on EPMA point measurements amount to: fl: $\text{Mg/Ca} = 3.8 \text{ mmol mol}^{-1} \pm 1.7 \text{ mmol mol}^{-1}$, $\text{Sr/Ca} = 7.4 \text{ mmol mol}^{-1} \pm 1.2 \text{ mmol mol}^{-1}$, $\text{Na/Ca} = 24.4 \text{ mmol mol}^{-1} \pm 5.4 \text{ mmol mol}^{-1}$, $\text{S/Ca} = 5.5 \text{ mmol mol}^{-1} \pm 2.7 \text{ mmol mol}^{-1}$; nfl: $\text{Mg/Ca} = 3.2 \text{ mmol mol}^{-1} \pm 1.8 \text{ mmol mol}^{-1}$, $\text{Sr/Ca} = 4.6 \text{ mmol mol}^{-1} \pm 1.9 \text{ mmol mol}^{-1}$, $\text{Na/Ca} = 26.6 \text{ mmol mol}^{-1} \pm 1.3 \text{ mmol mol}^{-1}$, $\text{S/Ca} = 2.3 \text{ mmol mol}^{-1} \pm 0.9 \text{ mmol mol}^{-1}$. Significant mean differences between fluorescent and non-fluorescent layers, based on Wilcoxon-Mann-Whitney test, are evident with regards to the S/Ca ($p < 0.001$) and Sr/Ca ratios ($p = 0.006$).

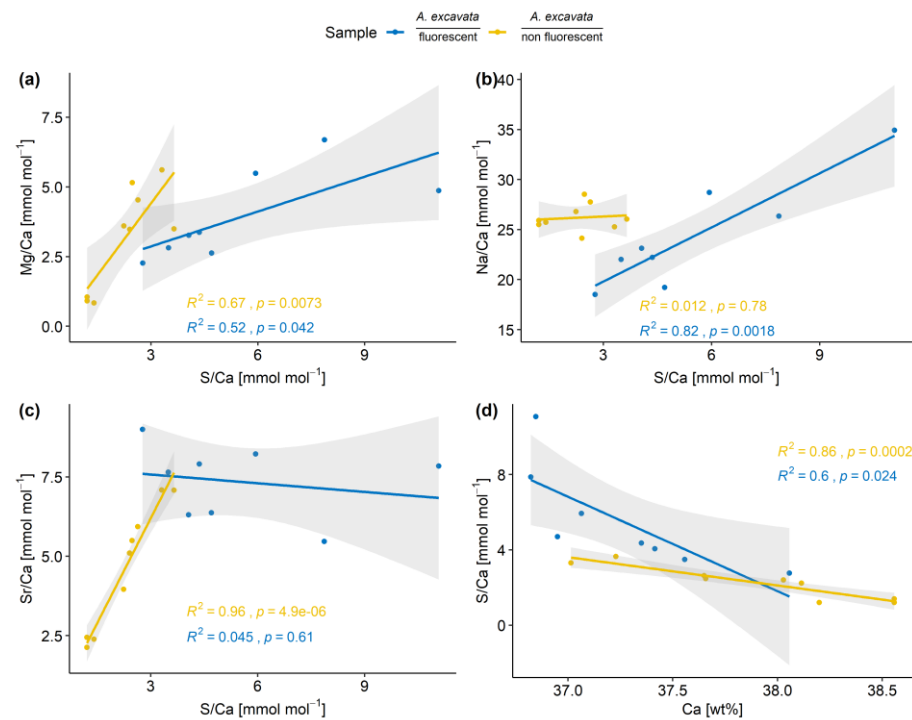
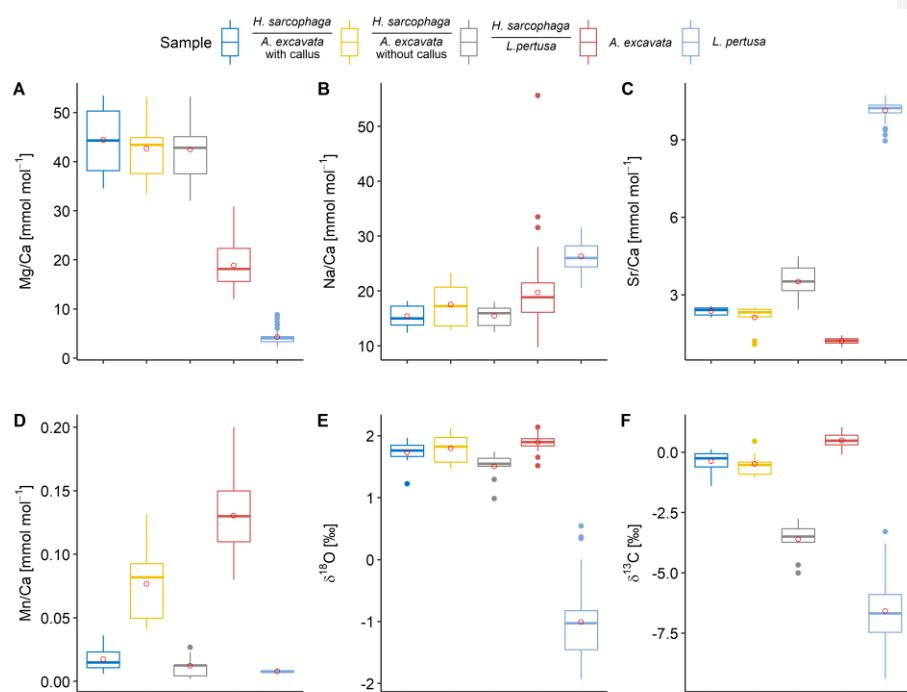


Figure 4 Elemental composition of the SRZ divided according to their fluorescence. Linear correlations are shown for both layers with 95% confidence intervals in gray.

Mg/Ca and S/Ca as well as Na/Ca and S/Ca display significant correlations in the fluorescent layers (Fig. 4). In the non-fluorescent shell layers, Mg/Ca and S/Ca, Sr/Ca and S/Ca are significantly correlated. In both layers, S/Ca ratios are inverse correlated with Ca wt% (Fig. 4).

3.5.3.4. Stable carbon and oxygen isotope



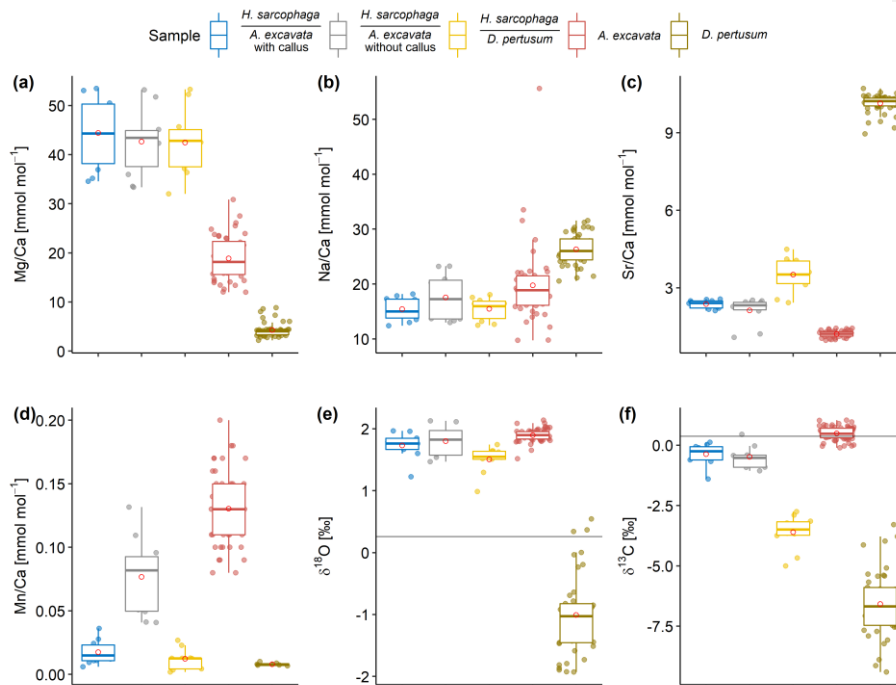


Figure 5 Box- and whisker plots displaying the E/Ca (ICP-OES and ICP-MS) and stable isotope measurements analysis (MS) of the investigated specimens. Boxes display the interquartile range and lines the median values. The whiskers show min and max values that are within the range of $Q1 - 1.5 \times IQR - Q3 + 1.5 \times IQR$. Red circles show mean values. Lines in E and F show the isotopic composition of the ambient seawater. Text below the horizontal lines in the legend is the host organism that *H. sarcophaga* grew on.

The different *H. sarcophaga* shells exhibit differences in their isotopic composition based on their host organism (Fig. 4 E/F). In particular, $\delta^{18}O$ values are similar in HL and HA with $+1.6451 \pm 0.22$ ‰ and $+1.80 \pm 0.25$ ‰, respectively. These values are in accordance with $\delta^{18}O$ values from the host organism *A. excavata*, which range from $+1.52$ ‰ to $+2.2$ ‰. *L. pertusa* $+1$ ‰. *D. pertusum* displays lower more depleted $\delta^{18}O$ and $\delta^{13}C$ values, ranging from -1.93 ‰ to $+0.54$ ‰ and -9.4041 ‰ to -3.2930 ‰.

Bigger Larger differences between the different *H. sarcophaga* samples, are observable in the carbon isotopic signature of specimens taken from different host organisms. HA display $\delta^{13}C$ values of -0.43 ± 0.47 ‰ which is close to the ratios of their host organism, being $+0.549 \pm 0.28$ ‰. HL are more depleted in heavy carbon isotopes with a measured value of -3.9761 ± 0.71 ‰. For reference, the isotopic composition of the ambient seawater is $\delta^{18}O = +0.26$ ‰ and $\delta^{13}C = +0.38$ ‰.

The isotopic composition of HAW and HAO can be described by linear functions whereas the isotopic composition in HL cannot:

417

$$\delta^{13}\text{C}_{\text{HAW}} = 1.8 \pm 0.4 \pm \delta^{18}\text{O} - 3.4 \pm 0.8 \text{ (} r^2 = 0.7, p = 0.004, \text{ df} = 7 \text{)}$$

[1]

418

$$\delta^{13}\text{C}_{\text{HAO}} = 1.1 \pm 0.3 \pm \delta^{18}\text{O} - 2.6 \pm 0.6 \text{ (} r^2 = 0.6, p = 0.02, \text{ df} = 6 \text{)}$$

[2]

419

$$\delta^{13}\text{C}_{\text{HL}} = 1.7 \pm 1.0 \pm \delta^{18}\text{O} - 6.2 \pm 1.5 \text{ (} r^2 = 0.18, p = 0.12, \text{ df} = 8 \text{)}$$

[3]

420

3.6.3.5. ICP-OES results from *H. sarcophaga* grown on different host organisms

421

H. sarcophaga samples from different host organisms are similar in their chemical composition with regard to Mg/Ca and Na/Ca (Fig. 45 A/B). Mean Mg/Ca ratios range from 42.47 ± 6.8 to 44.4 ~~mmol mol⁻¹~~ ^{mmol mol⁻¹}, with intra-individual variations of 6.8 ± 7.2 mmol mol⁻¹ (SD). Both host organisms have lower mean Mg/Ca ratios of 4.23 ± 1.5 mmol mol⁻¹ and 18.9 ± 4.5 mmol mol⁻¹ in *L. pertusa* *D. pertusum* and *A. excavata*, respectively.

422

423

424

425

426

Mean Na/Ca ratios range between 15.5 ~~16.4 ± 2.1 to 17.6 ± 4.3~~ mmol mol⁻¹ for *H. sarcophaga*. The highest Na/Ca ratios and variations are measured in HAO. *L. pertusa* *D. pertusum* displays overall higher Na/Ca ratios than *H. sarcophaga* (25.6 ~~26.3 ± 2.8~~ mmol mol⁻¹). The highest variation is measured in *A. excavata* ranging from 9.8 ~~to~~ 55.6 mmol mol⁻¹ with a mean of 19.8 ± 7.3 mmol mol⁻¹.

427

428

429

430

A clear difference in Sr/Ca of 1.1 ± 0.16 ~~(2SD of MACS3)~~ mmol mol⁻¹ is evident between *H. sarcophaga* from the different host organisms (Fig. 45 C). HAW and HAO show mean Sr/Ca ratios of 2.3 ~~74 ± 0.2~~ and 2.3 ~~61 ± 0.5~~ mmol mol⁻¹, respectively. The host organism *A. excavata* has lower Sr/Ca ratios (1.2 ± 0.1 mmol mol⁻¹). On the contrary, HL and *L. pertusa* *D. pertusum*, display higher mean Sr/Ca ratios of 3.5 ± 0.7 and 10.2 ~~13 ± 0.3~~ mmol mol⁻¹ respectively.

431

432

433

434

435

Prominent differences between *H. sarcophaga* groups are also evident in their Mn/Ca ratios (Fig. 45 D). HAW, HL and *L. pertusa* *D. pertusum* display Mn/Ca ratios of 0.0 ~~10~~ 0.017 ± 0.01 mmol mol⁻¹, 0.012 ± 0.008 mmol mol⁻¹ and 0.008 ± 0.001 mmol mol⁻¹, whereas HAO and *A. excavata* show higher Mn/Ca ratios of 0.0 ~~66~~ 0.077 ± 0.03 mmol mol⁻¹ and 0.13 ± 0.03 mmol mol⁻¹, respectively.

436

437

438

439

3.7.3.6. Compositional differences in *H. sarcophaga* related to their host organism

440

Table 42 Results of the one-way ANOVA and Kruskal-Wallis analysis with the host organism as predictor variable. Bold fields show elemental and isotopic ratios in *H. sarcophaga* that may be significantly influenced by the chemistry of the host organism. *p*-values are Bonferroni adjusted.

441

442

ANOVA						
	Mg/Ca	Na/Ca	Sr/Ca	Mn/Ca	δ ¹⁸ O	δ ¹³ C
DFn	2					
DFd	25					
F	0.2	0.22	23	32	4.1	97
p	0.82	0.8	<0.001	<0.001	0.029	<0.001
Generalized eta squared	0.015	0.018	0.65	0.74	0.26	0.89
Kruskal-Wallis test						
n	28					

Formatiert: Nicht Hochgestellt/ Tiefgestellt

df	2					
p	0.83	0.92	<0.001	<0.001	0.03	<0.001

We conducted a one-way ANOVA and Kruskal-Wallis test (Table 4.2) in order to explore if the investigated *H. sarcophaga* groups (HAW, HAO, HL) show significant differences in their geochemical composition related to their host organism. We used the measured elemental- and isotopic composition as target ~~variable~~variables and the host organisms (*A. excavata* with callus, *A. excavata* without callus, ~~*L. pertusa*~~*D. pertusum*) as the factor variable. Tukey-HSD (Table 2.3) was used as post-hoc test to investigate group specific mean differences.

Table 2.3 Tukey-HSD test results. Bold fields show significant differences between the two groups. *HAW* = *H. sarcophaga* that infested *A. excavata* with callus formation, *HAO* = *H. sarcophaga* that infested *A. excavata* without callus formation, *HL* = *H. sarcophaga* that infested *D. pertusum*. *p*-values are Bonferroni adjusted.

Tukey-HSD test				
	Group 1	Group 2	Difference	p
Mg/Ca	HAW	HAO	-1.22	0.93
	HAW	HL	-1.95	0.81
	HAO	HL	-0.73	0.97
Na/Ca	HAW	HAO	0.74	0.81
	HAW	HL	0.05	0.99
	HAO	HL	-0.68	0.84
Sr/Ca	HAW	HAO	-0.004	1
	HAW	HL	1.14	<0.001
	HAO	HL	1.14	<0.001
Mn/Ca	HAW	HAO	0.05	<0.001
	HAW	HL	-0.005	0.75
	HAO	HL	-0.05	<0.001
$\delta^{18}\text{O}$	HAW	HAO	0.07	0.81
	HAW	HL	-0.23	0.11
	HAO	HL	-0.30	0.032
$\delta^{13}\text{C}$	HAW	HAO	-0.11	0.91
	HAW	HL	-3.24	<0.001
	HAO	HL	-3.12	<0.001

Formatiert: Schriftart: Fett

Formatiert: Schriftart: Fett

Formatiert: Schriftart: Fett

Formatiert: Schriftart: Fett

Formatiert: Schriftart: Fett

Formatiert: Schriftart: Fett

Formatiert: Schriftart: Fett

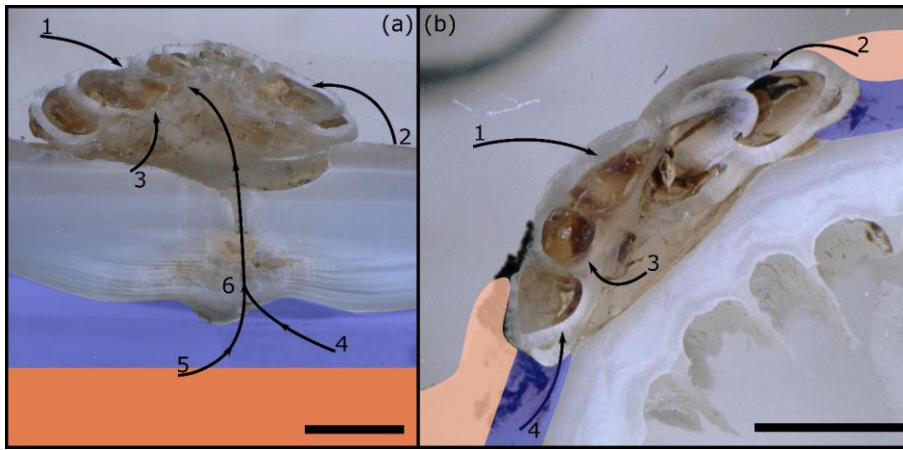
The one-way ANOVA reveals no significant ~~difference~~ in the Mg/Ca and Na/Ca ratios of the foraminifera that were collected from the different host organisms (Table 4.2). In contrast, the ANOVA suggests a significant difference between Sr/Ca and Mn/Ca ratios between these two groups. In the case of Sr/Ca, significant differences based on the Tukey-HSD post-hoc test are observable between HL and HA, whereas we find no significant differences between HAW and HAO. In addition, we observe no significant differences between HAW and HL in their Mn/Ca composition, but significant differences are present between both these groups and HAO.

461 In the case of the stable oxygen isotope composition, we observe significant differences between *H.*
462 *sarcophaga* specimens from different host organisms. The $\delta^{18}\text{O}$ -ratio measured in HL is significantly
463 lower than in HAO. Significant differences are also observable for $\delta^{13}\text{C}$ ratios. Here, differences in the
464 isotopic composition are detectable between HL and HA, with the latter showing higher $\delta^{13}\text{C}$ ratio.

465 The Kruskal-Wallis test, which was used as a non-parametric cross validation for the ANOVA test, shows
466 the same results as the ANOVA test

467 4. Discussion

468 4.1. Mechanisms of etching and boring



470 4.1.1.1. Figure 6 Sr/Ca differences in *H. sarcophaga* related to the host organism

471 We observe significant differences in the Sr/Ca and Mn/Ca composition between *H. sarcophaga* from
472 different host organisms.

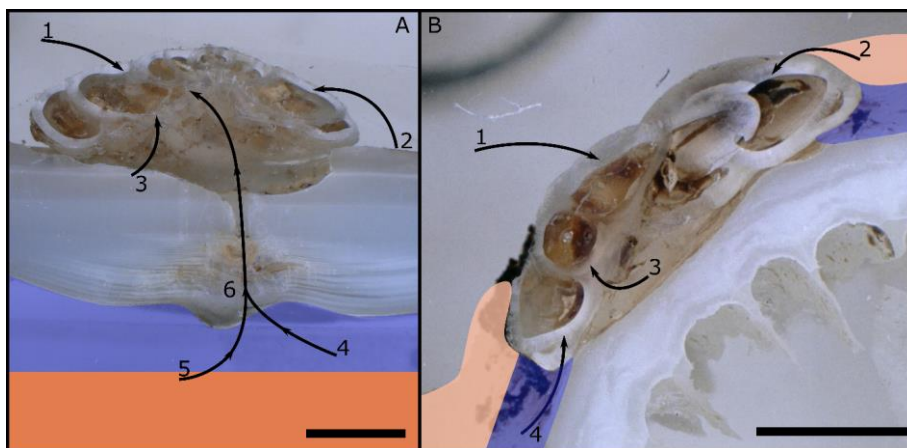


Figure 5 Possible pathways of E/Ca and isotopic signals into the foraminiferal calcite. A: *H. sarcophaga* on *A. excavata*, B: *H. sarcophaga* on *L. pertusa*. Blue areas represent the calcifying space, orange areas represent mantle tissue in *A. excavata* (A) and organic layer (coenosarc/mucus) in *L. pertusa* (B). Uptake of seawater and free-floating particles (1), Ingestion of host organic material (periostracum, coral tissue/mucus) (2), Ingestion of dissolved carbonate material (3), Ingestion of extracellular calcifying fluid (ECF) (4), Ingestion of Mantle tissue (5), ingestion of carbonate and organic material from the deposited callus (6). Scalebar is 100 μ m. Please note that the calcifying space and organic layers are displayed enlarged for improved visibility. Actual size of the calcifying space amounts to 1–100 nm (Nakahara, 1991; Tambutté et al., 2007). The organic layer (coenosarc) is \sim 25 μ m in thickness (Tambutté et al., 2007).

Possible pathways of E/Ca and isotopic signals into the foraminiferal calcite. A: *H. sarcophaga* on *A. excavata*, B: *H. sarcophaga* on *D. pertusum*. Blue areas represent the calcifying space, orange areas represent mantle tissue in *A. excavata* (A) and organic layer (coenosarc/mucus) in *D. pertusum* (B). Uptake of seawater and free-floating particles (1), Ingestion of host organic material (periostracum, coral tissue/mucus) (2), Ingestion of dissolved carbonate material (3), Ingestion of extracellular calcifying fluid (ECF) (4), Ingestion of Mantle tissue (5), ingestion of carbonate and organic material from the deposited callus (6). Scalebar is 100 μ m. Please note that the calcifying space and organic layers are displayed enlarged for improved visibility. Actual size of the calcifying space amounts to 1–100 nm (Nakahara, 1991; Tambutté et al., 2007). The organic layer (coenosarc) is \sim 25 μ m in thickness (Tambutté et al., 2007).

The boring and etching of *H. sarcophaga* in *A. excavata* and *D. pertusum* can serve multiple purposes. The attachment etchings of foraminifera have been proposed to serve as an anchoring function and increase protection from predators and the hydrodynamic regime. Possibly, the foraminifera also dissolve the host's carbonate material to satisfy the calcium and/or DIC requirements of *H. sarcophaga* for the calcification of its shell (Cedhagen, 1994; Vénec-Peyré, 1996; Todd, 1965), rather than expending further energy to source Ca/DIC from the surrounding seawater (Fig 6A).

The boring in *A. excavata* is presumably produced to access the softbody of the bivalve, indicated by the mantle damage in the vicinity of the boring (Cedhagen, 1994). Additionally, the foraminifera may benefit from ingesting the ECF of the bivalve, containing carbohydrates, proteins, glycoproteins and amino acids therefore constituting a valuable nutrient source (Yin et al., 2005). The ECF is also enriched in Ca and CO₂ compared to the ambient seawater, maybe providing additional ions for the calcification of *H. sarcophaga* (Crenshaw, 1972). Feeding on mantle fluids of bivalves by parasitic foraminifera is also supported by tracer experiments on *C. refulgens* (Alexander and Delaca, 1987). With *D. pertusum*

as host, the foraminifera can access the coenosarc and underlying calcifying space of the coral without having to bore through the carbonate skeleton (Fig. 6B).

H. sarcophaga probably uses chemical etching, as indicated by the xenoglyph surface texture of the trace that changes in correlation with the host's microstructure (Beuck et al., 2008; Todd, 1965). A possible mechanism was investigated in the non-symbiotic benthic foraminifera *Ammonia* sp., which uses H⁺-ATPase to actively pump H⁺-ions out of their protoplasm to facilitate calcification (Toyofuku et al., 2017). This proton-flux causes a pH decrease by up to 1.1 in a 100 µm wide zone around the foraminifera (Toyofuku et al., 2017). Similar effects are reported from excavating sponges. *Cliona* varians displays pH values as low as 5 in their filopodia during carbonate dissolution (Webb et al., 2019).

4.2. Sr/Ca differences in *H. sarcophaga* related to the host organism

We observe significant differences in the Sr/Ca and Mn/Ca composition between *H. sarcophaga* from different host organisms.

HL show significantly higher Sr/Ca ratios than HA. Given that this result is based on measurements from multiple individuals distributed across more than one host organism, we suggest that this is most likely a signal of the high Sr/Ca aragonite precipitated from *L. pertusa* that is imprinted into the test of *H. sarcophaga*. In both host organisms, *H. sarcophaga* produces an attachment etching on the host (Fig. 3) to firmly anchor itself (Bromley and Heinberg, 2006). It subsequently penetrates the host shell in order with their pseudopodia to access the hosts soft tissue (Beuck et al., 2008). The attachment etching may additionally serve to satisfy the calcium requirements of *H. sarcophaga* for the calcification of its shell (Cedhagen, 1994), rather than expending further energy to source Ca from the surrounding seawater. By chemically corroding the attachment etching as well as by the penetrating boring and by taking up the resulting solutions, the foraminifer gains access to a pre-concentrated calcium carbonate solution from which it can precipitate its shell (Fig. 5). Naturally, the foraminifer would also reflect other characteristics of the host, such as the high Sr/Ca ratio from the aragonite of *L. pertusa* (Raddatz et al., 2013; Schleinkofer et al., 2019). In agreement with the much lower Sr/Ca ratios in calcite and aragonite in *A. excavata* (Schleinkofer et al., 2021) compared to the coralline aragonite, we do not observe such high Sr/Ca ratios in HA. Still, the observed Sr/Ca ratios in HA are higher by a factor of two than in the host organism. Since we do not observe differences between HAW and HAO, the Sr/Ca surplus cannot be derived from the ingestion of organic material from within the shell cavity. A further control is likely provided through the mixture of dissolved host CaCO₃ material

~~and ambient seawater from which the foraminifer calcifies, which is explored further in the next section.~~

HL show significantly higher Sr/Ca ratios than HA. Given that this result is based on measurements from multiple individuals distributed across more than one host organism, we suggest that this is most likely a signal of the high Sr/Ca aragonite precipitated from *D. pertusum* that is imprinted into the test of *H. sarcophaga*. By chemically corroding the attachment etching as well as by the penetrating boring and by taking up the resulting solutions, the foraminifera gains access to a pre-concentrated calcium carbonate solution from which it can precipitate its shell (Fig. 6). Naturally, the foraminifera would also reflect other characteristics of the host, such as the high Sr/Ca ratio from the aragonite of *D. pertusum* (Raddatz et al., 2013; Schleinkofer et al., 2019). In agreement with the much lower Sr/Ca ratios in calcite and aragonite in *A. excavata* (Schleinkofer et al., 2021) compared to the coralline aragonite, we do not observe such high Sr/Ca ratios in HA. Still, the observed Sr/Ca ratios in HA are higher by a factor of two than in the host organism. Since we do not observe differences between HAW and HAO, the Sr/Ca surplus cannot be derived from the ingestion of organic material from within the shell cavity. We hypothesize that a possible further control is likely provided through the mixture of dissolved host CaCO₃ material and ambient seawater from which the foraminifera calcify, which is explored in more detail in the next section.

4.2.4.3. Mixing model

In order to further investigate ~~underlying mechanisms of~~ the observed results, we created a simple two-component model to explore how the trace-element chemistry of *H. sarcophaga* could change by delivery of ions to the calcification site that were derived from dissolution of the host organism. In this model we calculate changes of the foraminifera composition in dependence from an assumed calcification from a variable mixture of seawater and dissolved host carbonate material. We excluded the addition of the hosts calcifying fluid in the model because there is no data available for the chemical composition of the calcifying fluid of ~~*L. pertusa*~~*D. pertusum* nor *A. excavata*, and because the model is intended only as an initial exploration of whether the geochemistry of *H. sarcophaga* can be explained ~~in this way by calcification from a mixture of seawater and dissolved host material.~~ Furthermore, measurements of the chemical composition of the calcifying fluid of other bivalve species indicate that the composition is close to the composition of seawater ~~(Crenshaw, 1972; Wada and Fujinuki, 1974).~~(Wada and Fujinuki, 1976; Crenshaw, 1972).

The model calculates element/Ca ratios based on calcite precipitation from a fluid that is derived from a mix of seawater (transported to the calcification site, see e.g. ~~(Erez, 2003))~~, (Erez, 2003)), and CaCO₃ dissolved from the host organism:

$$\frac{\frac{E}{Ca_{Hyrrokkin}}}{\frac{E}{Ca_{Hyrrokkin}}} = \frac{E_{SW} + \frac{10^R}{M_{Carb}} \frac{E}{Ca_{Host}}}{Ca_{SW} + \frac{10^R}{M_{Carb}}} * D_E * 1000 \quad [4]$$

570 Where E_{SW} = element concentration in seawater, E/Ca_{Host} = element/Ca in host carbonate [mmol mol⁻¹]
571 ¹], Ca_{SW} = Calcium concentration in seawater (~~10 mmol~~**0.010 mol** L⁻¹), D_e = Calcite-Water distribution
572 coefficient, M_{carb} = atomic mass of CaCO₃ (100.08 g mol⁻¹) and R = log mixing ratio between carbonate
573 and seawater [g L⁻¹].

Table 34 Parameters used in the proposed model to explore the effects of carbonate and water uptake of *H. sarcophaga* on the shell chemistry. Host element/Ca ratios are derived from this study. D_E^{-1} & D_E^{-2} = Distribution coefficient

Model parameters				
	E_{sw} [mmol mol ⁻¹ L ⁻¹]	E/Ca_{Acesta} [mmol mol ⁻¹]	$E/Ca_{Lophelia}$ $Ca_{Desmophyllum}$ [mmol mol ⁻¹]	
Mg/Ca	530.053	19	4.2	0.015 (Segev and Erez, 2006) 0.015 (Segev and Erez, 2006) 0.009 (Oomori et al., 1987)
Na/Ca	0.450	20	26	0.0016 (Allen et al., 2016) 0.00028 (Evans et al., 2015) 0.0001 (Füger et al., 2019)
Sr/Ca	0.10001	1.2	10.1	0.28 (Raitzsch et al., 2010) 0.16 (Raitzsch et al., 2010) 0.2 (Mucci and Morse, 1983; Evans et al., 2015)
Mn/Ca	5*10⁻⁶⁹	0.131	0.008	13 (Mucci, 1988) 0.5 (van Dijk et al., 2020) 10 (Mucci, 1988)

576

577 As we have no information about the amount of dissolved material and water that is taken up by *H.*

578 *sarcophaga*, we modelled it over eight~~six~~ orders of magnitude (log dissolved CaCO_3 /seawater ratios of

579 -4 to +4). ~~This corresponds to a range from 99.99 % seawater and 0.01 % host CaCO_3 contribution to~~

580 ~~0.01 % seawater and 99.99 % host CaCO_3 contribution.~~2). The parameters used are reported in Table

581 34.

Eingefügte Zellen

Formatierte Tabelle

Formatiert: Hochgestellt

Formatiert: Zentriert

Formatiert: Zentriert

Formatiert: Zentriert

Formatiert: Zentriert

Formatiert: Zentriert

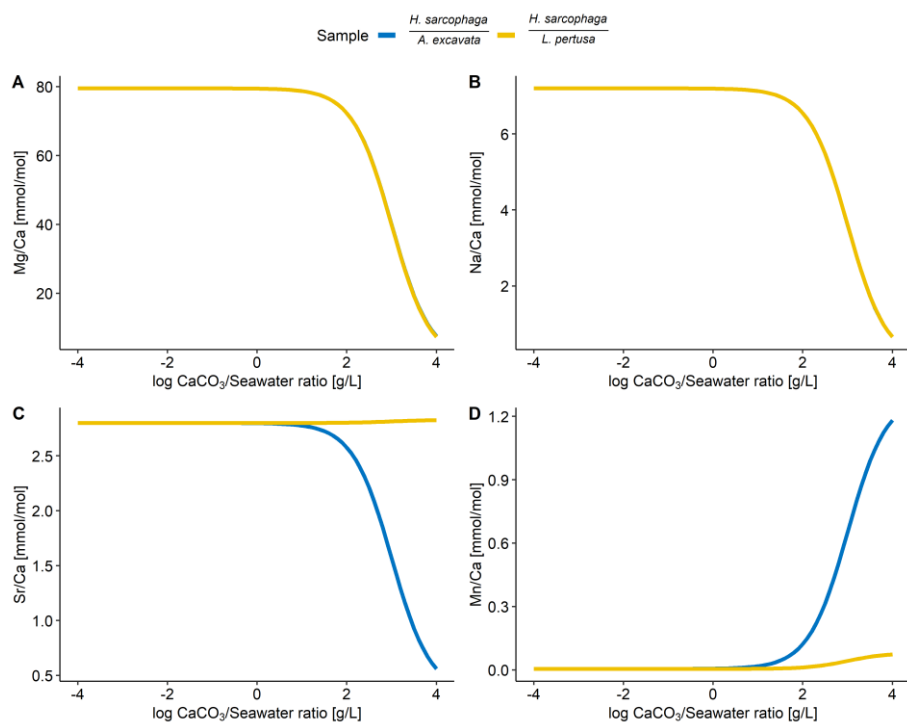
Formatiert: Zentriert

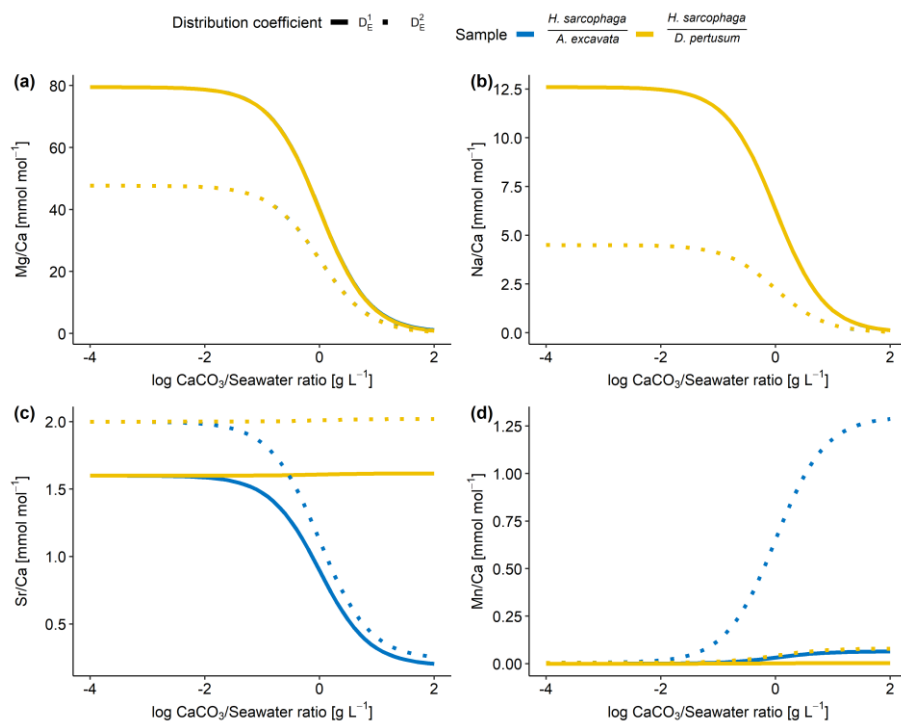
Formatiert: Zentriert

Formatiert: Zentriert

Formatiert: Zentriert

Formatiert: Schriftart: Kursiv





585 Figure 7 Results of model calculations with the ~~aforementioned~~ parameters ~~listed in Tab. 4~~ for the measured E/Ca ratios. ~~Text~~
 586 ~~below the horizontal lines in the legend is the host organism that *H. sarcophaga* grew on.~~ Independently of the mixing ratio
 587 of dissolved host CaCO₃ and ambient water, no differences of the geochemical signature is predictable in Mg/Ca and Na/Ca.
 588 On the contrary, Sr/Ca and Mn/Ca ratios are predicted to diverge at mixing ratios > 10 g CaCO₃/L seawater. ~~0.01 g CaCO₃ L⁻¹~~
 589 ~~seawater. Solid lines are produced with D_E¹ for the calculation and dotted lines are produced with D_E² for the calculation (see~~
 590 ~~Tab. 4). In panel a and b, the different samples overlap each other.~~

591 Based on the ~~proposed model, we can see that shown in Fig. 7,~~ the Mg/Ca and Na/Ca ratios in *H.*
 592 *sarcophaga* are independent of the geochemical signature of the host it lived on, ~~which is in~~
 593 ~~agreement with our measurements.~~ This is caused by the high concentration of these elements in the
 594 ambient seawater in comparison to the host's carbonate. The composition of the mixture is largely
 595 controlled by the addition of Ca, which is equal for both host organisms.

596 In contrast, the model predicts that, at high ratios of CaCO₃ derived from the host compared to the
 597 surrounding seawater, different Sr/Ca and Mn/Ca ratios should be observed between foraminifera
 598 living on different host organisms. ~~The modelled Sr/Ca ratios for HL are constant at 2.8 mmol mol⁻¹~~
 599 ~~independent from the mixing ratio (Fig. 6C). This is because when the foraminifera dissolves aragonitic~~
 600 ~~material of *L. pertusa* and mixes it with seawater, the resulting Sr/Ca ratios in this solution do not~~
 601 ~~change due to the aragonitic D_s being close to 1. Consequently, if the shell Sr/Ca ratio in *H. sarcophaga*~~

depends on calcite D_{Sr} and the Sr/Ca ratio in the calcifying fluid of *H. sarcophaga*, the resulting Sr/Ca ratio in HL is equivalent to a specimen that calcifies solely from seawater (specimen without a host). As the calcitic D_{Sr} is below 1 (Mucci and Morse, 1983; Raitzsch et al., 2010), the addition of dissolved material from *A. excavata* in the calcifying space results in decreasing Sr/Ca ratios in the calcifying fluid and consequently lower Sr/Ca ratios in the precipitated calcite of the foraminifera. The modelled Sr/Ca ratios for HL are constant at $2.0 \text{ mmol mol}^{-1}$ independent from the mixing ratio (Fig. 7C). When the foraminifera dissolves aragonitic material of *D. pertusum* and this material is mixed with seawater, the resulting Sr/Ca ratios in this solution do not change due to the aragonitic D_{Sr} being close to 1. Consequently, if the shell Sr/Ca ratio in *H. sarcophaga* depends on calcite D_{Sr} and the Sr/Ca ratio in the calcifying fluid of *H. sarcophaga*, the resulting Sr/Ca ratio in HL is equivalent to a specimen that calcifies solely from seawater (specimen without a host). As the calcitic D_{Sr} is below 1 (Raitzsch et al., 2010; Mucci and Morse, 1983; Evans et al., 2015), the addition of dissolved material from *A. excavata* in the calcifying space results in decreasing Sr/Ca ratios in the calcifying fluid and lower Sr/Ca ratios in the precipitated calcite of the foraminifera. Similar results are obtained in the case of Mn/Ca ratios. The addition of dissolved host material to the calcifying space of *H. sarcophaga* results in an increase of the Mn/Ca ratio in the calcifying fluid, which leads to increasing Mn/Ca ratios in the foraminiferal calcite.

~~While the proposed model can explain why we do not see changes in the Mg/Ca and Na/Ca composition of *H. sarcophaga* from different host organisms, and can also explain why Sr/Ca ratios differ between these groups (Fig. 2) it cannot explain the occurring processes entirely. The model can only predict Na/Ca ratios up to 7 mmol mol^{-1} (Fig. 6B), whereas we measure ratios of 15 mmol mol^{-1} . As already mentioned, this is a simplified model that disregards possible influences of other reservoirs such as the calcifying fluid of the bivalve that might also form part of the calcifying fluid of *H. sarcophaga*. Additionally, the distribution coefficients used in this model are not empirically determined on *H. sarcophaga* but derive from other benthic foraminifera (Mg/Ca, Na/Ca, Sr/Ca) or inorganic precipitation experiments (Mn/Ca), and the model also does not account for growth rate driven differences in trace element partitioning, which are especially relevant in the case of Na and Mn (Füger et al., 2019; Mucci, 1988).~~

The proposed model can help us understand why we do not see changes in the Mg/Ca and Na/Ca composition of *H. sarcophaga* from different host organisms and why Sr/Ca and Mn/Ca ratios differ between these groups (Fig. 2). Nonetheless, other processes are clearly required to explain the details of trace element uptake in *H. sarcophaga*. Sr/Ca ratios in HL, for instance, can only be modelled up to 2 mmol mol^{-1} , whereas we measure a mean of $3.5 \text{ mmol mol}^{-1}$. The results of this model are largely driven by the distribution coefficients used, however, the distribution coefficients used in this model

are not empirically determined on *H. sarcophaga* but derive from other foraminifera species (D_e^1) or inorganic precipitation experiments (D_e^2). The model does also not account for growth-rate driven differences in trace element partitioning, while this is especially relevant in the case of Na and Mn (Mucci, 1988; Föger et al., 2019). In addition, we have to consider lattice strain-effects that increase the distribution coefficient for other elements such as Sr and Na, as *H. sarcophaga* has relatively high concentrations of Mg (Evans et al., 2015; Mucci and Morse, 1983).

As discussed above, this is a simplified model that uses seawater and dissolved carbonate as endmembers. An additional possibility is that the foraminifera pumps or channels ions into and out of the calcifying fluid. In particular, it has been suggested foraminifera are able to transport Mg out of the calcifying space (Nehrke et al., 2013; Toyofuku et al., 2017; Bentov and Erez, 2006), but intermediate and high-Mg foraminifera such as *A. lessonii* appear to exert a lower degree of control over the composition of their calcifying fluid compared to low-Mg species (Evans et al., 2018; Geerken et al., 2018). Assuming the calcifying fluid is depleted in Mg in comparison to seawater, the model would predict lower Mg/Ca ratios, although importantly, it would still not predict a difference in the Mg/Ca ratios of *H. sarcophaga* influenced by the host organism.

Another factor that should be considered is the transport pathway of the dissolved material into the foraminifera's calcifying fluid. The dissolution process of the host organism could modify the chemistry of the ambient seawater in a limited area around the foraminifera (Toyofuku et al., 2017), although this process is hard to imagine in an environment (cold-water coral reef) that relies on constant water movement to provide nutrients to the main inhabitants (Mienis et al., 2007). As such, we suggest it is more likely, that the dissolved material is transported through the cytoplasm to the calcification site (Spero, 1988; Erez, 2003), although further work is required to confirm this.

4.3.4.4. Mn/Ca differences in *H. sarcophaga* related to the host organism

Based on the ANOVA analysis (Table 1), significant differences are also observable in the Mn/Ca ratios. HAO display four times higher Mn/Ca ratios than in the other two observed groups. HL show similar Mn/Ca ratios as their host organism, both HAW and HAO show lower Mn/Ca ratios. Based on the differences, we observe between the samples that were picked from *A. excavata*, it is unlikely that the Mn/Ca signal in *H. sarcophaga* derives from the host shell material (Fig. 5/A3 & B3). In this case we would expect to see differences between HA and HL as Mn/Ca in *A. excavata* is approximately one order of magnitude higher than in *L. pertusa*. Influences of the surrounding water cannot explain the observed differences either. Manganese, as a redox-sensitive element, is controlled by the oxygen concentration of the ambient water. Under well-oxygenated conditions, the main species Mn^{2+} is oxidized to Mn-oxyhydroxides and precipitated (Calvert and Pedersen, 1993, 1996). Low-oxygen

conditions lead to a reduction of Mn-oxhydroxides to the bioavailable Mn^{2+} and an consequent increase of Mn/Ca ratios in biogenic carbonates (Groeneveld and Filipsson, 2013; Koho et al., 2015; Tribouillard et al., 2006). However, the Leksa Reef is well oxygenated (Jacobson, 1983; Milzer et al., 2013).

An influence of the calcification rate on Mn/Ca ratio was shown in inorganic precipitated calcite overgrowths and the planktic foraminifer *Orbulina universa* (Holland et al., 2017; Lorens, 1981; Mucci, 1988). Generally speaking, increased calcification rates cause Mn/Ca ratios in the precipitates to decrease (Holland et al., 2017; Mucci, 1988). In our investigated samples, this effect would imply lower calcification rates in HAO compared to HAW and HL. The possibility of HAO having low calcification rates is likely, as it is missing its primary nutrient source. Due to the high distribution coefficient of manganese, Rayleigh fractionation, might add an additional control on Mn/Ca ratios in the foraminifera shell (Holland et al., 2017). The model of Rayleigh fractionation relies on a number of assumptions about the internal reservoir of the foraminifera concerning size, initial composition, refreshment rate and calcification rate (Elderfield, 1996). As these parameters are not fully understood we cannot provide further information about the possible influence.

A significant influence of possibly Mn-enriched bodily fluids of bivalves (Wada and Fujinuki, 1974) can also not explain the differences in the chemical composition as the samples that discern from the others are picked from HAO. These foraminifera did not have access to the internal organic material of the bivalve (Fig. 5/A4). Instead, the high Mn signal in HAO must derive from a source that is located on the outside of the bivalve host (Fig. 5/A2). When the foraminifera initially infests the bivalve and starts boring into the shell, nutrient sources other than the internal organic parts of the bivalve have to be utilised by *H. sarcophaga*. The organic periostracum of the bivalve could depict this nutrient source as it is a highly nutritional source for organic material on the outside of the bivalves shell (Secor et al., 1993). High concentrations of Mn and Fe were measured in the periostracum of freshwater and marine bivalves (Allen, 1960; Swinehart and Smith, 1979). The mechanistic explanation for this enrichment of Mn and Fe is reported to be the high amount of the amino acids containing glycine and tyrosin in the periostracum of bivalves (Hare, 1965; Whitney et al., 2019), which act as complexing sites for metal ions (Swinehart and Smith, 1979). The existence of living *H. sarcophaga* attached to rocks demonstrates that they do not necessarily rely on a living host but can also supply themselves through other feeding strategies (Cedhagen, 1994). Since algae take up Mn and concentrate it internally (Sunda and Huntsman, 1985), the increased Mn/Ca in HAO could also be caused by an facultative suspension feeding mode of *H. sarcophaga* during its early ontogeny.

Based on the ANOVA analysis (Table 2), significant differences are also observable in the Mn/Ca ratios. HAO display four times higher Mn/Ca ratios then in the other two observed groups. HL show similar

Mn/Ca ratios as their host organism, both HAW and HAO show lower Mn/Ca ratios. Based on the differences we observe between the samples that were picked from *A. excavata*, it is unlikely that the Mn/Ca signal in *H. sarcophaga* derives from the host shell material (Fig. 6/A3 & B3). In this case we would expect to see differences between HA and HL as Mn/Ca in *A. excavata* is approximately one order of magnitude higher than in *D. pertusum*. Influences of the surrounding water cannot explain the observed differences either. Manganese, as a redox-sensitive element, is controlled by the oxygen concentration of the ambient water. Under well oxygenated conditions, the main species Mn^{2+} is oxidized to Mn-oxyhydroxides and precipitated (Calvert and Pedersen, 1996, 1993). Low-oxygen conditions lead to a reduction of Mn-oxyhydroxides to the bioavailable Mn^{2+} and a consequent increase of Mn/Ca ratios in biogenic carbonates (Tribovillard et al., 2006; Groeneveld and Filipsson, 2013; Koho et al., 2015). The Leksa Reef, however, is well oxygenated (Milzer et al., 2013; Jacobson, 1983).

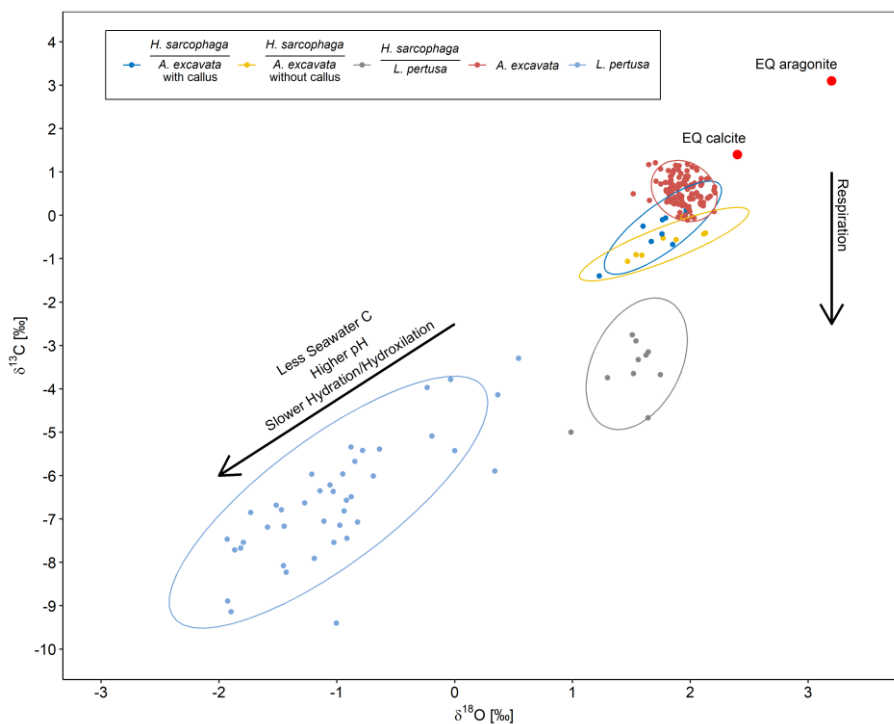
An influence of the precipitation rate on Mn/Ca ratio was shown in inorganically precipitated calcite overgrowths and the planktic foraminifera *Orbulina universa* (Mucci, 1988; Lorens, 1981; Holland et al., 2017). Generally speaking, increased calcification rates cause Mn/Ca ratios in the precipitates to decrease (Mucci, 1988; Holland et al., 2017). In our investigated samples, this effect would imply lower calcification rates in HAO compared to HAW and HL. The possibility of HAO having low calcification rates is likely, as it is missing a valuable nutrient source (Fig. 6). Due to the high distribution coefficient of manganese, Rayleigh fractionation might add an additional control on Mn/Ca ratios in the foraminifera shell (Holland et al., 2017). The model of Rayleigh fractionation relies on a number of assumptions about the internal reservoir of the foraminifera regarding the size, initial composition, refreshment rate and calcification rate (Elderfield, 1996). As these parameters are not fully understood, both for *H. sarcophaga* and foraminifera in general, we cannot provide further information about the possible influence.

A significant influence of the potentially Mn-enriched bodily fluids of bivalves (Wada and Fujinuki, 1976) also cannot explain the differences in the chemical composition as the samples that discern from the others are picked from HAO. These foraminifera did not have access to the internal organic material of the bivalve (Fig. 6/A4). Instead, the high Mn signal in HAO must derive from a source that is located on the outside of the bivalve host (Fig. 6/A2). When the foraminifera initially infests the bivalve and starts boring into the shell, nutrient sources other than the internal organic parts of the bivalve have to be utilised by *H. sarcophaga*. The organic periostracum of the bivalve could depict this nutrient source as it is a highly nutritional source for organic material on the outside of the bivalve's shell (Secor et al., 1993). High concentrations of Mn and Fe were measured in the periostracum of freshwater and marine bivalves (Swinehart and Smith, 1979; Allen, 1960). The mechanistic explanation

for this enrichment of Mn and Fe is reported to be the high amount of the amino acids containing glycine and tyrosine in the periostracum of bivalves (Piez, 1961; Whitney et al., 2019), which act as complexing sites for metal ions (Swinehart and Smith, 1979). The existence of living *H. sarcophaga* attached to rocks demonstrates that they do not necessarily rely on a living host but can also supply themselves through other feeding strategies (Cedhagen, 1994). Since algae take up Mn and concentrate it internally (Sunda and Huntsman, 1985), the increased Mn/Ca in HAO could also be caused by a facultative suspension feeding mode of *H. sarcophaga* during its juvenile stage.

At this point we can only speculate about the mechanistic explanation for the enrichment of Mn/Ca in HAO. Future research on *H. sarcophaga* should involve spatially resolved Mn and Fe measurements, to explore if there is an ontogenetic decrease of Mn/Ca ratios in the test of *H. sarcophaga* picked from *A. excavata*. This decrease would mark the time of the first penetration of the bivalve shell.

4.4.4.5. Carbonate isotopic composition in *H. sarcophaga* based on the host organism



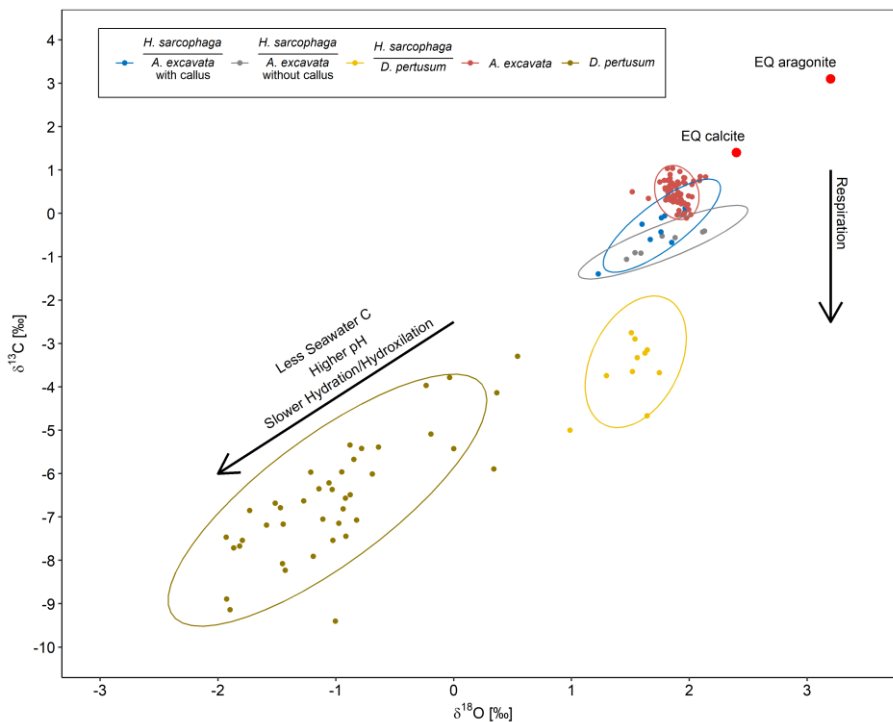


Figure 8 $\delta^{18}\text{O}$ plotted against $\delta^{13}\text{C}$ for *H. sarcophaga* from different host organisms and for the host organisms *A. excavata* and *D. pertusum* with 95 % confidence ellipse. Arrows show compositional changes induced by kinetic effects and respiration. Text below the horizontal lines in the denominator legend is the host organism that *H. sarcophaga* grew on. Red points show the equilibrium composition for calcite and aragonite as calculated from the isotopic composition of the ambient seawater.

The oxygen and carbon isotopic composition of the different organisms are characterised by large differences. *A. excavata* does not show signs of kinetic effects which would be indicated by a correlation of $\delta^{13}\text{C}$ and $\delta^{18}\text{O}$ values (Adkins et al., 2003; Bajnai et al., 2018; McCaunaghey, 2003). Bivalves are largely considered to calcify in equilibrium with the surrounding water (Immenhauser et al., 2016), which appears to be valid for *A. excavata* as it displays an isotopic composition close to the expected equilibrium (Fig. 7). The host organism *L. pertusa* displays higher departures from the expected aragonite equilibrium, which is mainly caused by additional incorporation of isotopically lighter, metabolic CO_2 and by kinetic isotope effects associated with hydration/hydroxylation reactions given that this coral raises the calcification site pH to values significantly exceeding seawater pH (Adkins et al., 2003; Chen et al., 2018; Holcomb et al., 2009). *excavata* does not show signs of kinetic effects which would be indicated by a correlation of $\delta^{13}\text{C}$ and $\delta^{18}\text{O}$ values (McCaunaghey, 2003; Adkins et al., 2003; Bajnai et al., 2018). Bivalves are largely considered to calcify in equilibrium with the surrounding water (Immenhauser et al., 2016), which appears to be valid for *A. excavata* as it

displays an isotopic composition close to the expected equilibrium (Fig. 8). The host organism *D. pertusum* displays higher departures from the expected aragonite equilibrium, which is mainly caused by additional incorporation of isotopically lighter, metabolic CO₂ and by kinetic isotope effects associated with hydration/hydroxylation reactions given that this coral raises the calcification site pH to values significantly exceeding seawater pH (Chen et al., 2018; McCulloch et al., 2012).

Interestingly, the HA samples display an isotopic composition very similar to the composition of its host organism (Fig. 78). The 95% confidence ellipsoids of HAW, HAO and *A. excavata* all overlap at highest $\delta^{18}\text{O}$ values. However, in contrast to *A. excavata*, HAW and HAO display positive correlations between $\delta^{18}\text{O}$ and $\delta^{13}\text{C}$. This may indicate that all three organisms closely mineralize their carbon from the same source, but hydration/hydroxylation kinetics occur more pronounced in HAW and HAO relative to *A. excavata*.

The observable differences in the carbon isotopic composition between HA and HL can also be caused by different proportions of the carbon sources. HL presumably have constant access to the host's carbon pool, whereas the access of HA to the host's carbon pool is limited due to the defence mechanism of *A. excavata* (Fig. 3). When the bivalve has successfully closed the boring of the foraminifer, the foraminifer must use seawater DIC as a carbon source until it penetrates the shell again. This mixing of different carbon sources in HA in contrast to the stable carbon source of HL can explain the lower $\delta^{13}\text{C}$ values in HL due to an increased influence of host derived carbon.

~~HL is characterized by significantly more positive $\delta^{18}\text{O}$ values than its host, and it also shows a slightly steeper positive correlation between $\delta^{13}\text{C}$ and $\delta^{18}\text{O}$. Both circumstances point to faster hydration/hydroxylation kinetics to be effective during the mineralization of HL compared to its host (Chen et al., 2018). If the pH at which HA precipitates its carbonate is lower than the pH of the calcifying fluid in *L. pertusa*, the hydration kinetics would be accelerated as a result (Cohen, 2003; Crenshaw, 1972; Raddatz et al., 2014). Both organisms may derive their carbon from the same source which likely occurs depleted in ^{13}C relative to seawater, possibly due to significant admixture from metabolic CO₂. This assertion is supported by the fact that HL has constant access to the host's carbon pool.~~

HL is characterized by significantly more positive $\delta^{18}\text{O}$ values than its host, and is also characterized by a slightly steeper positive correlation between $\delta^{13}\text{C}$ and $\delta^{18}\text{O}$. Both circumstances point to faster hydration/hydroxylation kinetics to be effective during the mineralization of HL compared to its host (Chen et al., 2018). If the pH at which HA precipitates carbonate is lower than the pH of the calcifying fluid in *D. pertusum*, the hydration kinetics would be accelerated as a result (Raddatz et al., 2014; Cohen, 2003; Crenshaw, 1972). Both organisms may derive their carbon from the same source which

likely occurs depleted in ^{13}C relative to seawater, possibly due to significant admixture from metabolic CO_2 . This assertion is supported by the fact that HL has constant access to the host's carbon pool. Another mechanism potentially altering the $\delta^{13}\text{C}$ from equilibrium might be the etching mechanism that pumps H^+ -ions in the ambient water around the foraminifera (Toyofuku et al., 2017). The decreasing pH around the foraminifera shifts the carbon speciation towards CO_2 . As CO_2 is depleted in ^{13}C compared to the total inorganic carbon pool, the utilization of CO_2 for calcification would also explain the deviations of the foraminifera's shell $\delta^{13}\text{C}$ from isotopic equilibrium (Toyofuku et al., 2017; McCorkle et al., 1997).

4.5.4.6. Implications for paleoceanographic reconstructions

The results presented here have implications for paleoreconstructions in two ways. When using bivalves for paleo reconstructions or geochemical investigations in general, the shells must be carefully examined for potential traces of bioerosion. In case of callus formation, the carbonate formed can have a significantly different composition than the original carbonate mineralogy.

~~Even more critical are the implications for paleoreconstructions using foraminifera which are regularly analyzed for this purpose. Several foraminifera species are known to live on different host organisms and act as parasites and/or bioeroders (Dupuy et al., 2010; Freiwald and Schönfeld, 1996; Walker et al., 2017). Some of these are also used for isotope and element based paleoenvironmental reconstructions or geochemical investigations in general, such as *Cibicides refulgens* (García-Gallardo et al., 2017; Mackensen and Nam, 2014; Rathburn and De Deckker, 1997), *Hanzawaia concentrica* (Smith and Emiliani, 1968) and *Discanomalina coronata* (Baranwal et al., 2014).~~

~~As an example we use a $\delta^{18}\text{O}$ -temperature conversion formula for benthic foraminifera (Marchitto et al., 2014). Even more critical are the implications for paleoceanographic reconstructions using foraminifera which are regularly analyzed for this purpose. Several foraminifera species are known to live on different host organisms and act as parasites and/or bioeroders (Walker et al., 2017; Dupuy et al., 2010; Freiwald and Schönfeld, 1996). Some of these are also used for isotope and element based paleoenvironmental reconstructions or geochemical investigations in general, such as *Cibicides refulgens* (Mackensen and Nam, 2014; Rathburn and de Deckker, 1997; García-Gallardo et al., 2017), *Hanzawaia concentrica* (Smith and Emiliani, 1968) and *Discanomalina coronata* (Baranwal et al., 2014).~~

~~As an example, we use a $\delta^{18}\text{O}$ -temperature conversion formula for benthic foraminifera (Marchitto et al., 2014) and our measured $\delta^{18}\text{O}$ ratios to reconstruct a temperature for the Leksa Reef of 7.5 °C using HAO and 7.8 °C using HAW- with $\delta^{18}\text{O}_{\text{SW}}$ derived from seawater measurements. In-situ measurements of the water temperature in the Leksa Reef by CTD show a mean temperature of 7.8°C (min= 7.1°C, max=8.8°C) (Bücher, 2018). (Bücher, 2018). If we however use $\delta^{18}\text{O}$ ratios from HL we would~~

834 reconstruct a water temperature of 8.8°C and consequently overestimate the water temperature by
835 1.0 °C

836 If the aforementioned species show similar host specific alterations of their isotopic and elemental
837 composition, paleotemperature reconstructions on the basis of these species could be biased. Given
838 that our results indicate that host specific isotopic and elemental composition changes can be present
839 in the parasitic ~~foraminifer~~foraminifera *H. sarcophaga* we draw attention to other parasitic
840 foraminifera that should be investigated for similar host-parasite relations, especially if they are used
841 for geochemical investigations.

842 4.7. Chemical composition of *H. sarcophaga* compared to other benthic foraminifera

843 *H. sarcophaga* displays significantly higher Mg/Ca ratios than most other benthic foraminifera species
844 with comparable ecology, that show Mg/Ca ratios between 0.5 and 10 mmol/mol (Lear et al., 2002).
845 Foraminifera that have comparable Mg/Ca ratios to *H. sarcophaga* include *Amphistegina* (23– 77 mmol
846 mol⁻¹ (van Dijk et al., 2019; Raja et al., 2005; Geerken et al., 2018)), *Quinqueloculina* (50 – 135 mmol
847 mol⁻¹ (Gussone et al., 2016; Toyofuku et al., 2000)) and *Pyrqo* (4 – 85 mmol mol⁻¹ (Gussone et al., 2016))
848 but these species are biologically and mineralogically distinct from *H. sarcophaga*. *Quinqueloculina* and
849 *Pyrqo* are porcelaneous, whereas *H. sarcophaga* is hyaline. Furthermore, *H. sarcophaga* is not
850 inhabited by photosymbionts in contrast to *Amphistegina*.

851 The exact processes involved in ion transportation, seawater vacuolization and pH-regulation utilized
852 by *H. sarcophaga* remain to be discovered. High Mg/Ca ratios in *H. sarcophaga* that are similar to
853 inorganic precipitated calcite (Oomori et al., 1987; Mucci and Morse, 1983) may indicate a calcification
854 mechanism without ways of discriminating against elements such as magnesium. These species rely
855 on an increase of the calcification site pH (Erez, 2003; de Nooijer et al., 2009; Toyofuku et al., 2017) to
856 facilitate calcification. The main control on calcite Mg/Ca ratios is then provided by the composition of
857 the calcifying fluid (Raitzsch et al., 2010). The high Mg content would therefore indicate a calcifying
858 space that is more similar to ambient seawater i.e. with no or minor modification via ion channels or
859 pumps (de Nooijer et al., 2014; Bentov and Erez, 2006). Additionally, high Mg/Ca ratios in the calcifying
860 space might be necessary for the stabilization of ACC, a suggested metastable calcite precursor phase
861 in foraminifera and other calcifying organisms (Addadi et al., 2003; Jacob et al., 2011, 2017). High
862 amounts of Mg in the calcite can also cause lattice strain effects, due to the size difference of Mg and
863 Ca ions that causes lattice distortion (Evans et al., 2015; Mucci and Morse, 1983). The lattice distortion
864 can cause an increased incorporation of elements such as Sr and Na (Mucci and Morse, 1983; Evans et
865 al., 2015), a feature that we observe in our samples compared to the species *A. lessonii*, that has slightly

Formatiert: Englisch (Vereinigte Staaten), Muster:
Transparent (Weiß)

lower Mg/Ca ratios than *H. sarcophaga* (35 vs. 45 mmol mol⁻¹) and consequently lower Na/Ca and Sr/Ca ratios (Geerken et al., 2018)

4.6.4.8. Biomineralization in the callus region

In order to protect itself from the parasitizing foraminifer, *A. excavata* seals the canal etched through the shell. This is accomplished by rapidly calcifying over the foraminifera boring (Beuck et al., 2008; Cedhagen, 1994). The calcification process produces a callus on the inside of the bivalve shell that is 3-5 mm in diameter and 1-2 mm in height. In the SRZ we can observe the proposed model of biomineralization in bivalves that starts with the formation of an organic sheet, indicated by the high fluorescence, high S concentration and low Ca concentration, which acts as a framework during calcification (Addadi et al., 2006; Checa et al., 2005; Wada, 1976). The following layer is depleted in S and enriched in Ca and therefore represents a higher CaCO₃ concentration (Fig. 1 & 3). This sequence is repeated multiple times leading to the formation of the visible callus. As long as the foraminifera does not stop the boring process, the bivalve needs to continually counter calcify the region of infestation to defend itself.

The callus displays high concentrations of organic material, that isIn order to protect itself from the parasitizing foraminifera, *A. excavata* seals the canal etched through the shell. This is accomplished by rapidly calcifying over the foraminifera boring (Beuck et al., 2008; Cedhagen, 1994). The calcification process produces a callus on the inside of the bivalve shell that is 3-5 mm in diameter and 1-2 mm in height. In the SRZ, evidence can be found for the biomineralization model for bivalves proposed by (Addadi et al., 2006; Checa et al., 2005; Wada and Fujinuki, 1976), i.e. that this process starts with the formation of an organic sheet indicated by the high fluorescence, high S concentration and low Ca concentration of this region, which then acts as a framework during calcification The following layer is depleted in S and enriched in Ca and therefore represents a higher Ca concentration (Fig. 3 & 4). This sequence is repeated multiple times leading to the formation of the visible callus. As long as the foraminifera does not stop the boring process, the bivalve needs to continually counter the boring process by calcifying in the region of infestation.

The callus displays high concentrations of organic material that are not observable in the undisturbed regions. The layers that are characterised by high organic contents appear to be preferentially dissolved (Fig. 3B) In cross sections, organic rich areas make up 50 % of the callus (Fig 4/D1D). It appears unlikely that the high amounts of organic material in the SRZ are solely deposited as a calcification framework, considering the differences between undisturbed shell areas and the SRZ. Therefore, the high amount of deposited organic material probably serves some other purpose, such as an increase

Formatiert: Englisch (Vereinigte Staaten)

898 of the overall material deposition rate and the provision of an initial sealant from the surrounding
899 water.

900 ~~The boring organisms pose a threat to the bivalve in multiple ways. It has been shown that *H.*~~
901 ~~*sarcophaga* penetrated the mantle of *A. excavata* which led to a destruction of the mantle epithelium~~
902 ~~of the bivalve due to ingestion by *H. sarcophaga* (Cedhagen, 1994). Infested sections showed larger~~
903 ~~numbers of cell nuclei, indicating higher cell division rates and higher metabolic rates (Cedhagen,~~
904 ~~1994). The pathway through the bivalve shell furthermore allows pathogens to reach and attack the~~
905 ~~bivalve and allows surrounding water to permeate into the extra pallial fluid (EPF) of the bivalve. Even~~
906 ~~though the EPF in several bivalve species shows trace element concentrations close to seawater~~
907 ~~(Crenshaw, 1972; Wada and Fujinuki, 1974), the bivalve still has to actively concentrate Ca in the~~
908 ~~calcifying space to reach concentrations that exceed the solubility product (Bonucci and Wheeler,~~
909 ~~2020; Wilbur and Saleuddin, 1983). This concentration of Ca is accomplished through active pumping~~
910 ~~by means of enzymes such as Ca-ATPase (Klein et al., 1996) or through ion channels (Carré et al., 2006).~~
911 ~~In case of an unsealed calcifying space, the dilution with seawater makes high concentrations of Ca-~~
912 ~~ions to levels needed for calcification in the extra-EPF less likely. A fast sealing method, by means of~~
913 ~~organic deposition, is therefore necessary to ensure that the bivalve's calcification capability is not~~
914 ~~compromised.~~

915 Geochemically, the SRZ shows the largest differences to the undisturbed aragonite in Mg/Ca and Sr/Ca
916 ratios (Fig. 2 & 3). Mg/Ca ratios are five times higher in the SRZ than in undisturbed aragonite.
917 Magnesium is regarded to be enriched in organic matrices secreted by the bivalve compared to the
918 shell CaCO_3 (Schöne et al., 2010). The distribution of magnesium in the SRZ, especially its enrichments
919 in fluorescent layers rich in sulfur (Fig. 1 & 3), makes an enrichment of Mg due to high organic
920 concentrations likely. Beside an enrichment of Mg in the secreted organic matter, peptides similar to
921 that found in sites of calcification (Moradian-Oldak et al., 1990) can increase the Mg concentration in
922 precipitated calcite by reducing the dehydration enthalpy (Stephenson et al., 2008). These peptides
923 are also regularly found in molluscs (Falini et al., 1996; Halloran and Donachy, 1995; Marin et al., 2007;
924 Zhang and Zhang, 2006). As these peptides do furthermore increase the growth rate by 25 % to 50 %
925 (Stephenson et al., 2008), due to the need of fast calcification (Beuck et al., 2008), a high concentration
926 of the peptides in SRZ is supported. Higher growth rates can furthermore lead to an increase of crystal
927 impurities which could alter other elements besides Mg (Lorens, 1981).

928 In contrast to magnesium, strontium was not found to be enriched in organic matter compared to shell
929 CaCO_3 (Takesue et al., 2008). However, the influence of peptides on other elements such as Sr is
930 speculated on (Stephenson et al., 2008). Sr in aragonitic bivalves is considered to be controlled by
931 growth rate effects (Carré et al., 2006; Füllenbach et al., 2017; Lorrain et al., 2005; Takesue et al., 2008).

A calcification rate control on Sr incorporation is also supported from abiogenic calcite (Gabitov et al., 2014) but not from abiogenic aragonite (Gabitov et al., 2006). Accordingly, this growth rate effect is probably of biologic nature in aragonite precipitates.

Sr probably arrives into the calcifying space via similar pathways to Ca, as was shown by the effects of calcium channel blockers in corals (Ferrier-Pagès et al., 2002). However, Ca-ATPase has a higher affinity for Ca (Yu and Inesi, 1995). Therefore, a higher Ca-ATPase activity, as a result of increased growth rates, should lead to decreasing Sr/Ca ratios in the precipitates, which was shown in corals (Ferrier-Pagès et al., 2002; de Villiers et al., 1995). As we expect high growth rates in the SRZ, Ca channels that also transport Sr cannot explain the observed Sr signature in this zone. Alternatively, the organisms metabolic rate has been suggested to control Sr/Ca in bivalves through metabolic pumping (Klein et al., 1996). High metabolic activity was observed in *A. excavata* infested by *H. sarcophaga*, indicated by a high concentration of nuclei, (Cedhagen, 1994). However, the model of Klein et al. would predict lower Sr/Ca ratios in these areas, thus a mechanism other than metabolic pumping must control the high Sr/Ca ratios in the SRZ.

Füllenbach et al. (2015) proposed that in slow growing areas of bivalves, the organisms exerts less biological control over element incorporation, leading to elevated Sr/Ca ratios. While this hypothesis does not fit our observation of elevated Sr/Ca ratios in a potentially fast growing shell area, a similar hypothesis was suggested concerning Mg/Ca in *Mytilus edulis* (Lorens and Bender, 1980). The authors found strongly elevated Mg/Ca ratios in shells sections that were precipitated after handling the specimens for size measurements and attributed this effect to stress (Lorens and Bender, 1980). The boring of *H. sarcophaga* is very likely to be a stress factor on *A. excavata*. An influence of such stress related effects on Mg/Ca and potentially Sr/Ca are, therefore, possible. The high Mg concentrations in the EPF due to a potential breakdown of Mg regulating mechanisms however, would inhibit the organism from calcification due to the inhibiting effects of Mg on crystal nucleation and growth (Lorens and Bender, 1980; Pytkowicz, 1965). *A. excavata* might circumvent this by releasing additional sulfate bearing organic molecules that provide additional nucleation sites and higher Ca concentrations at the nucleation sites (Lorens and Bender, 1980), which we can observe by the increased S/Ca ratios in the SRZ.

5.—Conclusion

Our results demonstrate that the elemental and isotopic composition of the parasitic foraminifer *H. The Boring organisms pose a threat to the bivalve in multiple ways. It has been shown that *H. sarcophaga* penetrated the mantle of *A. excavata* which led to a destruction of the mantle epithelium of the bivalve due to ingestion by *H. sarcophaga* (Cedhagen, 1994). Infested sections showed larger numbers of cell*

nuclei, indicating higher cell division rates and higher metabolic rates (Cedhagen, 1994). The pathway through the bivalve shell furthermore allows pathogens to reach and attack the bivalve and could allow surrounding water to permeate into the extra pallial fluid (EPF) of the bivalve. Even though the EPF in several bivalve species shows trace element concentrations close to seawater (Wada and Fujinuki, 1976; Crenshaw, 1972), the bivalve still has to actively concentrate Ca in the calcifying space to reach concentrations that exceed the solubility product (Wilbur and Saleuddin, 1983; Bonucci and Wheeler, 2020). This concentration of Ca is accomplished through active pumping by means of enzymes such as Ca-ATPase (Klein et al., 1996) or through ion channels (Carré et al., 2006). In case of an unsealed calcifying space, the dilution with seawater makes high concentrations of Ca-ions to levels needed for calcification in the extra EPF less likely. A fast-sealing method, by means of organic deposition, is therefore necessary to ensure that the bivalve's calcification capability is not compromised.

Geochemically, the SRZ shows the largest differences to the undisturbed aragonite in Mg/Ca and Sr/Ca ratios (Fig 2 & 3). Mg/Ca ratios are five times higher in the SRZ than in undisturbed aragonite. Magnesium is thought to be enriched in organic matrices secreted by the bivalve compared to the shell CaCO_3 (Schöne et al., 2010). The distribution of magnesium in the SRZ, especially its enrichment in fluorescent layers rich in sulfur (Fig. 1,3 and 4), makes an enrichment of Mg due to high organic concentrations likely. Beside an enrichment of Mg in the secreted organic matter, peptides similar to that found at the site of calcification in bivalves (Moradian-Oldak et al., 1990) can increase the Mg concentration in precipitated calcite by reducing the dehydration enthalpy (Stephenson et al., 2008). These peptides are also regularly found in molluscs (Marin et al., 2007; Falini et al., 1996; Halloran and Donachy, 1995; Zhang and Zhang, 2006). As these peptides do furthermore increase the growth rate by 25 % to 50 % (Stephenson et al., 2008), due to the need of fast calcification (Beuck et al., 2008), it may suggest that a high concentration of peptides in the SRZ is likely. Higher growth rates can additionally lead to an increase of crystal impurities which could alter other elements besides Mg (Lorens, 1981).

In contrast to Mg, Sr was not found to be enriched in organic matter compared to shell CaCO_3 (Takesue et al., 2008), and therefore the presence of organics cannot explain the observed high Sr/Ca of the aragonite in the SRZ. Yet, there is evidence for the influence of peptides on the incorporation of other elements such as Sr (Stephenson et al., 2008). Sr incorporation in the aragonitic bivalves is considered to be controlled in-part by growth rate effects (Lorrain et al., 2005; Füllenbach et al., 2017; Takesue et al., 2008; Carré et al., 2006). A calcification rate control on Sr incorporation is also supported from abiogenic calcite (Gabitov et al., 2014) but not from abiogenic aragonite (Gabitov et al., 2006). Accordingly, this growth rate effect is probably of biologic nature in aragonite precipitates.

Sr likely arrives into the calcifying space via similar pathways as Ca, as was shown by the effects of calcium channel blockers in corals (Ferrier-Pagès et al., 2002). However, Ca-ATPase has a higher affinity for Ca than Sr (Yu and Inesi, 1995). Therefore, a higher Ca-ATPase activity, as a result of increased growth rates, should lead to decreasing Sr/Ca ratios in the precipitates, which was shown in corals (Ferrier-Pagès et al., 2002; de Villiers et al., 1995). As we expect high growth rates in the SRZ, Ca channels that also transport Sr cannot explain the observed Sr distribution in this zone. Alternatively, the organism's metabolic rate has been suggested to control Sr/Ca in bivalves through metabolic pumping (Klein et al., 1996). High metabolic activity was observed in *A. excavata* infested by *H. sarcophaga*, indicated by a high concentration of cell-nuclei (Cedhagen, 1994). The model of Klein et al. (1996) would predict lower Sr/Ca ratios in these areas, thus a mechanism other than metabolic pumping must control the high Sr/Ca ratios in the SRZ.

Füllenbach et al. (2015) proposed that in slow growing areas of bivalves, the organisms exert less biological control over element incorporation, leading to elevated Sr/Ca ratios. While this hypothesis does not fit to our observation of elevated Sr/Ca ratios in a potentially fast-growing shell area, a similar hypothesis was suggested concerning Mg/Ca in *Mytilus edulis* (Lorens and Bender, 1980). The authors found strongly elevated Mg/Ca ratios in shells sections that were precipitated after handling the specimens for size measurements and attributed this effect to stress (Lorens and Bender, 1980). The boring of *H. sarcophaga* is very likely to be a stress factor on *A. excavata*. An influence of such stress related effects on Mg/Ca and potentially Sr/Ca (Fig. 4) are, therefore, possible. The high Mg-concentrations in the EPF due to a potential breakdown of Mg-regulating mechanisms however, would inhibit the organism from calcification due to the inhibiting effects of Mg on crystal nucleation and growth (Pytkowicz, 1965; Lorens and Bender, 1980). *A. excavata* might circumvent this by releasing additional sulphate bearing organic molecules that provide additional nucleation sites and higher Ca-concentrations at the nucleation sites (Lorens and Bender, 1980), which might potentially be the cause of the observed increased S/Ca ratios in the SRZ (Fig. 4).

5. Conclusion

Our results demonstrate that the elemental and isotopic composition of the parasitic foraminifera *H. sarcophaga* varies depending on the host organisms that the foraminifer settles on. *H. sarcophaga* that lived on the coral *L. pertusa* shows significantly higher Sr/Ca ratios than those that lived on the bivalve *A. excavata*. Combining these data with a simple mixing model, we propose that this could point towards a biomineralization pathway that is influenced by uptake of

Formatiert: Englisch (Vereinigte Staaten)

1030 carbonate material derived from the host. The dissolution of the host shell could serve to satisfy the
1031 ~~foraminifers~~foraminifera's demand for calcium and DIC.

1032 We also observe significant differences between *H. sarcophaga* specimens that grew on *A. excavata*
1033 that can be correlated to the success of the penetration progress. Foraminifera that fully penetrated
1034 the bivalve's shell, recognizable by the hosts callus formation, display significantly lower Mn/Ca ratios
1035 than foraminifera that did not completely penetrate the shell. This could be an effect of a suspension
1036 feeding period of the foraminifera or grazing of Mn-rich material of the periostracum until it
1037 penetrated the bivalve's shell when switching to a parasitic mode of feeding. Other possibilities include
1038 differences in the growth rate caused by changes of the nutrient availability or Rayleigh fractionation.

1039 The oxygen and carbon isotopic composition of *H. sarcophaga* also appears to be influenced by ~~its~~
1040 ~~specific~~the type of host organism ~~that it infests~~. Again, this might be an effect of a direct uptake of the
1041 host's organic material and/or CaCO₃ ~~however other~~. Other effects such as different pH regimes in the
1042 host organisms and varying equilibration may also play a role. Different extents of the calcification site
1043 carbonate system equilibration between ~~HL and HA~~*H. sarcophaga* that infested *D. pertusum* (HL) and
1044 *H. sarcophaga* that infested *A. excavata* (HA) could also explain the missing signs of kinetic
1045 fractionation in HL compared to HA.

1046 As the elemental and isotopic composition of some parasitic foraminifera is used for
1047 paleoceanographic reconstructions, our results ~~clearly~~ indicate that ~~if these findings are also~~
1048 ~~applicable to other species~~, such studies should only be performed when the host organism ~~and its~~
1049 ~~chemical composition are~~is known.

1050 **Author contribution**

1051 **NS:** Investigation, Conceptualization, Data curation, formal analysis, Investigation, Visualization,
1052 Writing (Original Draft)

1053 **DE:** Methodology, Formal Analysis, Writing (Review & Editing)

1054 **MW:** Resources, Writing (Review & Editing)

1055 **JVB:** Resources, Writing (Review & Editing)

1056 **JF:** Investigation, Resources, Writing (Review & Editing)

1057 **AF:** Resources, Writing (Review & Editing)

1058 **SH:** Investigation, Writing (Review & Editing)

1059 **HM:** Investigation, Resources, Writing (Review & Editing)

1060 **SV:** Supervision, Resources, Writing (Review & Editing)

1061 **JR:** Funding Acquisition, [Investigation](#), Project administration, Supervision, Resources, Writing (Review
1062 & Editing)

1063 Acknowledgments

1064 We are grateful to all cruise captains, crew members and cruise participants of research cruises
1065 POS473 and POS525. We are also grateful for the help of Celestine Beyer and Luciano Zolezzi, who
1066 aided with the ~~measurements~~ [EPMA measurements](#). [We also want to thank Lennart de Nooijer and](#)
1067 [Inge van Dijk, whose detailed comments substantially improved our manuscript](#). This work was
1068 funded by the Deutsche Forschungsgemeinschaft, RA 2156-5/1 to JR. This is FIERCE contribution No.
1069 70

1070 Supplements

1071 [1] Pictures of Meigen test

1072 [\[2\] Measurement data](#)

1073 [\[3\] RAW and TIFF pictures of Fig.1](#)

1074 Competing Interests

1075 The authors declare that they have no conflict of interest.

1076 References

1077 ~~Addadi, L., Joester, D., Nudelman, F. and Weiner, S.: Mollusk Shell Formation : A Source of New~~
1078 ~~Concepts for Understanding Biomineralization Processes, , 980–987, doi:10.1002/chem.200500980,~~
1079 ~~2006.~~

1080 ~~Adkins, J. F., Boyle, E. A., Curry, W. B. and Lutringer, A.: Stable isotopes in deep-sea corals and a new~~
1081 ~~mechanism for “vital effects,” Geochim. Cosmochim. Acta, 67(6), 1129–1143, doi:10.1016/S0016-~~
1082 ~~7037(02)01203-6, 2003.~~

1083 ~~Alexander, S. P. and Delaca, T. E.: Feeding adaptations of the foraminiferan Cibicides refulgens living~~
1084 ~~epizoically and parasitically on the Antarctic scallop Adamussium colbecki, Biol. Bull.,~~
1085 ~~doi:10.2307/1541868, 1987.~~

1086 ~~Allen, J. A.: Manganese deposition on the shells of living molluscs, Nature, doi:10.1038/185336b0,~~
1087 ~~1960.~~

1088 ~~Allen, K. A., Hönisch, B., Eggins, S. M., Haynes, L. L., Rosenthal, Y. and Yu, J.: Trace element proxies for~~

1089 surface-ocean conditions: A synthesis of culture calibrations with planktic foraminifera, *Geochim.*
1090 *Cosmochim. Acta*, 193, 197–221, doi:10.1016/j.gca.2016.08.015, 2016.

1091 Bajnai, D., Fiebig, J., Tomašových, A., Milner Garcia, S., Rollion-Bard, C., Raddatz, J., Löffler, N., Primo-
1092 Ramos, C. and Brand, U.: Assessing kinetic fractionation in brachiopod calcite using clumped
1093 isotopes, *Sci. Rep.*, 8(1), 533, doi:10.1038/s41598-017-17353-7, 2018.

1094 Baranwal, S., Sauer, S., Knies, J., Chand, S., Jensen, H. and Klug, M.: Benthic foraminifera as tools in
1095 interpretation of subsurface hydrocarbon fluid flow at Veslemøy High and Høla-Vesterålen areas of
1096 the Barents Sea. [online] Available from:
1097 <https://ui.adsabs.harvard.edu/abs/2014EGUGA...16.1843B/abstract> (Accessed 10 December 2020),
1098 2014.

1099 Beuck, L., López-Correa, M. and Freiwald, A.: Biogeographical distribution of Hyrrokkin (Rosalinidae,
1100 Foraminifera) and its host-specific morphological and textural trace variability, *Curr. Dev. Bioerosion*,
1101 329–360, doi:10.1007/978-3-540-77598-0_17, 2008.

1102 Bonucci, E. and Wheeler, A. P.: Mechanisms of Molluscan Shell Formation, in *Calcification in*
1103 *Biological Systems*, pp. 179–216, Plenum Press., 2020.

1104 Bromley, R. G. and Heinberg, C.: Attachment strategies of organisms on hard substrates: A
1105 palaeontological view, *Palaeogeogr. Palaeoclimatol. Palaeoecol.*, 232(2–4), 429–453,
1106 doi:10.1016/j.palaeo.2005.07.007, 2006.

1107 Büscher, J.: Cold-water coral habitat characterisation and in situ physiological state analyses of four
1108 spatially distinct reefs in North- and mid-Norway ? Cruise Report RV POSEIDON 525 [POS525],
1109 GEOMAR, Kiel, Germany., 2018.

1110 Calvert, S. E. and Pedersen, T. F.: Geochemistry of Recent oxic and anoxic marine sediments:
1111 Implications for the geological record, *Mar. Geol.*, doi:10.1016/0025-3227(93)90150-T, 1993.

1112 Calvert, S. E. and Pedersen, T. F.: Sedimentary geochemistry of manganese: Implications for the
1113 environment of formation of mangiferous black shales, *Econ. Geol.*,
1114 doi:10.2113/gsecongeo.91.1.36, 1996.

1115 Carré, M., Bentaleb, I., Bruguier, O., Ordinola, E., Barrett, N. T. and Fontugne, M.: Calcification rate
1116 influence on trace element concentrations in aragonitic bivalve shells: Evidences and mechanisms,
1117 *Geochim. Cosmochim. Acta*, 70(19), 4906–4920, doi:10.1016/j.gca.2006.07.019, 2006.

1118 Cedhagen, T.: Taxonomy and biology of hyrrokkin sarcophaga gen. Et Sp. N., a parasitic foraminiferan
1119 (rosalinidae), *Sarsia*, 79(1), 65–82, doi:10.1080/00364827.1994.10413549, 1994.

1120 Checa, A. G., Rodríguez-Navarro, A. B. and Esteban-Delgado, F. J.: The nature and formation of
 1121 calcitic columnar prismatic shell layers in pteriomorphian bivalves, *Biomaterials*, 26(32), 6404–6414,
 1122 doi:10.1016/j.biomaterials.2005.04.016, 2005.
 1123 Chen, S., Gagnon, A. C. and Adkins, J. F.: Carbonic anhydrase, coral calcification and a new model of
 1124 stable isotope vital effects, *Geochim. Cosmochim. Acta*, 236, 179–197,
 1125 doi:10.1016/j.gca.2018.02.032, 2018.
 1126 Cheng, Y. R. and Dai, C. F.: A bioeroding foraminifer, *Hyrrokin sarcophaga*, on deepwater corals from
 1127 the South China Sea, *Coral Reefs*, 35(3), 901, doi:10.1007/s00338-016-1447-7, 2016.
 1128 Cohen, A. L.: Geochemical Perspectives on Coral Mineralization, *Rev. Mineral. Geochemistry*, 54(1),
 1129 151–187, doi:10.2113/0540151, 2003.
 1130 Costa, K. B., Cabarcos, E., Santarosa, A. C. A., Battaglin, B. B. F. and Toledo, F. A. L.: A multiproxy
 1131 approach to the climate and marine productivity variations along MIS-5 in SE-Brazil: A comparison
 1132 between major components of calcareous nannofossil assemblages and geochemical records,
 1133 *Palaeogeogr. Palaeoclimatol. Palaeoecol.*, 449, 275–288, doi:10.1016/j.palaeo.2016.02.032, 2016.
 1134 Crenshaw, M. A.: The Inorganic Composition Of Molluscan Extrapallial Fluid, *Biol. Bull.*, 143(3), 506–
 1135 512, doi:10.2307/1540180, 1972.
 1136 Dupuy, C., Rossignol, L., Geslin, E. and Pascal, P. Y.: Predation of mudflat meio-macrofaunal
 1137 metazoans by a calcareous foraminifer, *Ammonia tepida* (Cushman, 1926), *J. Foraminifer. Res.*, 40(4),
 1138 305–312, doi:10.2113/gsjfr.40.4.305, 2010.
 1139 Elderfield, H.: A biomineralization model for the incorporation of trace elements into foraminiferal
 1140 calcium carbonate, *Earth Planet. Sci. Lett.*, 142(3–4), 409–423, doi:10.1016/0012-821X(96)00105-7,
 1141 1996.
 1142 Erez, J.: The Source of Ions for Biomineralization in Foraminifera and Their Implications for
 1143 Paleooceanographic Proxies, *Rev. Mineral. Geochemistry*, 54(1), 115–149, doi:10.2113/0540115,
 1144 2003.
 1145 Falini, G., Albeck, S., Weiner, S. and Addadi, L.: Control of Aragonite or Calcite Polymorphism by
 1146 Mollusk Shell Macromolecules, *Science (80-.)*, 271(5245), 67–69, doi:10.1126/science.271.5245.67,
 1147 1996.
 1148 Ferrier-Pagès, C., Boisson, F., Allemand, D. and Tambutti, E.: Kinetics of strontium uptake in the
 1149 scleractinian coral *Stylophora pistillata*, *Mar. Ecol. Prog. Ser.*, 245(Milliman 1974), 93–100,
 1150 doi:10.3354/meps245093, 2002.

1151 Form, A. U., Büscher, J. V., Hissmann, K., Flögel, S., Wisshak, M., Rüggeberg, A., Bannister, R., Kutti, T.,
 1152 Stapp, L., Bennecke, S., Küter, M., Nachtigall, K., Schauer, J. and Fenske, M.: RV POSEIDON Cruise
 1153 Report POS473 LORELEI II: LOphelia REef Lander Expedition and Investigation II, Tromsø—Bergen—
 1154 Esbjerg, 15.08.—31.08.—04.09.2014., 2015.
 1155 Freiwald, A. and Schönfeld, J.: Substrate pitting and boring pattern of *Hyrrokkin sarcophaga*
 1156 *Cedhagen*, 1994 (Foraminifera) in a modern deep-water coral reef mound, *Mar. Micropaleontol.*,
 1157 28(2), 199–207, 1996.
 1158 Föger, A., Konrad, F., Leis, A., Dietzel, M. and Mavromatis, V.: Effect of growth rate and pH on lithium
 1159 incorporation in calcite, *Geochim. Cosmochim. Acta*, 248, 14–24, doi:10.1016/j.gca.2018.12.040,
 1160 2019.
 1161 Füllenbach, C. S., Schöne, B. R., Shirai, K., Takahata, N., Ishida, A. and Sano, Y.: Minute co-variations
 1162 of Sr/Ca ratios and microstructures in the aragonitic shell of *Cerastoderma edule* (Bivalvia)—Are
 1163 geochemical variations at the ultra-scale masking potential environmental signals?, *Geochim.*
 1164 *Cosmochim. Acta*, 205, 256–271, doi:10.1016/j.gca.2017.02.019, 2017.
 1165 Gabitov, R. I., Cohen, A. L., Gaetani, G. A., Holcomb, M. and Watson, E. B.: The impact of crystal
 1166 growth rate on element ratios in aragonite: An experimental approach to understanding vital effects,
 1167 *Geochim. Cosmochim. Acta*, 70(18), A187, doi:10.1016/j.gca.2006.06.377, 2006.
 1168 Gabitov, R. I., Sadekov, A. and Leinweber, A.: Crystal growth rate effect on Mg/Ca and Sr/Ca
 1169 partitioning between calcite and fluid: An in situ approach, *Chem. Geol.*, 367, 70–82,
 1170 doi:10.1016/j.chemgeo.2013.12.019, 2014.
 1171 García-Gallardo, Á., Grunert, P., Voelker, A. H. L., Mendes, I. and Piller, W. E.: Re-evaluation of the
 1172 “elevated epifauna” as indicator of Mediterranean Outflow Water in the Gulf of Cadiz using stable
 1173 isotopes ($\delta^{13}\text{C}$, $\delta^{18}\text{O}$), *Glob. Planet. Change*, 155, 78–97, doi:10.1016/j.gloplacha.2017.06.005, 2017.
 1174 Goldstein, J. I., Newbury, D. E., Michael, J. R., Ritchie, N. W. M., Scott, J. H. J. and Joy, D. C.: Scanning
 1175 electron microscopy and x-ray microanalysis., 2017.
 1176 Goldstein, S. T.: Foraminifera: A biological overview, in *Modern Foraminifera.*, 1999.
 1177 Gray, W. R. and Evans, D.: Nonthermal Influences on Mg/Ca in Planktonic Foraminifera: A Review of
 1178 Culture Studies and Application to the Last Glacial Maximum, *Paleoceanogr. Paleoclimatology*, 34(3),
 1179 306–315, doi:10.1029/2018PA003517, 2019.
 1180 Greaves, M., Caillon, N., Rebaubier, H., Bartoli, G., Bohaty, S., Cache, I., Clarke, L., Cooper, M., Daunt,
 1181 C., Delaney, M., DeMenocal, P., Dutton, A., Eggins, S., Elderfield, H., Garbe-Schoenberg, D., Goddard,

1182 E., Green, D., Groeneveld, J., Hastings, D., Hathorne, E., Kimoto, K., Klinkhammer, G., Labeyrie, L., Lea,
 1183 D. W., Marchitto, T., Martínez-Botí, M. A., Mortyn, P. G., Ni, Y., Nuernberg, D., Paradis, G., Quinn, T.,
 1184 Rosenthal, Y., Russel, A., Sagawa, T., Sosdian, S., Stett, L., Tachikawa, K., Tappa, E., Thunell, R. and
 1185 Wilson, P. A.: Interlaboratory comparison study of calibration standards for foraminiferal Mg/Ca
 1186 thermometry, *Geochemistry, Geophys. Geosystems*, 9(8), 1–27, doi:10.1029/2008GC001974, 2008.

1187 Groeneveld, J. and Filipsson, H. L.: Mg/Ca and Mn/Ca ratios in benthic foraminifera: the potential to
 1188 reconstruct past variations in temperature and hypoxia in shelf regions, *Biogeosciences*, 10(7), 5125–
 1189 5138, doi:10.5194/bg-10-5125-2013, 2013.

1190 Sen Gupta, B. K.: *Modern Foraminifera*, 2003.

1191 Halloran, B. A. and Donachy, J. E.: Characterization of organic matrix macromolecules from the shells
 1192 of the antarctic scallop, *Adamussium colbecki*, *Comp. Biochem. Physiol. — Part B Biochem.*, 111(2),
 1193 221–231, doi:10.1016/0305-0491(94)00245-P, 1995.

1194 Hancock, L. G., Walker, S. E., Pérez Huerta, A. and Bowser, S. S.: Population Dynamics and Parasite
 1195 Load of a Foraminifer on Its Antarctic Scallop Host with Their Carbonate Biomass Contributions,
 1196 edited by G. J. Vermeij, *PLoS One*, 10(7), e0132534, doi:10.1371/journal.pone.0132534, 2015.

1197 Hare, P. E.: Amino acid composition of some calcified proteins, *Carnegie Inst. Washingt. Yearbk.*, 64,
 1198 223–232, 1965.

1199 Hissmann, K. and Schauer, J.: Manned submersible „JAGO“, *J. large-scale Res. Facil. JLSRF*, 3,
 1200 doi:10.17815/jlsrf-3-157, 2017.

1201 Holcomb, M., Cohen, A. L., Gabitov, R. I. and Hutter, J. L.: Compositional and morphological features
 1202 of aragonite precipitated experimentally from seawater and biogenically by corals, *Geochim.*
 1203 *Cosmochim. Acta*, 73(14), 4166–4179, doi:10.1016/j.gca.2009.04.015, 2009.

1204 Holland, K., Eggins, S. M., Hönisch, B., Haynes, L. L. and Branson, O.: Calcification rate and shell
 1205 chemistry response of the planktic foraminifer *Orbulina universa* to changes in microenvironment
 1206 seawater carbonate chemistry, *Earth Planet. Sci. Lett.*, 464, 124–134, doi:10.1016/j.epsl.2017.02.018,
 1207 2017.

1208 Hönisch, B., Allen, K. A., Russell, A. D., Eggins, S. M., Bijma, J., Spero, H. J., Lea, D. W. and Yu, J.:
 1209 Planktic foraminifers as recorders of seawater Ba/Ca, *Mar. Micropaleontol.*, 79(1–2), 52–57,
 1210 doi:10.1016/j.marmicro.2011.01.003, 2011.

1211 Horton, T., Kroh, A., Ahyong, S., Bailly, N., Boyko, C. B., Brandão, S. N., Gofas, S., Hooper, J. N. A.,
 1212 Hernandez, F., Holovachov, O., Mees, J., Molodtsova, T. N., Paulay, G., Decock, W., Dekeyser, S.,

1213 Poffyn, G., Vandepitte, L., Vanhoorne, B., Adlard, R., Agatha, S., Ahn, K. J., Akkari, N., Alvarez, B.,
 1214 Anderberg, A., Anderson, G., Angel, M. V., Antic, D., Arango, C., Artois, T., Atkinson, S., Auffenberg, K.,
 1215 Baldwin, B. G., Bank, R., Barber, A., Barbosa, J. P., Bartsch, I., Bellan-Santini, D., Bergh, N., Bernot, J.,
 1216 Berta, A., Bezerra, T. N., Bieler, R., Blanco, S., Blasco-Costa, I., Blazewicz, M., Bock, P., Bonifacio de
 1217 León, M., Böttger-Schnack, R., Bouchet, P., Boury-Esnault, N., Boxshall, G., Bray, R., Bruce, N. L.,
 1218 Cairns, S., Calvo-Casas, J., Carballo, J. L., Cárdenas, P., Carstens, E., Chan, B. K., Chan, T. Y., Cheng, L.,
 1219 Christenhusz, M., Churchill, M., Coleman, C. O., Collins, A. G., Collins, G. E., Corbari, L., Cordeiro, R.,
 1220 Cornils, A., Coste, M., Costello, M. J., Crandall, K. A., Cremonese, F., Cribb, T., Cutmore, S., Dahdouh-
 1221 Guebas, F., Daly, M., Daneliya, M., Dauvin, J. C., Davie, P., De Broyer, C., De Grave, S., de Mazancourt,
 1222 V., de Voogd, N. J., Decker, P., Defaye, D., d'Hondt, J. L., Dippenaar, S., Dohrmann, M., Dolan, J.,
 1223 Domning, D., Downey, R., Ector, L., Eisendle-Flöckner, U., Eitel, M., Encarnação, S. C. d., Enghoff, H.,
 1224 Epler, J., Ewers-Saucedo, C., et al.: World Register of Marine Species (WoRMS), [online] Available
 1225 from: <http://www.marinespecies.org>, 2021.
 1226 Immenhauser, A., Schöne, B. R., Hoffmann, R. and Niedermayr, A.: Mollusc and brachiopod skeletal
 1227 hard parts: Intricate archives of their marine environment, *Sedimentology*, **63**(1), 1–59,
 1228 doi:10.1111/sed.12231, 2016.
 1229 Jacobson, P.: Physical Oceanography of the Trondheimsfjord, *Geophys. Astrophys. Fluid Dyn.*, **26**(1–
 1230 2), 3–26, doi:10.1080/03091928308221761, 1983.
 1231 Jochum, K. P., Nohl, U., Herwig, K., Lammel, E., Stoll, B. and Hofmann, A. W.: GeoReM: A New
 1232 Geochemical Database for Reference Materials and Isotopic Standards, *Geostand. Geoanalytical Res.*,
 1233 **29**(3), 333–338, doi:10.1111/j.1751-908x.2005.tb00904.x, 2005.
 1234 Kato, K., Wada, H. and Fujioka, K.: The application of chemical staining to separate calcite and
 1235 aragonite minerals for micro-scale isotopic analyses, *Geochem. J.*, **37**(2), 291–297,
 1236 doi:10.2343/geochemj.37.291, 2003.
 1237 Klein, R. T., Lohmann, K. C. and Thayer, C. W.: Sr/Ca and $^{13}\text{C}/^{12}\text{C}$ ratios in skeletal calcite of *Mytilus*
 1238 *trossulus*: Covariation with metabolic rate, salinity, and carbon isotopic composition of seawater,
 1239 *Geochim. Cosmochim. Acta*, doi:10.1016/S0016-7037(96)00232-3, 1996.
 1240 Koho, K. A., de Nooijer, L. J. and Reichert, G. J.: Combining benthic foraminiferal ecology and shell
 1241 Mn/Ca to deconvolve past bottom water oxygenation and paleoproductivity, *Geochim. Cosmochim.*
 1242 *Acta*, **165**, 294–306, doi:10.1016/j.gca.2015.06.003, 2015.
 1243 Lackschewitz, K. and Heinitz, M.: Research Vessel POSEIDON, J. large scale Res. Facil. JLSRF, **1**, 60–63,
 1244 doi:10.17815/jlsrf-1-62, 2015.

1245 Lantz, B.: The impact of sample non-normality on ANOVA and alternative methods, *Br. J. Math. Stat.*
1246 *Psychol.*, 66(2), 224–244, doi:10.1111/j.2044-8317.2012.02047.x, 2013.

1247 Lear, C. H. and Rosenthal, Y.: Benthic foraminiferal Li/Ca: Insights into Cenozoic seawater carbonate
1248 saturation state, *Geology*, 34(11), 985, doi:10.1130/G22792A.1, 2006.

1249 Lorens, R. B.: Sr, Cd, Mn and Co distribution coefficients in calcite as a function of calcite precipitation
1250 rate, *Geochim. Cosmochim. Acta*, 45(4), 553–561, doi:10.1016/0016-7037(81)90188-5, 1981.

1251 Lorens, R. B. and Bender, M. L.: The impact of solution chemistry on *Mytilus edulis* calcite and
1252 aragonite, *Geochim. Cosmochim. Acta*, 44(9), 1265–1278, doi:10.1016/0016-7037(80)90087-3, 1980.

1253 Lorrain, A., Gillikin, D. P., Paulet, Y. M., Chauvaud, L., Le Mercier, A., Navez, J. and André, L.: Strong
1254 kinetic effects on Sr/Ca ratios in the calcitic bivalve *Pecten maximus*, *Geology*, 33(12), 965–968,
1255 doi:10.1130/G22048.1, 2005.

1256 Mackensen, A. and Nam, S. II: Taxon-specific epibenthic foraminiferal $\delta^{18}\text{O}$ in the Arctic Ocean:
1257 Relationship to water masses, deep circulation, and brine release, *Mar. Micropaleontol.*, 113, 34–43,
1258 doi:10.1016/j.marmicro.2014.09.002, 2014.

1259 Marchitto, T. M., Curry, W. B., Lynch Stieglitz, J., Bryan, S. P., Cobb, K. M. and Lund, D. C.: Improved
1260 oxygen isotope temperature calibrations for cosmopolitan benthic foraminifera, *Geochim.*
1261 *Cosmochim. Acta*, 130, 1–11, doi:10.1016/j.gca.2013.12.034, 2014.

1262 Marin, F., Luquet, G., Marie, B. and Medakovic, D.: Molluscan Shell Proteins: Primary Structure,
1263 Origin, and Evolution, *Curr. Top. Dev. Biol.*, 80(November 2018), 209–276, doi:10.1016/S0070-
1264 2153(07)80006-8, 2007.

1265 McCauley, T. A.: Sub-equilibrium oxygen-18 and carbon-13 levels in biological carbonates:
1266 Carbonate and kinetic models, *Coral Reefs*, 22(4), 316–327, doi:10.1007/s00338-003-0325-2, 2003.

1267 Milzer, G., Giraudeau, J., Faust, J., Knies, J., Eynaud, F. and Rühlemann, C.: Spatial distribution of
1268 benthic foraminiferal stable isotopes and dinocyst assemblages in surface sediments of the
1269 Trondheimsfjord, central Norway, *Biogeosciences*, 10(7), 4433–4448, doi:10.5194/bg-10-4433-2013,
1270 2013.

1271 Moradian-Oldak, J., Addadi, L., Weiner, S. and Berman, A.: Tuning of Crystal Nucleation and Growth
1272 by Proteins: Molecular Interactions at Solid-Liquid Interfaces in Biomineralization, *Croat. Chem. Acta*,
1273 63(3), 539–544 [online] Available from: <https://hrcak.srce.hr/137390> (Accessed 1 December 2020),
1274 1990.

1275 Mucci, A.: Manganese uptake during calcite precipitation from seawater: Conditions leading to the

1276 formation of a pseudokutnahorite, *Geochim. Cosmochim. Acta*, 52(7), 1859–1868, doi:10.1016/0016-
1277 7037(88)90009-9, 1988.

1278 Mucci, A. and Morse, J. W.: The incorporation of Mg²⁺ and Sr²⁺ into calcite overgrowths: influences
1279 of growth rate and solution composition, *Geochim. Cosmochim. Acta*, 47(2), 217–233, 1983.

1280 Nakahara, H.: Nacre Formation in Bivalve and Gastropod Molluscs, in *Mechanisms and Phylogeny of*
1281 *Mineralization in Biological Systems*, pp. 343–350, Springer Japan, Tokyo., 1991.

1282 Petersen, J., Barras, C., Bézos, A., La, C., De Nooijer, L. J., Meysman, F. J. R., Mouret, A., Slomp, C. P.
1283 and Jorissen, F. J.: Mn/Ca intra- and inter-test variability in the benthic foraminifer *Ammonia tepida*,
1284 *Biogeosciences*, 15(1), 331–348, doi:10.5194/bg-15-331-2018, 2018.

1285 Pytkowicz, R. M.: Rates of Inorganic Calcium Carbonate Nucleation, *J. Geol.*, 73(1), 196–199,
1286 doi:10.1086/627056, 1965.

1287 Raddatz, J., Rüggeberg, A., Margreth, S. and Dullo, W. C.: Paleoenvironmental reconstruction of
1288 Challenger Mound initiation in the Porcupine Seabight, NE Atlantic, *Mar. Geol.*, 282(1–2), 79–90,
1289 doi:10.1016/j.margeo.2010.10.019, 2011.

1290 Raddatz, J., Liebetrau, V., Rüggeberg, A., Hathorne, E., Krabbenhöft, A., Eisenhauer, A., Böhm, F.,
1291 Vollstaedt, H., Fietzke, J., López Correa, M., Freiwald, A. and Dullo, W. C.: Stable Sr isotope, Sr/Ca,
1292 Mg/Ca, Li/Ca and Mg/Li ratios in the scleractinian cold-water coral *Lophelia pertusa*, *Chem. Geol.*,
1293 352, 143–152, doi:10.1016/j.chemgeo.2013.06.013, 2013.

1294 Raddatz, J., Rüggeberg, A., Flögel, S., Hathorne, E. C., Liebetrau, V., Eisenhauer, A. and Dullo, W. C.:
1295 The influence of seawater pH on U/Ca ratios in the scleractinian cold-water coral *Lophelia pertusa*,
1296 *Biogeosciences*, 11(7), 1863–1871, doi:10.5194/bg-11-1863-2014, 2014.

1297 Raddatz, J., Nürnberg, D., Tiedemann, R. and Rippert, N.: Southeastern marginal West Pacific Warm
1298 Pool sea surface and thermocline dynamics during the Pleistocene (2.5–0.5 Ma), *Palaeogeogr.*
1299 *Palaeoclimatol. Palaeoecol.*, 471, 144–156, doi:10.1016/j.palaeo.2017.01.024, 2017.

1300 Raitzsch, M., Duenas-Bohórquez, A., Reichert, G. J., De Nooijer, L. J. and Bickert, T. T.: Incorporation
1301 of Mg and Sr in calcite of cultured benthic foraminifera: Impact of calcium concentration and
1302 associated calcite saturation state, *Biogeosciences*, 7(3), 869–881, doi:10.5194/bg-7-869-2010, 2010.

1303 Rathburn, A. E. and De Deckker, P.: Magnesium and strontium compositions of Recent benthic
1304 foraminifera from the Coral Sea, Australia and Prydz Bay, Antarctica, *Mar. Micropaleontol.*, 32(3–4),
1305 231–248, doi:10.1016/S0377-8398(97)00028-5, 1997.

1306 Schleinkofer, N., Raddatz, J., Freiwald, A., Evans, D., Beuck, L., Rüggeberg, A. and Liebetrau, V.:

1307 Environmental and biological controls on Na/Ca ratios in scleractinian cold-water corals,
 1308 Biogeosciences, 16(18), 3565–3582, doi:10.5194/bg-16-3565-2019, 2019.
 1309 Schöne, B. R., Zhang, Z., Jacob, D., Gillikin, D. P., Tütken, T., Garbe-Schönberg, D., McConnaughey, T.
 1310 and Soldati, A.: Effect of organic matrices on the determination of the trace element chemistry (Mg,
 1311 Sr, Mg/Ca, Sr/Ca) of aragonitic bivalve shells (*Arctica islandica*)—Comparison of ICP-OES and LA-ICP-
 1312 MS data, Geochem. J., 44(1), 23–37, doi:10.2343/geochemj.1.0045, 2010.
 1313 Schweizer, M., Bowser, S. S., Korsun, S. and Pawlowski, J.: Emendation of *Cibicides antarcticus*
 1314 (Saidova, 1975) based on molecular, morphological, and ecological data, J. Foraminifer. Res.,
 1315 doi:10.2113/gsjfr.42.4.340, 2012.
 1316 Secor, C. L., Mills, E. L., Harshbarger, J., Kuntz, H. T., Gutenmann, W. H. and Lisk, D. J.:
 1317 Bioaccumulation of toxicants, element and nutrient composition, and soft tissue histology of zebra
 1318 mussels (*Dreissena polymorpha*) from New York State waters, Chemosphere, doi:10.1016/0045-
 1319 6535(93)90224-S, 1993.
 1320 Segev, E. and Erez, J.: Effect of Mg/Ca ratio in seawater on shell composition in shallow benthic
 1321 foraminifera, Geochemistry, Geophys. Geosystems, 7(2), 1–8, doi:10.1029/2005GC000969, 2006.
 1322 Smith, P. B. and Emiliani, C.: Oxygen-isotope analysis of recent tropical pacific benthonic
 1323 foraminifera, Science (80-), doi:10.1126/science.160.3834.1335, 1968.
 1324 Spötl, C. and Vennemann, T. W.: Continuous flow isotope ratio mass spectrometric analysis of
 1325 carbonate minerals, Rapid Commun. Mass Spectrom., 17(9), 1004–1006, doi:10.1002/rcm.1010,
 1326 2003.
 1327 Stephenson, A. E., Deyoreo, J. J., Wu, L., Wu, K. J., Hoyer, J. and Dove, P. M.: Peptides enhance
 1328 magnesium signature in calcite: Insights into origins of vital effects, Science (80-), 322(5902), 724–
 1329 727, doi:10.1126/science.1159417, 2008.
 1330 Sunda, W. G. and Huntsman, S. A.: Regulation of cellular manganese and manganese transport rates
 1331 in the unicellular alga *Chlamydomonas*, Limnol. Oceanogr., 30(1), 71–80,
 1332 doi:10.4319/lo.1985.30.1.0071, 1985.
 1333 Swinehart, J. H. and Smith, K. W.: Iron And Manganese Deposition In The Periostraca Of Several
 1334 Bivalve Molluscs, Biol. Bull., 156(3), 369–381, doi:10.2307/1540924, 1979.
 1335 Takesue, R. K., Bacon, C. R. and Thompson, J. K.: Influences of organic matter and calcification rate on
 1336 trace elements in aragonitic estuarine bivalve shells, Geochim. Cosmochim. Acta, 72(22), 5431–5445,
 1337 doi:10.1016/j.gca.2008.09.003, 2008.

1338 ~~Tambutté, E., Allemand, D., Zoccola, D., Meibom, A., Lotto, S., Caminiti, N. and Tambutté, S.:
 1339 Observations of the tissue-skeleton interface in the scleractinian coral *Stylophora pistillata*, *Coral*
 1340 *Reefs*, 26(3), 517–529, doi:10.1007/s00338-007-0263-5, 2007.~~
 1341 Tribouillard, N., Algeo, T. J., Lyons, T. and Riboulleau, A.: Trace metals as paleoredox and
 1342 paleoproductivity proxies: An update, *Chem. Geol.*, 232(1–2), 12–32,
 1343 doi:10.1016/j.chemgeo.2006.02.012, 2006.
 1344 de Villiers, S., Nelson, B. K. and Chivas, A.: Biological Control on Coral Sr/Ca and $\delta^{18}\text{O}$
 1345 Reconstructions of Sea Surface Temperatures, *Science* (80-.), 269, 1247–1249, 1995.
 1346 Wada, K.: Biomineralization in bivalve molluscs with emphasis on the chemical composition of the
 1347 extrapallial fluid, *Mech. Miner. Invertebr. plants*, 1976.
 1348 Wada, K. and Fujinuki, T.: Physiological regulation of shell formation in molluscs, I. Chemical
 1349 composition of extrapallial fluid, *Bull. Natl. Pearl Res. Lab.*, 18, 2085–2110, 1974.
 1350 Walker, S. E., Hancock, L. G. and Bowser, S. S.: Diversity, biogeography, body size and fossil record of
 1351 parasitic and suspected parasitic foraminifera: A review, *J. Foraminifer. Res.*, 47(1), 34–55,
 1352 doi:10.2113/gsjfr.47.1.34, 2017.
 1353 Whitney, N. M., Johnson, B. J., Dostie, P. T., Luzier, K. and Wanamaker, A. D.: Paired bulk organic and
 1354 individual amino acid $\delta^{15}\text{N}$ analyses of bivalve shell periostracum: A paleoceanographic proxy for
 1355 water source variability and nitrogen cycling processes, *Geochim. Cosmochim. Acta*, 254, 67–85,
 1356 doi:10.1016/j.gca.2019.03.019, 2019.
 1357 Wilbur, K. M. and Saleuddin, A. S. M.: Shell Formation, in *The Mollusca*, pp. 235–287, Elsevier., 1983.
 1358 Yu, X. and Inesi, G.: Variable stoichiometric efficiency of Ca^{2+} and Sr^{2+} transport by the sarcoplasmic
 1359 reticulum ATPase, *J. Biol. Chem.*, 270(9), 4361–4367, doi:10.1074/jbc.270.9.4361, 1995.
 1360 Zhang, C. and Zhang, R.: Matrix proteins in the outer shells of molluscs, *Mar. Biotechnol.*, 8(6), 572–
 1361 586, doi:10.1007/s10126-005-6029-6, 2006.
 1362
 1363 Addadi, L., Raz, S., and Weiner, S.: Taking Advantage of Disorder: Amorphous Calcium Carbonate and
 1364 Its Roles in Biomineralization, *Advanced Materials*, 15, 959–970,
 1365 <https://doi.org/10.1002/adma.200300381>, 2003.

1366 [Addadi, L., Joester, D., Nudelman, F., and Weiner, S.: Mollusk Shell Formation: A Source of New](#)
 1367 [Concepts for Understanding Biomineralization Processes, Chemistry - A European Journal, 12, 980–](#)
 1368 [987, <https://doi.org/10.1002/chem.200500980>, 2006.](#)
 1369 [Addamo, A. M., Vertino, A., Stolarski, J., García-Jiménez, R., Taviani, M., and Machordom, A.: Merging](#)
 1370 [scleractinian genera: The overwhelming genetic similarity between solitary *Desmophyllum* and](#)
 1371 [colonial *Lophelia*, BMC Evolutionary Biology, 16, <https://doi.org/10.1186/s12862-016-0654-8>, 2016.](#)
 1372 [Adkins, J. F., Boyle, E. A., Curry, W. B., and Lutringer, A.: Stable isotopes in deep-sea corals and a new](#)
 1373 [mechanism for “vital effects,” *Geochimica et Cosmochimica Acta*, 67, 1129–1143,](#)
 1374 [https://doi.org/10.1016/S0016-7037\(02\)01203-6, 2003.](#)
 1375 [Alexander, S. P. and Delaca, T. E.: Feeding adaptations of the foraminiferan *Cibicides refulgens* living](#)
 1376 [epizoically and parasitically on the Antarctic scallop *Adamussium colbecki*, *Biological Bulletin*, 173,](#)
 1377 [136–159, <https://doi.org/10.2307/1541868>, 1987.](#)
 1378 [Allen, J. A.: Manganese deposition on the shells of living molluscs, *Nature*, 185, 336–337,](#)
 1379 [https://doi.org/10.1038/185336b0, 1960.](#)
 1380 [Bajnai, D., Fiebig, J., Tomašových, A., Milner Garcia, S., Rollion-Bard, C., Raddatz, J., Löffler, N., Primo-](#)
 1381 [Ramos, C., and Brand, U.: Assessing kinetic fractionation in brachiopod calcite using clumped](#)
 1382 [isotopes, *Scientific Reports*, 8, 533, <https://doi.org/10.1038/s41598-017-17353-7>, 2018.](#)
 1383 [Baranwal, S., Sauer, S., Knies, J., Chand, S., Jensen, H., and Klug, M.: Benthic foraminifera as tools in](#)
 1384 [interpretation of subsurface hydrocarbon fluid flow at Veslemøy High and Hola-Vesterålen areas of](#)
 1385 [the Barents Sea, *Geophysical Research Abstracts*, 2014-1843 pp., 2014.](#)
 1386 [Bentov, S. and Erez, J.: Impact of biomineralization processes on the Mg content of foraminiferal](#)
 1387 [shells: A biological perspective, *Geochemistry, Geophysics, Geosystems*, 7,](#)
 1388 [https://doi.org/10.1029/2005GC001015, 2006.](#)
 1389 [Beuck, L., López Correa, M., and Freiwald, A.: Biogeographical distribution of *Hyrrokin* \(*Rosalinidae*,](#)
 1390 [Foraminifera\) and its host-specific morphological and textural trace variability, *Current*](#)
 1391 [Developments in Bioerosion, 329–360, <https://doi.org/10.1007/978-3-540-77598-0-17>, 2008.](#)
 1392 [Bonucci, E. and Wheeler, A. P.: Mechanisms of Molluscan Shell Formation, in: *Calcification in*](#)
 1393 [Biological Systems, Plenum Press, 179–216, <https://doi.org/10.1201/9781003068396-10>, 2020.](#)
 1394 [Büscher, J.: Cold-water coral habitat characterisation and in situ physiological state analyses of four](#)
 1395 [spatially distinct reefs in North- and mid-Norway-Cruise Report RV POSEIDON 525 \[POS525\],](#)
 1396 [GEOMAR, Kiel, Germany, \[https://doi.org/10.3289/CR_POS525\]\(https://doi.org/10.3289/CR_POS525\), 2018.](#)

1397 [Calvert, S. E. and Pedersen, T. F.: Geochemistry of Recent oxic and anoxic marine sediments:](#)
1398 [Implications for the geological record, Marine Geology, https://doi.org/10.1016/0025-](#)
1399 [3227\(93\)90150-T, 1993.](#)

1400 [Calvert, S. E. and Pedersen, T. F.: Sedimentary geochemistry of manganese: Implications for the](#)
1401 [environment of formation of manganiferous black shales, Economic Geology,](#)
1402 [https://doi.org/10.2113/gsecongeo.91.1.36, 1996.](#)

1403 [Carré, M., Bentaleb, I., Bruguier, O., Ordinola, E., Barrett, N. T., and Fontugne, M.: Calcification rate](#)
1404 [influence on trace element concentrations in aragonitic bivalve shells: Evidences and mechanisms,](#)
1405 [Geochimica et Cosmochimica Acta, 70, 4906–4920, https://doi.org/10.1016/j.gca.2006.07.019, 2006.](#)

1406 [Cedhagen, T.: Taxonomy and biology of hyrrokkin sarcophaga gen. Et Sp. N., a parasitic foraminiferan](#)
1407 [\(rosalinidae\), Sarsia, 79, 65–82, https://doi.org/10.1080/00364827.1994.10413549, 1994.](#)

1408 [Checa, A. G., Rodríguez-Navarro, A. B., and Esteban-Delgado, F. J.: The nature and formation of](#)
1409 [calcitic columnar prismatic shell layers in pteriomorphian bivalves, Biomaterials, 26, 6404–6414,](#)
1410 [https://doi.org/10.1016/j.biomaterials.2005.04.016, 2005.](#)

1411 [Cheng, Y. R. and Dai, C. F.: A bioeroding foraminifer, Hyrrokkin sarcophaga, on deepwater corals from](#)
1412 [the South China Sea, Coral Reefs, 35, 901, https://doi.org/10.1007/s00338-016-1447-7, 2016.](#)

1413 [Chen, S., Gagnon, A. C., and Adkins, J. F.: Carbonic anhydrase, coral calcification and a new model of](#)
1414 [stable isotope vital effects, Geochimica et Cosmochimica Acta, 236, 179–197,](#)
1415 [https://doi.org/10.1016/j.gca.2018.02.032, 2018.](#)

1416 [Cohen, A. L.: Geochemical Perspectives on Coral Mineralization, Reviews in Mineralogy and](#)
1417 [Geochemistry, 54, 151–187, https://doi.org/10.2113/0540151, 2003.](#)

1418 [Crenshaw, M. A.: The inorganic composition of molluscan extrapallial fluid, The Biological Bulletin,](#)
1419 [143, 506–512, https://doi.org/10.2307/1540180, 1972.](#)

1420 [van Dijk, I., Mouret, A., Cotte, M., le Houedec, S., Oron, S., Reichart, G. J., Reyes-Herrera, J., Filipsson,](#)
1421 [H. L., and Barras, C.: Chemical Heterogeneity of Mg, Mn, Na, S, and Sr in Benthic Foraminiferal](#)
1422 [Calcite, Frontiers in Earth Science, 7, 281, https://doi.org/10.3389/feart.2019.00281, 2019.](#)

1423 [van Dijk, I., de Nooijer, L. J., Barras, C., and Reichart, G. J.: Mn Incorporation in Large Benthic](#)
1424 [Foraminifera: Differences Between Species and the Impact of pCO₂, Frontiers in Earth Science,](#)
1425 [https://doi.org/10.3389/feart.2020.567701, 2020.](#)

1426 [Dupuy, C., Rossignol, L., Geslin, E., and Pascal, P. Y.: Predation of mudflat meio-macrofaunal](#)
 1427 [metazoans by a calcareous foraminifer, *Ammonia tepida* \(Cushman, 1926\), *Journal of Foraminiferal*](#)
 1428 [Research](#), 40, 305–312, <https://doi.org/10.2113/gsf.40.4.305>, 2010.

1429 [Elderfield, H.: A biomineralization model for the incorporation of trace elements into foraminiferal](#)
 1430 [calcium carbonate, *Earth and Planetary Science Letters*](#), 142, 409–423, [https://doi.org/10.1016/0012-](https://doi.org/10.1016/0012-821X(96)00105-7)
 1431 [821X\(96\)00105-7](#), 1996.

1432 [Erez, J.: The Source of Ions for Biomineralization in Foraminifera and Their Implications for](#)
 1433 [Paleoceanographic Proxies, *Reviews in Mineralogy and Geochemistry*](#), 54, 115–149,
 1434 <https://doi.org/10.2113/0540115>, 2003.

1435 [Evans, D., Erez, J., Oron, S., and Müller, W.: Mg/Ca-temperature and seawater-test chemistry](#)
 1436 [relationships in the shallow-dwelling large benthic foraminifera *Operculina ammonoides*, *Geochimica*](#)
 1437 [et *Cosmochimica Acta*](#), 148, 325–342, <https://doi.org/10.1016/j.gca.2014.09.039>, 2015.

1438 [Evans, D., Müller, W., and Erez, J.: Assessing foraminifera biomineralisation models through trace](#)
 1439 [element data of cultures under variable seawater chemistry, *Geochimica et Cosmochimica Acta*](#), 236,
 1440 [198–217, https://doi.org/10.1016/j.gca.2018.02.048](https://doi.org/10.1016/j.gca.2018.02.048), 2018.

1441 [Falini, G., Albeck, S., Weiner, S., and Addadi, L.: Control of Aragonite or Calcite Polymorphism by](#)
 1442 [Mollusk Shell Macromolecules, *Science*](#), 271, 67–69, <https://doi.org/10.1126/science.271.5245.67>,
 1443 [1996.](#)

1444 [Ferrier-Pagès, C., Boisson, F., Allemand, D., and Tambutté, E.: Kinetics of strontium uptake in the](#)
 1445 [scleractinian coral *Stylophora pistillata*, *Marine Ecology Progress Series*](#), 245, 93–100,
 1446 <https://doi.org/10.3354/meps245093>, 2002.

1447 [Form, A. U., Büscher, J. v., Hissmann, K., Flögel, S., Wisshak, M., Rüggeberg, A., Bannister, R., Kutti, T.,](#)
 1448 [Stapp, L., Bennecke, S., Küter, M., Nachtigall, K., Schauer, J., and Fenske, M.: RV POSEIDON Cruise](#)
 1449 [Report POS473 LORELEI II: LOphelia REef Lander Expedition and Investigation II, Tromsø – Bergen –](#)
 1450 [Esbjerg, 15.08. – 31.08. – 04.09.2014., 25 pp., https://doi.org/10.3289/CR_POS_473](#), 2015.

1451 [Freiwald, A. and Schönfeld, J.: Substrate pitting and boring pattern of *Hyrrokkin sarcophaga*](#)
 1452 [Cedhagen, 1994 \(Foraminifera\) in a modern deep-water coral reef mound, *Marine*](#)
 1453 [Micropaleontology](#), 28, 199–207, 1996.

1454 [Füger, A., Konrad, F., Leis, A., Dietzel, M., and Mavromatis, V.: Effect of growth rate and pH on](#)
 1455 [lithium incorporation in calcite, *Geochimica et Cosmochimica Acta*](#), 248, 14–24,
 1456 <https://doi.org/10.1016/j.gca.2018.12.040>, 2019.

1457 [Füllenbach, C. S., Schöne, B. R., Shirai, K., Takahata, N., Ishida, A., and Sano, Y.: Minute co-variations](#)
 1458 [of Sr/Ca ratios and microstructures in the aragonitic shell of *Cerastoderma edule* \(Bivalvia\) – Are](#)
 1459 [geochemical variations at the ultra-scale masking potential environmental signals?, *Geochimica et*](#)
 1460 [Cosmochimica Acta](#), 205, 256–271, <https://doi.org/10.1016/j.gca.2017.02.019>, 2017.

1461 [Gabitov, R. I., Cohen, A. L., Gaetani, G. A., Holcomb, M., and Watson, E. B.: The impact of crystal](#)
 1462 [growth rate on element ratios in aragonite: An experimental approach to understanding vital effects,](#)
 1463 [Geochimica et Cosmochimica Acta](#), 70, A187, <https://doi.org/10.1016/j.gca.2006.06.377>, 2006.

1464 [Gabitov, R. I., Sadekov, A., and Leinweber, A.: Crystal growth rate effect on Mg/Ca and Sr/Ca](#)
 1465 [partitioning between calcite and fluid: An in situ approach, *Chemical Geology*](#), 367, 70–82,
 1466 <https://doi.org/10.1016/j.chemgeo.2013.12.019>, 2014.

1467 [García-Gallardo, Á., Grunert, P., Voelker, A. H. L., Mendes, L., and Piller, W. E.: Re-evaluation of the](#)
 1468 [“elevated epifauna” as indicator of Mediterranean Outflow Water in the Gulf of Cadiz using stable](#)
 1469 [isotopes \(\$\delta^{13}\text{C}\$, \$\delta^{18}\text{O}\$ \), *Global and Planetary Change*](#), 155, 78–97,
 1470 <https://doi.org/10.1016/j.gloplacha.2017.06.005>, 2017.

1471 [Geerken, E., Jan De Nooijer, L., van Dijk, L., and Reichert, G. J.: Impact of salinity on element](#)
 1472 [incorporation in two benthic foraminiferal species with contrasting magnesium contents,](#)
 1473 [Biogeosciences](#), 15, 2205–2218, <https://doi.org/10.5194/bg-15-2205-2018>, 2018.

1474 [GEOMAR Helmholtz-Zentrum für Ozeanforschung: Research Vessel POSEIDON, *Journal of large-scale*](#)
 1475 [research facilities JLSRF](#), 1, 60–63, <https://doi.org/10.17815/jlsrf-1-62>, 2015.

1476 [GEOMAR Helmholtz-Zentrum für Ozeanforschung: Manned submersible „JAGO“, *Journal of large-*](#)
 1477 [scale research facilities JLSRF](#), 3, 1–12, <https://doi.org/10.17815/jlsrf-3-157>, 2017.

1478 [Goldstein, J. I., Newbury, D. E., Michael, J. R., Ritchie, N. W. M., Scott, J. H. J., and Joy, D. C.: Scanning](#)
 1479 [Electron Microscopy and X-Ray Microanalysis, Springer New York, New York, NY,](#)
 1480 <https://doi.org/10.1007/978-1-4939-6676-9>, 2018.

1481 [Goldstein, S. T.: Foraminifera: A biological overview, in: *Modern Foraminifera*,](#)
 1482 https://doi.org/10.1007/0-306-48104-9_3, 1999.

1483 [Gray, W. R. and Evans, D.: Nonthermal Influences on Mg/Ca in Planktonic Foraminifera: A Review of](#)
 1484 [Culture Studies and Application to the Last Glacial Maximum, *Paleoceanography and*](#)
 1485 [Paleoclimatology](#), 34, 306–315, <https://doi.org/10.1029/2018PA003517>, 2019.

1486 [Greaves, M., Barker, S., Daunt, C., and Elderfield, H.: Accuracy, standardization, and interlaboratory](#)
1487 [calibration standards for foraminiferal Mg/Ca thermometry, *Geochemistry, Geophysics, Geosystems*,](#)
1488 [6, 2–13, <https://doi.org/10.1029/2004GC000790>, 2005.](#)

1489 [Greaves, M., Caillon, N., Rebaubier, H., Bartoli, G., Bohaty, S., Cacho, I., Clarke, L., Cooper, M., Daunt,](#)
1490 [C., Delaney, M., DeMenocal, P., Dutton, A., Eggins, S., Elderfield, H., Garbe-Schoenberg, D., Goddard,](#)
1491 [E., Green, D., Groeneveld, J., Hastings, D., Hathorne, E., Kimoto, K., Klinkhammer, G., Labeyrie, L., Lea,](#)
1492 [D. W., Marchitto, T., Martínez-Botí, M. A., Mortyn, P. G., Ni, Y., Nuernberg, D., Paradis, G., Quinn, T.,](#)
1493 [Rosenthal, Y., Russel, A., Sagawa, T., Sosdian, S., Stott, L., Tachikawa, K., Tappa, E., Thunell, R., and](#)
1494 [Wilson, P. A.: Interlaboratory comparison study of calibration standards for foraminiferal Mg/Ca](#)
1495 [thermometry, *Geochemistry, Geophysics, Geosystems*, 9, 1–27,](#)
1496 [https://doi.org/10.1029/2008GC001974, 2008.](#)

1497 [Groeneveld, J. and Filipsson, H. L.: Mg/Ca and Mn/Ca ratios in benthic foraminifera: the potential to](#)
1498 [reconstruct past variations in temperature and hypoxia in shelf regions, *Biogeosciences*, 10, 5125–](#)
1499 [5138, <https://doi.org/10.5194/bg-10-5125-2013>, 2013.](#)

1500 [Gussone, N., Filipsson, H. L., and Kuhnert, H.: Mg/Ca, Sr/Ca and Ca isotope ratios in benthonic](#)
1501 [foraminifers related to test structure, mineralogy and environmental controls, *Geochimica et*](#)
1502 [Cosmochimica Acta](#), 173, 142–159, <https://doi.org/10.1016/j.gca.2015.10.018>, 2016.

1503 [Halloran, B. A. and Donachy, J. E.: Characterization of organic matrix macromolecules from the shells](#)
1504 [of the antarctic scallop, *Adamussium colbecki*, *Comparative Biochemistry and Physiology -- Part B:*](#)
1505 [Biochemistry and](#), 111, 221–231, [https://doi.org/10.1016/0305-0491\(94\)00245-P](https://doi.org/10.1016/0305-0491(94)00245-P), 1995.

1506 [Hancock, L. G., Walker, S. E., Pérez-Huerta, A., and Bowser, S. S.: Population Dynamics and Parasite](#)
1507 [Load of a Foraminifer on Its Antarctic Scallop Host with Their Carbonate Biomass Contributions, *PLOS*](#)
1508 [ONE](#), 10, e0132534, <https://doi.org/10.1371/journal.pone.0132534>, 2015.

1509 [Holland, K., Eggins, S. M., Hönisch, B., Haynes, L. L., and Branson, O.: Calcification rate and shell](#)
1510 [chemistry response of the planktic foraminifer *Orbulina universa* to changes in microenvironment](#)
1511 [seawater carbonate chemistry, *Earth and Planetary Science Letters*, 464, 124–134,](#)
1512 [https://doi.org/10.1016/j.epsl.2017.02.018, 2017.](#)

1513 [Hönisch, B., Allen, K. A., Russell, A. D., Eggins, S. M., Bijma, J., Spero, H. J., Lea, D. W., and Yu, J.:](#)
1514 [Planktic foraminifers as recorders of seawater Ba/Ca, *Marine Micropaleontology*, 79, 52–57,](#)
1515 [https://doi.org/10.1016/j.marmicro.2011.01.003, 2011.](#)

1516 [Horton, T., Kroh, A., Ah Yong, S., Bailly, N., Boyko, C. B., Brandão, S. N., Gofas, S., Hooper, J. N. A.,](#)
1517 [Hernandez, F., Holovachov, O., Mees, J., Molodtsova, T. N., Paulay, G., Decock, W., Dekeyser, S.,](#)

1518 [Poffyn, G., Vandepitte, L., Vanhoorne, B., Adlard, R., Agatha, S., Ahn, K. J., Akkari, N., Alvarez, B.,](#)
 1519 [Anderberg, A., Anderson, G., Angel, M. v., Antic, D., Arango, C., Artois, T., Atkinson, S., Auffenberg, K.,](#)
 1520 [Baldwin, B. G., Bank, R., Barber, A., Barbosa, J. P., Bartsch, I., Bellan-Santini, D., Bergh, N., Bernot, J.,](#)
 1521 [Berta, A., Bezerra, T. N., Bieler, R., Blanco, S., Blasco-Costa, I., Blazewicz, M., Bock, P., Bonifacio de](#)
 1522 [León, M., Böttger-Schnack, R., Bouchet, P., Boury-Esnault, N., Boxshall, G., Bray, R., Bruce, N. L.,](#)
 1523 [Cairns, S., Calvo Casas, J., Carballo, J. L., Cárdenas, P., Carstens, E., Chan, B. K., Chan, T. Y., Cheng, L.,](#)
 1524 [Christenhusz, M., Churchill, M., Coleman, C. O., Collins, A. G., Collins, G. E., Corbari, L., Cordeiro, R.,](#)
 1525 [Cornils, A., Coste, M., Costello, M. J., Crandall, K. A., Cremonese, F., Cribb, T., Cutmore, S., Dahdouh-](#)
 1526 [Guebas, F., Daly, M., Daneliya, M., Dauvin, J. C., Davie, P., de Broyer, C., de Grave, S., de Mazancourt,](#)
 1527 [V., de Voogd, N. J., Decker, P., Defaye, D., d'Hondt, J. L., Dippenaar, S., Dohrmann, M., Dolan, J.,](#)
 1528 [Domning, D., Downey, R., Ector, L., Eisendle-Flöckner, U., Eitel, M., Encarnação, S. C. d., Enghoff, H.,](#)
 1529 [Epler, J., Ewers-Saucedo, C., et al.: World Register of Marine Species \(WoRMS\),](#)
 1530 <http://www.marinespecies.org>, 2021.

1531 [Immenhauser, A., Schöne, B. R., Hoffmann, R., and Niedermayr, A.: Mollusc and brachiopod skeletal](#)
 1532 [hard parts: Intricate archives of their marine environment, *Sedimentology*, 63, 1–59,](#)
 1533 <https://doi.org/10.1111/sed.12231>, 2016.

1534 [Jacob, D. E., Wirth, R., Soldati, A. L., Wehrmeister, U., and Schreiber, A.: Amorphous calcium](#)
 1535 [carbonate in the shells of adult Unionoida, *Journal of Structural Biology*, 173, 241–249,](#)
 1536 <https://doi.org/10.1016/j.jsb.2010.09.011>, 2011.

1537 [Jacob, D. E., Wirth, R., Agbaje, O. B. A., Branson, O., and Eggins, S. M.: Planktic foraminifera form](#)
 1538 [their shells via metastable carbonate phases, *Nature Communications*, 8, 1–8,](#)
 1539 <https://doi.org/10.1038/s41467-017-00955-0>, 2017.

1540 [Jacobson, P.: Physical Oceanography of the Trondheimsfjord, *Geophysical & Astrophysical Fluid*](#)
 1541 [Dynamics](#), 26, 3–26, <https://doi.org/10.1080/03091928308221761>, 1983.

1542 [Jochum, K. P., Nohl, U., Herwig, K., Lammel, E., Stoll, B., and Hofmann, A. W.: GeoReM: A New](#)
 1543 [Geochemical Database for Reference Materials and Isotopic Standards, *Geostandards and*](#)
 1544 [Geoanalytical Research](#), 29, 333–338, <https://doi.org/10.1111/j.1751-908X.2005.tb00904.x>, 2005.

1545 [Kato, K., Wada, H., and Fujioka, K.: The application of chemical staining to separate calcite and](#)
 1546 [aragonite minerals for micro-scale isotopic analyses, *Geochemical Journal*, 37, 291–297,](#)
 1547 <https://doi.org/10.2343/geochemj.37.291>, 2003.

1548 [Klein, R. T., Lohmann, K. C., and Thayer, C. W.: Sr/Ca and \$^{13}\text{C}/^{12}\text{C}\$ ratios in skeletal calcite of *Mytilus*](#)
 1549 [trossulus: Covariation with metabolic rate, salinity, and carbon isotopic composition of seawater,](#)
 1550 [Geochimica et Cosmochimica Acta, \[https://doi.org/10.1016/S0016-7037\\(96\\)00232-3\]\(https://doi.org/10.1016/S0016-7037\(96\)00232-3\), 1996.](#)
 1551 [Koho, K. A., de Nooijer, L. J., and Reichart, G. J.: Combining benthic foraminiferal ecology and shell](#)
 1552 [Mn/Ca to deconvolve past bottom water oxygenation and paleoproductivity, Geochimica et](#)
 1553 [Cosmochimica Acta, 165, 294–306, <https://doi.org/10.1016/j.gca.2015.06.003>, 2015.](#)
 1554 [Lantz, B.: The impact of sample non-normality on ANOVA and alternative methods, British Journal of](#)
 1555 [Mathematical and Statistical Psychology, 66, 224–244, \[https://doi.org/10.1111/j.2044-\]\(https://doi.org/10.1111/j.2044-8317.2012.02047.x\)](#)
 1556 [8317.2012.02047.x](#), 2013.
 1557 [Lear, C. H. and Rosenthal, Y.: Benthic foraminiferal Li/Ca: Insights into Cenozoic seawater carbonate](#)
 1558 [saturation state, Geology, 34, 985, <https://doi.org/10.1130/G22792A.1>, 2006.](#)
 1559 [Lear, C. H., Rosenthal, Y., and Slowey, N.: Benthic foraminiferal Mg/Ca-paleothermometry: A revised](#)
 1560 [core-top calibration, Geochimica et Cosmochimica Acta, 66, 3375–3387,](#)
 1561 [https://doi.org/10.1016/S0016-7037\(02\)00941-9, 2002.](#)
 1562 [Lorens, R. B.: Sr, Cd, Mn and Co distribution coefficients in calcite as a function of calcite precipitation](#)
 1563 [rate, Geochimica et Cosmochimica Acta, 45, 553–561, \[https://doi.org/10.1016/0016-7037\\(81\\)90188-\]\(https://doi.org/10.1016/0016-7037\(81\)90188-5\)](#)
 1564 [5](#), 1981.
 1565 [Lorens, R. B. and Bender, M. L.: The impact of solution chemistry on *Mytilus edulis* calcite and](#)
 1566 [aragonite, Geochimica et Cosmochimica Acta, 44, 1265–1278, \[https://doi.org/10.1016/0016-\]\(https://doi.org/10.1016/0016-7037\(80\)90087-3\)](#)
 1567 [7037\(80\)90087-3](#), 1980.
 1568 [Lorrain, A., Gillikin, D. P., Paulet, Y. M., Chauvaud, L., le Mercier, A., Navez, J., and André, L.: Strong](#)
 1569 [kinetic effects on Sr/Ca ratios in the calcitic bivalve *Pecten maximus*, Geology, 33, 965–968,](#)
 1570 [https://doi.org/10.1130/G22048.1, 2005.](#)
 1571 [Mackensen, A. and Nam, S. il: Taxon-specific epibenthic foraminiferal \$\delta^{18}\text{O}\$ in the Arctic Ocean:](#)
 1572 [Relationship to water masses, deep circulation, and brine release, Marine Micropaleontology, 113,](#)
 1573 [34–43, <https://doi.org/10.1016/j.marmicro.2014.09.002>, 2014.](#)
 1574 [Marchitto, T. M., Curry, W. B., Lynch-Stieglitz, J., Bryan, S. P., Cobb, K. M., and Lund, D. C.: Improved](#)
 1575 [oxygen isotope temperature calibrations for cosmopolitan benthic foraminifera, Geochimica et](#)
 1576 [Cosmochimica Acta, 130, 1–11, <https://doi.org/10.1016/j.gca.2013.12.034>, 2014.](#)

1577 [Marin, F., Luquet, G., Marie, B., and Medakovic, D.: Molluscan Shell Proteins: Primary Structure,](#)
1578 [Origin, and Evolution, Current Topics in Developmental Biology, 80, 209–276,](#)
1579 [https://doi.org/10.1016/S0070-2153\(07\)80006-8](https://doi.org/10.1016/S0070-2153(07)80006-8), 2007.

1580 [McConnaughey, T. A.: Sub-equilibrium oxygen-18 and carbon-13 levels in biological carbonates:](#)
1581 [Carbonate and kinetic models, Coral Reefs, 22, 316–327, https://doi.org/10.1007/s00338-003-0325-](#)
1582 [2](#), 2003.

1583 [McCorkle, D. C., Corliss, B. H., and Farnham, C. A.: Vertical distributions and stable isotopic](#)
1584 [compositions of live \(stained\) benthic foraminifera from the North Carolina and California continental](#)
1585 [margins, Deep-Sea Research Part I: Oceanographic Research Papers, 44, 983–1024,](#)
1586 [https://doi.org/10.1016/S0967-0637\(97\)00004-6](https://doi.org/10.1016/S0967-0637(97)00004-6), 1997.

1587 [McCulloch, M., Falter, J., Trotter, J., and Montagna, P.: Coral resilience to ocean acidification and](#)
1588 [global warming through pH up-regulation, Nature Climate Change, 2, 623–627,](#)
1589 <https://doi.org/10.1038/nclimate1473>, 2012.

1590 [Mienis, F., de Stigter, H. C., White, M., Duineveld, G., de Haas, H., and van Weering, T. C. E.:](#)
1591 [Hydrodynamic controls on cold-water coral growth and carbonate-mound development at the SW](#)
1592 [and SE Rockall Trough Margin, NE Atlantic Ocean, Deep-Sea Research Part I: Oceanographic Research](#)
1593 [Papers, 54, 1655–1674, https://doi.org/10.1016/j.dsr.2007.05.013](#), 2007.

1594 [Milzer, G., Giraudeau, J., Faust, J., Knies, J., Eynaud, F., and Rühlemann, C.: Spatial distribution of](#)
1595 [benthic foraminiferal stable isotopes and dinocyst assemblages in surface sediments of the](#)
1596 [Trondheimsfjord, central Norway, Biogeosciences, 10, 4433–4448, https://doi.org/10.5194/bg-10-](#)
1597 [4433-2013](#), 2013.

1598 [Moradian-Oldak, J., Addadi, L., Weiner, S., and Berman, A.: Tuning of Crystal Nucleation and Growth](#)
1599 [by Proteins: Molecular Interactions at Solid-Liquid Interfaces in Biomineralization, Croatica Chemica](#)
1600 [Acta, 63, 539–544, 1990.](#)

1601 [Mucci, A.: Manganese uptake during calcite precipitation from seawater: Conditions leading to the](#)
1602 [formation of a pseudokutnahorite, Geochimica et Cosmochimica Acta, 52, 1859–1868,](#)
1603 [https://doi.org/10.1016/0016-7037\(88\)90009-9](https://doi.org/10.1016/0016-7037(88)90009-9), 1988.

1604 [Mucci, A. and Morse, J. W.: The incorporation of Mg 2+ and Sr 2+ into calcite overgrowths: influences](#)
1605 [of growth rate and solution composition, Geochimica et Cosmochimica Acta, 47, 217–233, 1983.](#)

1606 [Nakahara, H.: Nacre Formation in Bivalve and Gastropod Molluscs, in: Mechanisms and Phylogeny of](#)
1607 [Mineralization in Biological Systems, Springer Japan, Tokyo, 343–350, \[https://doi.org/10.1007/978-4-\]\(https://doi.org/10.1007/978-4-431-68132-8_55\)](#)
1608 [431-68132-8_55, 1991.](#)

1609 [Nehrke, G., Keul, N., Langer, G., de Nooijer, L. J., Bijma, J., and Meibom, A.: A new model for](#)
1610 [biomineralization and trace-element signatures of Foraminifera tests, *Biogeosciences*,](#)
1611 [https://doi.org/10.5194/bg-10-6759-2013, 2013.](#)

1612 [de Nooijer, L. J., Toyofuku, T., and Kitazato, H.: Foraminifera promote calcification by elevating their](#)
1613 [intracellular pH, *Proceedings of the National Academy of Sciences of the United States of America*,](#)
1614 [106, 15374–15378, <https://doi.org/10.1073/pnas.0904306106>, 2009.](#)

1615 [de Nooijer, L. J., Spero, H. J., Erez, J., Bijma, J., and Reichart, G. J.: Biomineralization in perforate](#)
1616 [foraminifera, *Earth-Science Reviews*, 135, 48–58, <https://doi.org/10.1016/j.earscirev.2014.03.013>,](#)
1617 [2014.](#)

1618 [Oomori, T., Kaneshima, H., Maezato, Y., and Kitano, Y.: Distribution Coefficient of Mg²⁺ ions between](#)
1619 [calcite and solution at 10–50°C, *Marine Chemistry*, 20, 327–336, \[https://doi.org/10.1016/B978-\]\(https://doi.org/10.1016/B978-044452228-3/50006-6\)](#)
1620 [044452228-3/50006-6, 1987.](#)

1621 [Petersen, J., Barras, C., Bézous, A., La, C., de Nooijer, L. J., Meysman, F. J. R., Mouret, A., Slomp, C. P.,](#)
1622 [and Jorissen, F. J.: Mn/Ca intra- and inter-test variability in the benthic foraminifer *Ammonia tepida*,](#)
1623 [Biogeosciences, 15, 331–348, <https://doi.org/10.5194/bg-15-331-2018>, 2018.](#)

1624 [Piez, K. A.: Amino Acid Composition of Some Calcified Proteins, *Science*, 134, 841–842,](#)
1625 [https://doi.org/10.1126/science.134.3482.841, 1961.](#)

1626 [Pytkowicz, R. M.: Rates of Inorganic Calcium Carbonate Nucleation, *The Journal of Geology*, 73, 196–](#)
1627 [199, <https://doi.org/10.1086/627056>, 1965.](#)

1628 [Raddatz, J., Rüggeberg, A., Margreth, S., and Dullo, W. C.: Paleoenvironmental reconstruction of](#)
1629 [Challenger Mound initiation in the Porcupine Seabight, NE Atlantic, *Marine Geology*, 282, 79–90,](#)
1630 [https://doi.org/10.1016/j.margeo.2010.10.019, 2011.](#)

1631 [Raddatz, J., Liebetrau, V., Rüggeberg, A., Hathorne, E., Krabbenhöft, A., Eisenhauer, A., Böhm, F.,](#)
1632 [Vollstaedt, H., Fietzke, J., López Correa, M., Freiwald, A., and Dullo, W. C.: Stable Sr-isotope, Sr/Ca,](#)
1633 [Mg/Ca, Li/Ca and Mg/Li ratios in the scleractinian cold-water coral *Lophelia pertusa*, *Chemical*](#)
1634 [Geology, 352, 143–152, <https://doi.org/10.1016/j.chemgeo.2013.06.013>, 2013.](#)

1635 [Raddatz, J., Rüggeberg, A., Flögel, S., Hathorne, E. C., Liebetrau, V., Eisenhauer, A., and Dullo, W. C.:
 1636 The influence of seawater pH on U/Ca ratios in the scleractinian cold-water coral *Lophelia pertusa*,
 1637 *Biogeosciences*, 11, 1863–1871, <https://doi.org/10.5194/bg-11-1863-2014>, 2014.](#)
 1638 [Raddatz, J., Nürnberg, D., Tiedemann, R., and Rippert, N.: Southeastern marginal West Pacific Warm
 1639 Pool sea-surface and thermocline dynamics during the Pleistocene \(2.5–0.5 Ma\), *Palaeogeography*,
 1640 *Palaeoclimatology, Palaeoecology*, 471, 144–156, <https://doi.org/10.1016/j.palaeo.2017.01.024>,
 1641 2017.](#)
 1642 [Raitzsch, M., Duenas-Bohórquez, A., Reichart, G. J., de Nooijer, L. J., and Bickert, T. T.: Incorporation
 1643 of Mg and Sr in calcite of cultured benthic foraminifera: Impact of calcium concentration and
 1644 associated calcite saturation state, *Biogeosciences*, 7, 869–881, \[https://doi.org/10.5194/bg-7-869-\]\(https://doi.org/10.5194/bg-7-869-2010\)
 1645 2010, 2010.](#)
 1646 [Raja, R., Saraswati, P. K., Rogers, K., and Iwao, K.: Magnesium and strontium compositions of recent
 1647 symbiont-bearing benthic foraminifera, *Marine Micropaleontology*, 58, 31–44,
 1648 <https://doi.org/10.1016/j.marmicro.2005.08.001>, 2005.](#)
 1649 [Rathburn, A. E. and de Deckker, P.: Magnesium and strontium compositions of Recent benthic
 1650 foraminifera from the Coral Sea, Australia and Prydz Bay, Antarctica, *Marine Micropaleontology*, 32,
 1651 231–248, \[https://doi.org/10.1016/S0377-8398\\(97\\)00028-5\]\(https://doi.org/10.1016/S0377-8398\(97\)00028-5\), 1997.](#)
 1652 [Schleinkofer, N., Raddatz, J., Freiwald, A., Evans, D., Beuck, L., Rüggeberg, A., and Liebetrau, V.:
 1653 Environmental and biological controls on Na/Ca ratios in scleractinian cold-water corals,
 1654 *Biogeosciences*, 16, 3565–3582, <https://doi.org/10.5194/bg-16-3565-2019>, 2019.](#)
 1655 [Schleinkofer, N., Raddatz, J., Evans, D., Gerdes, A., Flögel, S., Voigt, S., Büscher, J. V., and Wisshak, M.:
 1656 Compositional variability of Mg/Ca, Sr/Ca, and Na/Ca in the deep-sea bivalve *Acesta excavata*
 1657 \(*Fabricius*, 1779\), *PLOS ONE*, 16, e0245605, <https://doi.org/10.1371/journal.pone.0245605>, 2021.](#)
 1658 [Schöne, B. R., Zhang, Z., Jacob, D., Gillikin, D. P., Tütken, T., Garbe-Schönberg, D., McConnaughey, T.,
 1659 and Soldati, A.: Effect of organic matrices on the determination of the trace element chemistry \(Mg,
 1660 Sr, Mg/Ca, Sr/Ca\) of aragonitic bivalve shells \(*Arctica islandica*\) - Comparison of ICP-OES and LA-ICP-
 1661 MS data, *Geochemical Journal*, 44, 23–37, <https://doi.org/10.2343/geochemj.1.0045>, 2010.](#)
 1662 [Schweizer, M., Bowser, S. S., Korsun, S., and Pawlowski, J.: Emendation of *Cibicides antarcticus*
 1663 \(*Saidova*, 1975\) based on molecular, morphological, and ecological data, *Journal of Foraminiferal*
 1664 *Research*, <https://doi.org/10.2113/gsjfr.42.4.340>, 2012.](#)

1665 [Secor, C. L., Mills, E. L., Harshbarger, J., Kuntz, H. T., Gutenmann, W. H., and Lisk, D. J.:
 1666 Bioaccumulation of toxicants, element and nutrient composition, and soft tissue histology of zebra
 1667 mussels \(*Dreissena polymorpha*\) from New York State waters, *Chemosphere*,
 1668 \[https://doi.org/10.1016/0045-6535\\(93\\)90224-S\]\(https://doi.org/10.1016/0045-6535\(93\)90224-S\), 1993.](#)

1669 [Segev, E. and Erez, J.: Effect of Mg/Ca ratio in seawater on shell composition in shallow benthic
 1670 foraminifera, *Geochemistry, Geophysics, Geosystems*, 7, 1–8,
 1671 <https://doi.org/10.1029/2005GC000969>, 2006.](#)

1672 [Smith, P. B. and Emiliani, C.: Oxygen-isotope analysis of recent tropical pacific benthonic
 1673 foraminifera, *Science*, <https://doi.org/10.1126/science.160.3834.1335>, 1968.](#)

1674 [Spero, H. J.: Ultrastructural examination of chamber morphogenesis and biomineralization in the
 1675 planktonic foraminifer *Orbulina universa*, *Marine Biology*, 99, 9–20,
 1676 <https://doi.org/10.1007/BF00644972>, 1988.](#)

1677 [Spötl, C. and Vennemann, T. W.: Continuous-flow isotope ratio mass spectrometric analysis of
 1678 carbonate minerals, *Rapid Communications in Mass Spectrometry*, 17, 1004–1006,
 1679 <https://doi.org/10.1002/rcm.1010>, 2003.](#)

1680 [Stephenson, A. E., Deyoreo, J. J., Wu, L., Wu, K. J., Hoyer, J., and Dove, P. M.: Peptides enhance
 1681 magnesium signature in calcite: Insights into origins of vital effects, *Science*, 322, 724–727,
 1682 <https://doi.org/10.1126/science.1159417>, 2008.](#)

1683 [Sunda, W. G. and Huntsman, S. A.: Regulation of cellular manganese and manganese transport rates
 1684 in the unicellular alga *Chlamydomonas*, *Limnology and Oceanography*, 30, 71–80,
 1685 <https://doi.org/10.4319/lo.1985.30.1.0071>, 1985.](#)

1686 [Swinehart, J. H. and Smith, K. W.: Iron And Manganese Deposition In The Periostraca Of Several
 1687 Bivalve Molluscs, *The Biological Bulletin*, 156, 369–381, <https://doi.org/10.2307/1540924>, 1979.](#)

1688 [Takesue, R. K., Bacon, C. R., and Thompson, J. K.: Influences of organic matter and calcification rate
 1689 on trace elements in aragonitic estuarine bivalve shells, *Geochimica et Cosmochimica Acta*, 72, 5431–
 1690 5445, <https://doi.org/10.1016/j.gca.2008.09.003>, 2008.](#)

1691 [Tambutté, E., Allemand, D., Zoccola, D., Meibom, A., Lotto, S., Caminiti, N., and Tambutté, S.:
 1692 Observations of the tissue-skeleton interface in the scleractinian coral *Stylophora pistillata*, *Coral
 1693 Reefs*, 26, 517–529, <https://doi.org/10.1007/s00338-007-0263-5>, 2007.](#)

1694 [Todd, R.: A new *Rosalina* \(foraminifera\) parasitic on a bivalve, *Deep-Sea Research and Oceanographic
 1695 Abstracts*, 12, 831–837, \[https://doi.org/10.1016/0011-7471\\(65\\)90806-5\]\(https://doi.org/10.1016/0011-7471\(65\)90806-5\), 1965.](#)

1696 [Toyofuku, T., Kitazato, H., Kawahata, H., Tsuchiya, M., and Nohara, M.: Evaluation of Mg/Ca](#)
 1697 [thermometry in foraminifera: Comparison of experimental results and measurements in nature,](#)
 1698 [Paleoceanography, 15, 456–464, <https://doi.org/10.1029/1999PA000460>, 2000.](#)
 1699 [Toyofuku, T., Matsuo, M. Y., de Nooijer, L. J., Nagai, Y., Kawada, S., Fujita, K., Reichart, G. J., Nomaki,](#)
 1700 [H., Tsuchiya, M., Sakaguchi, H., and Kitazato, H.: Proton pumping accompanies calcification in](#)
 1701 [foraminifera, Nature Communications, 8, 1–6, <https://doi.org/10.1038/ncomms14145>, 2017.](#)
 1702 [Tribovillard, N., Algeo, T. J., Lyons, T., and Riboulleau, A.: Trace metals as paleoredox and](#)
 1703 [paleoproductivity proxies: An update, Chemical Geology, 232, 12–32,](#)
 1704 [https://doi.org/10.1016/j.chemgeo.2006.02.012, 2006.](#)
 1705 [Véneç-Peyré, M. T.: Bioeroding foraminifera: A review, Marine Micropaleontology, 28, 19–30,](#)
 1706 [https://doi.org/10.1016/0377-8398\(95\)00037-2, 1996.](#)
 1707 [de Villiers, S., Nelson, B. K., and Chivas, A.: Biological Control on Coral Sr/Ca and d18O](#)
 1708 [Reconstructions of Sea Surface Temperatures, Science, 269, 1247–1249, 1995.](#)
 1709 [Wada, K. and Fujinuki, T.: Biomineralization in bivalve molluscs with emphasis on the chemical](#)
 1710 [composition of the extrapallial fluid, Book chapter, 1976.](#)
 1711 [Walker, S. E., Hancock, L. G., and Bowser, S. S.: Diversity, biogeography, body size and fossil record of](#)
 1712 [parasitic and suspected parasitic foraminifera: A review, Journal of Foraminiferal Research, 47, 34–](#)
 1713 [55, <https://doi.org/10.2113/jsifr.47.1.34>, 2017.](#)
 1714 [Webb, A. E., Pomponi, S. A., van Duyl, F. C., Reichart, G. J., and de Nooijer, L. J.: pH Regulation and](#)
 1715 [Tissue Coordination Pathways Promote Calcium Carbonate Bioerosion by Excavating Sponges,](#)
 1716 [Scientific Reports, 9, 1–10, <https://doi.org/10.1038/s41598-018-36702-8>, 2019.](#)
 1717 [Whitney, N. M., Johnson, B. J., Dostie, P. T., Luzier, K., and Wanamaker, A. D.: Paired bulk organic and](#)
 1718 [individual amino acid \$\delta^{15}\text{N}\$ analyses of bivalve shell periostracum: A paleoceanographic proxy for](#)
 1719 [water source variability and nitrogen cycling processes, Geochimica et Cosmochimica Acta, 254, 67–](#)
 1720 [85, <https://doi.org/10.1016/j.gca.2019.03.019>, 2019.](#)
 1721 [Wilbur, K. M. and Saleuddin, A. S. M.: Shell Formation, in: The Mollusca, Elsevier, 235–287,](#)
 1722 [https://doi.org/10.1016/B978-0-12-751404-8.50014-1, 1983.](#)
 1723 [Yin, Y., Huang, J., Paine, M. L., Reinhold, V. N., and Chasteen, N. D.: Structural Characterization of the](#)
 1724 [Major Extrapallial Fluid Protein of the Mollusc *Mytilus edulis* : Implications for Function,](#)
 1725 [Biochemistry, 44, 10720–10731, <https://doi.org/10.1021/bi0505565>, 2005.](#)

1726 [Yu, X. and Inesi, G.: Variable stoichiometric efficiency of Ca²⁺ and Sr²⁺ transport by the sarcoplasmic](#)
1727 [reticulum ATPase, Journal of Biological Chemistry, 270, 4361–4367,](#)
1728 <https://doi.org/10.1074/jbc.270.9.4361>, 1995.

1729 [Zhang, C. and Zhang, R.: Matrix proteins in the outer shells of molluscs, Marine Biotechnology, 8,](#)
1730 [572–586, https://doi.org/10.1007/s10126-005-6029-6](https://doi.org/10.1007/s10126-005-6029-6), 2006.

1731 -

1732 ▲

Formatiert: Englisch (Vereinigte Staaten)

Formatiert: Links